VOLUME 34 SEPTEMBER 1956 NUMBER 5

Canadian Journal of Technology

Editor: G. A. LEDINGHAM

Published by THE NATIONAL RESEARCH COUNCIL
OTTAWA CANADA

CANADIAN JOURNAL OF TECHNOLOGY

(Formerly Section F, Canadian Journal of Research)

Under the authority of the Chairman of the Committee of the Privy Council on Scientific and Industrial Research, the National Research Council issues THE CANADIAN JOURNAL OF TECHNOLOGY and six other journals devoted to the publication, in English or French, of the results of original scientific research. Matters of general policy concerning these journals are the responsibility of a joint Editorial Board consisting of: members representing the National Research Council of Canada; the Editors of the Journals; and members representing the Royal Society of Canada and four other scientific societies.

The Chemical Institute of Canada has chosen the Canadian Journal of Technology and the Canadian Journal of Chemistry as its medium of publication for scientific papers.

Manuscripts for publication should be submitted to Dr. Léo Marion, Editor-in-Chief, Canadian Journal of Technology, National Research Council, Ottawa 2, Canada.
(For instructions on preparation of copy, see **Notes to Contributors** (inside back cover).)

Proof, correspondence concerning proof, and orders for reprints should be sent to the Manager, Editorial Office (Research Journals), Division of Administration, National Research Council, Ottawa 2, Canada.

Subscriptions, renewals, requests for single or back numbers, and all remittances should be sent to Division of Administration, National Research Council, Ottawa 2, Canada. Remittances should be made payable to the Receiver General of Canada, credit National Research Council.

The journals published, frequency of publication, and prices are:

Canadian Journal of Biochemistry and Physiology	Bimonthly	$3.00 a year
Canadian Journal of Botany	Bimonthly	$4.00 a year
Canadian Journal of Chemistry	Monthly	$5.00 a year
Canadian Journal of Microbiology	Bimonthly	$3.00 a year
Canadian Journal of Physics	Monthly	$4.00 a year
Canadian Journal of Technology	Bimonthly	$3.00 a year
Canadian Journal of Zoology	Bimonthly	$3.00 a year

The price of single numbers of all journals is 75 cents.

Contents

Printed in Canada *by* University of Toronto Press

CANADIAN JOURNAL OF TECHNOLOGY

Notes to Contributors

Manuscripts

(i) ***General.*** Manuscripts, in English or French, should be typewritten, double spaced, on paper 8½ × 11 in. **The original and one copy are to be submitted.** Tables and captions for the figures should be placed at the end of the manuscript. Every sheet of the manuscript should be numbered.

Style, arrangement, spelling, and abbreviations should conform to the usage of this journal. Names of all simple compounds, rather than their formulas, should be used in the text. Greek letters or unusual signs should be written plainly or explained by marginal notes. Superscripts and subscripts must be legible and carefully placed.

Manuscripts and illustrations should be carefully checked before they are submitted. Authors will be charged for unnecessary deviations from the usual format and for changes made in the proof that are considered excessive or unnecessary.

(ii) ***Abstract.*** An abstract of not more than about 200 words, indicating the scope of the work and the principal findings, is required, except in Notes.

(iii) ***References.*** References should be listed **alphabetically by authors' names,** numbered, and typed after the text. The form of the citations should be that used in this journal; in references to papers in periodicals, titles should not be given and only initial page numbers are required. The names of periodicals should be abbreviated in the form given in the most recent *List of Periodicals Abstracted by Chemical Abstracts*. All citations should be checked with the original articles and each one referred to in the text by the key number.

(iv) ***Tables.*** Tables should be numbered in roman numerals and each table referred to in the text. Titles should always be given but should be brief; column headings should be brief and descriptive matter in the tables confined to a minimum. Vertical rules should be used only when they are essential. Numerous small tables should be avoided.

Illustrations

(i) ***General.*** All figures (including each figure of the plates) should be numbered consecutively from 1 up, in arabic numerals, and each figure referred to in the text. The author's name, title of the paper, and figure number should be written in the lower left corner of the sheets on which the illustrations appear. Captions should not be written on the illustrations (see Manuscripts (i)).

(ii) ***Line Drawings.*** Drawings should be carefully made with India ink on white drawing paper, blue tracing linen, or co-ordinate paper ruled in blue only; any co-ordinate lines that are to appear in the reproduction should be ruled in black ink. Paper ruled in green, yellow, or red should not be used unless it is desired to have all the co-ordinate lines show. All lines should be of sufficient thickness to reproduce well. Decimal points, periods, and stippled dots should be solid black circles large enough to be reduced if necessary. Letters and numerals should be neatly made, preferably with a stencil **(do NOT use typewriting)** and be of such size that the smallest lettering will be not less than 1 mm. high when reproduced in a cut 3 in. wide.

Many drawings are made too large; originals should not be more than 2 or 3 times the size of the desired reproduction. In large drawings or groups of drawings the ratio of height to width should conform to that of a journal page but the height should be adjusted to make allowance for the caption.

The original drawings and one set of clear copies (e.g. small photographs) are to be submitted.

(iii) ***Photographs.*** Prints should be made on glossy paper, with strong contrasts. They should be trimmed so that essential features only are shown and mounted carefully, with rubber cement, on white cardboard with no space or only a very small space (less than 1 mm.) between them. In mounting, full use of the space available should be made (to reduce the number of cuts required) and the ratio of height to width should correspond to that of a journal page (4¼ × 7½ in.); however, allowance must be made for the captions. Photographs or groups of photographs should not be more than 2 or 3 times the size of the desired reproduction.

Photographs are to be submitted in duplicate; if they are to be reproduced in groups one set should be mounted, the duplicate set unmounted.

Reprints

A total of 50 reprints of each paper, without covers, are supplied free. Additional reprints, with or without covers, may be purchased.

Charges for reprints are based on the number of printed pages, which may be calculated approximately by multiplying by 0.6 the number of manuscript pages (double-spaced typewritten sheets, 8½ × 11 in.) and including the space occupied by illustrations. An additional charge is made for illustrations that appear as coated inserts. The cost per page is given on the reprint requisition which accompanies the galley.

Any reprints required in addition to those requested on the author's reprint requisition form must be ordered officially as soon as the paper has been accepted for publication.

Canadian Journal of Technology

Issued by THE NATIONAL RESEARCH COUNCIL OF CANADA

VOLUME 34 SEPTEMBER 1956 NUMBER 5

THE POTENTIALS OF ZINC AND STEEL IN TAP WATER[1]

BY R. M. GUEST

ABSTRACT

At room temperature zinc normally is anodic to steel in water and protects it galvanically. At higher temperatures, it may become cathodic to steel under certain conditions and no longer give galvanic protection. In order to define these conditions, the potentials of zinc rods towards a commercially available steel were measured at 60°, 70°, 80°, 90° C., and at boiling point over a period of several months in Toronto tap water. Given time, potential reversals occurred at all these temperatures except at the boiling point but more quickly at 70°C. than at 60°, 80°, or 90°. The source of supply of Toronto tap water is Lake Ontario. Consequently the same type of behavior could be expected from other municipalities using Lake Ontario water. In fact, similar results could be expected with the waters of municipalities using Lake Erie, Lake Huron, or Lake Michigan water, as a source of supply, since they are all quite similar in chemical composition.

Zinc is normally anodic to steel and, when contact is made between the zinc and the steel, the zinc will corrode preferentially and protect the steel. If a reversal of potential should occur, that is, the zinc becoming cathodic to the steel, then the steel will corrode preferentially and protect the zinc. Other research workers (1, 2, 3, 4, 5, 6, 7) have noted this reversal of potential at 60° and above and have shown that oxygen must be present. They have also shown that the presence of bicarbonate and nitrate favor this reversal of potential whilst the presence of chloride, sulphate, silicate, and calcium retard it. Gilbert (4) has stated that zinc oxide is usually formed when zinc corrodes in hot water and suggests that the enoblement of zinc in hot aerated solutions may be due to the presence of zinc oxide having some electronic conductivity.

EXPERIMENTAL

Overflow spouts were attached to 1 liter beakers by making a suction joint. These beakers were placed on variable hot plates where the temperature was controlled to $\pm 1°$ C. By means of a constant levelling device, Toronto tap water was allowed to flow through these beakers at the rate of 2 liters per hour. The zinc and steel specimens were degreased in acetone and a hole drilled near one end. These samples were then slipped on a glass rod which was suspended

[1]*Manuscript received April 19, 1956.*
Contribution from the Department of Chemistry, Ontario Research Foundation, 43 Queen's Park, Toronto 5, Ontario.

across the top of the beaker. The samples remained on open circuit during the test and the potentials were measured with a potentiometer using a saturated calomel electrode as a reference electrode. The duration of the experiment was 70 days. An analysis of the zinc, the steel, and the Toronto tap water is given in Tables I, II, and III.

TABLE I

ZINC ANALYSIS

Aluminum	0.002%
Iron	0.082%
Cadmium	0.001%
Lead	0.840%
Tin	Nil
Copper	Present

TABLE II

ANALYSIS OF STEEL

Carbon	0.12
Manganese	0.73
Phosphorus	0.015
Sulphur	0.021
Silica	0.073
Chromium	0.05
Zirconium	0.05

TABLE III

ANALYSIS OF TORONTO TAP WATER

pH	7.8
Total solids	171 p.p.m.
Oxygen	11.4 p.p.m.
Carbon dioxide	2.9 p.p.m.
Hardness $CaCO_3$	129 p.p.m.
Bicarbonate alkalinity	91.3 p.p.m.
Calcium (Ca)	38.6 p.p.m.
Magnesium (Mg)	7.8 p.p.m.
Silica	0.2 p.p.m.
Sulphate (SO_4)	23.6 p.p.m.
Chloride (Cl)	20.4 p.p.m.

TABLE IV

POTENTIAL, VOLTS NEGATIVE TO SATURATED CALOMEL ELECTRODE

	Zinc			Steel		
Temp., °C.	Max.	Min.	Max. − Min.	Max.	Min.	Max. − Min.
60	0.9763	0.4555	0.5208	0.7250	0.5200	0.2050
70	0.9728	0.4410	0.5318	0.7280	0.5125	0.2155
80	1.0060	0.4000	0.6060	0.6958	0.5105	0.1853
90	0.9780	0.4813	0.4967	0.6903	0.5295	0.1608
100	0.9730	0.7450	0.2280	0.6532	0.5872	0.0660

The maximum and minimum potentials of the zinc and steel are given in Table IV. The difference between the maximum and minimum values of the zinc and of the steel is also given in this table. The change of potential in the cathodic direction was not continuous, that is, some potentials were more anodic than the potentials of the previous day.

The times elapsing before the first reversal of potential occurred, the times elapsing before a constant reversal occurred, and the magnitude of the maximum voltage reversal which occurred between zinc and steel are given in Table V.

TABLE V

Temp., °C.	Number of days elapsing before first reversal of potential	Number of days elapsing before constant reversal	Maximum (E steel–E zinc)
60	34	34	0.1128
70	13	13	0.1012
80	24	43	0.1145
90	23	58	0.0544

CONCLUSIONS

1. It has been demonstrated that a reversal of potential can occur in Toronto tap water between zinc and steel of the compositions given in Tables I and II.
2. This reversal of potential occurred at 60°, 70°, 80°, and 90° C. in Toronto tap water.
3. No reversal of potential occurred at the boiling point.
4. The time elapsing before a constant reversal occurred was less at 70° C. than at 60°, 80°, or 90° C.
5. The potentials of both the zinc and the steel became more cathodic with time. However, the change of potential for the zinc was much greater than the change of potential for the steel.

REFERENCES

1. GILBERT, P. T. Sheet Metal Inds. 25: 2003. 1948.
2. GILBERT, P. T. Sheet Metal Inds. 25: 2243. 1948.
3. GILBERT, P. T. Sheet Metal Inds. 25: 2441. 1948.
4. GILBERT, P. T. Trans. Electrochem. Soc. 99: 16. 1952.
5. HOXENG, R. B. Corrosion, 6: 308. 1950.
6. HOXENG, R. B. and PRUTTON, C. F. Corrosion, 5: 330. 1949.
7. SCHIKORR, G. Trans. Electrochem. Soc. 76: 247. 1939.

RECOVERY OF POLYHYDRIC ALCOHOLS FROM YEAST FERMENTATIONS[1]

By J. M. Roxburgh, J. F. T. Spencer, and H. R. Sallans

ABSTRACT

Recovery of polyhydric alcohols from two typical osmophilic yeast fermentations, grown in submerged culture, is described. One strain produces glycerol and D-arabitol, the other erythritol and small amounts of mannitol. Both D-arabitol and erythritol crystallize readily from ethanolic solutions in the presence of glycerol and other soluble fermentation products. Losses are shown to be primarily dependent on the glycerol and water content of the solvent mixture. Glycerol can be recovered in fair yield by vacuum distillation of the mother liquors from D-arabitol recovery. Mannitol crystallized with the erythritol in the fermentation studied and was separated by fractional crystallization.

INTRODUCTION

In earlier papers from this laboratory (3, 4) the production of glycerol, D-arabitol, erythritol, and traces of mannitol by osmophilic yeasts has been reported. These products are obtained in varying yields and proportions depending on the strain of the organism used and the conditions of the fermentation (3). The recovery of products from fermentations using two strains, one producing mainly glycerol and D-arabitol and the other erythritol and traces of mannitol, is described in this paper.

The recovery of glycerol from clarified fermentation slops has been extensively studied and practiced on an industrial scale (1), but the production has always been uneconomic compared with other sources, and justifiable only as an emergency measure in periods of short supply. Fermentation slops from "steered" fermentations are high in salts and nonvolatile organic substances. If these are not removed the recovery of glycerol by distillation is low, and it is the cost of their removal that is largely responsible for the uneconomic position of fermentation glycerol. The osmophilic yeasts do not require the addition of large amounts of inorganic salts, and the organic product occurring with glycerol in the slops is predominately D-arabitol or erythritol, either of which is readily recoverable and of probable commercial value. Whether these factors are sufficiently advantageous to make fermentation glycerol economic or not is uncertain, depending primarily on the markets which might be developed for the by-product polyols.

EXPERIMENTAL

The recovery procedure developed for this type of fermentation is based on the relatively low solubility of D-arabitol, erythritol, and mannitol in cold mixtures of glycerol and one of the lower alcohols. The polyols are only slightly

[1]*Manuscript received April 27, 1956.*
Contribution from the National Research Council of Canada, Prairie Regional Laboratory, Saskatoon, Saskatchewan, Canada. Issued as Paper No. 222 on the Uses of Plant Products and as N.R.C. No. 4007.

soluble in glycerol alone, but alcohol must be added for the removal of gums (chiefly polysaccharides) and to reduce viscosity for filtration. Briefly, the procedure involves a rough primary clarification of the acidified fermentation broth, then the removal of most of the water by evaporation. Hot alcohol is added and the gums are filtered off. Decolorizing with activated charcoal in this step improves the quality of the eventual product. Erythritol and D-arabitol crystallize readily from the alcoholic solution on cooling and are recovered by filtration. After recovery of the alcohol by atmospheric distillation, glycerol is vacuum distilled from the residue in fair yield in the conventional manner.

Factors affecting the quality and quantity of recovered products from a given fermentation broth are primarily (*a*) time, temperature, and agitation during crystallization of the solid polyols; (*b*) the extent to which water is removed in the evaporation step; (*c*) amounts of charcoal and alcohol used in decolorizing and degumming; and (*d*) the proportion of glycerol to solid polyols in the original broth.

Recovery of D-*Arabitol*

Residual solubilities of D-arabitol in synthetic mixtures of ethanol, glycerol, and water are shown in Table I. Four or five grams of D-arabitol, accurately

TABLE I

RECOVERIES OF D-ARABITOL FROM SYNTHETIC MIXTURES AT 0°C.

Sample	Composition,* gm./100 ml.			D-Arabitol recovered, gm./100 ml.	Loss of D-arabitol	
	D-Arabitol	Glycerol	Water		gm./100 ml. solvent	gm./gm. glycerol
1	5.00	7.5	0	4.30	0.70	0.093
2	5.00	10.0	0	4.05	0.95	0.095
3	5.00	12.0	0	3.88	1.12	0.093
4	5.00	15.0	0	3.57	1.43	0.095
5	4.00	0	0	3.40	0.60	
						gm./gm. water
6	5.00	0	2.0	4.38	0.62	0.31
7	5.00	0	5.0	4.11	0.89	0.18
8	5.00	0	10.0	3.12	1.88	0.19
9	5.00	0	15.0	1.27	3.73	0.25
10	5.00	7.5	2	3.85	1.15	
11	5.00	7.5	5	3.55	1.45	
12	5.00	10.0	2	3.75	1.25	

**Balance ethanol.*

weighed, was dissolved in 100 ml. of solvent of the specified composition, heat being applied as required. The solution was cooled with stirring in an ice bath for 30 min., then stored overnight at 0° C. Crystals were recovered in a weighed sintered glass crucible, washed with cold ethanol, dried at 70° C., and weighed. Equilibrium solubilities were determined by continuing the crystallization for six days at 0° C., and also by dissolving D-arabitol in the cold sol-

vent overnight with stirring. These ranged from 0.4 gm. per 100 ml. for pure ethanol to 0.7 gm. per 100 ml. for ethanol containing 10 gm. per 100 ml. of glycerol. However, the values given in Table I are reproducible and represent roughly the practically obtainable recoveries. Larger batches were crystallized for one to two hours at 0° C. with seeding and strong agitation with comparable results.

In solvent mixtures containing glycerol, but no water, the solubility loss of D-arabitol is dependent on the amount of glycerol present but independent of its concentration in the ethanol, in the practical range of $7\frac{1}{2}\%$ to 15%. The presence of even small amounts of water increases the losses substantially. This means that the maximum recovery of D-arabitol from a given fermentation broth is fixed by the proportion of glycerol to D-arabitol produced, and can only be achieved by removal of substantially all the water from the concentrate before addition of the alcohol. The amount of alcohol used should be the minimum that will ensure complete solubility of the D-arabitol present, precipitate gums satisfactorily, and give sufficiently low viscosity for filtration. Solubilities of D-arabitol in these solvent mixtures at the boiling point range from 5% in ethanol alone to 30% in ethanol containing 5 gm. of water per 100 ml. and to about 10% in ethanol containing 10 gm. of glycerol per 100 ml.

TABLE II

RECOVERY OF D-ARABITOL FROM FERMENTATION BROTHS

Sample	Composition,§ gm.			D-Arabitol, gm.		
	D-Arabitol*	Glycerol*	Water†	Recovered	Predicted loss	Actual loss
13A	16.0	12.4	13.0	17.0	2.5	‡
13B	16.0	12.4	13.0	16.9	2.5	‡
14A	16.0	12.8	12.0	12.8	2.5	3.2
14B	16.0	12.8	12.0	15.6	2.5	0.4
14C	16.0	12.8	12.0	13.7	2.5	2.3
15¶	160	128	0	158	11.6	2.0
14D	16.0	12.8	0	14.6	1.2	1.4

**By column chromatography.*
†Estimated by evaporation under vacuum.
‡High recoveries because of acid treatment. See text.
§In 100 ml. (balance ethanol) except No. 15.
¶In 1 liter (balance ethanol).

Recoveries from samples of three fermentations are shown in Table II. The whole fermentation was centrifuged, reduced in volume by evaporation, aliquots heated with ethanol and 1% each of celite and decolorizing charcoal, then filtered hot. The filtrates were cooled rapidly to 0° C. with stirring for 30 min. and stored overnight at 0° C. before recovery of the crystals. The fermentation from which samples 13A and 13B were taken was acidified with hydrochloric acid to pH 2 and boiled for three minutes before the initial centrifugation. This appears to release more D-arabitol from the cells, and since

samples for analysis were taken before this treatment the recoveries are higher than expected. Reasonable agreement with results predicted from experiments with synthetic mixtures was obtained in the other cases.

Recovery of Glycerol

Recoverable glycerol was estimated by distillation under vacuum using an apparatus similar to that described by Schlachter and Hoffman (2). A recovery of 91% was obtained from a pure glycerol–water mixture, and 78% to 83% from the combined filtrates of samples 1 to 4 inclusive used in estimating D-arabitol recoveries from synthetic mixtures. This implies that the presence of arabitol reduces the recoverable glycerol by approximately 10%.

Filtrates from fermentation samples 14 and 15 were similarly combined and distilled with recoveries of 65% to 67% of the glycerol indicated by chromatographic analysis (4). Presence of impurities other than D-arabitol probably accounts for the low yield but no investigation was made into specific reasons for these losses.

Recovery of Erythritol

Erythritol, unlike D-arabitol, in the fermentations studied so far is associated with little or no glycerol under conditions producing a maximum yield (3), and will be recovered therefore from mixtures of essentially ethanol and water. Data are presented in Table III for the recovery of erythritol from synthetic

TABLE III

RECOVERIES OF ERYTHRITOL FROM SYNTHETIC MIXTURES AT 0°C.

Sample	Composition,* gm./100 ml.			Erythritol recovered, gm./100 ml.	Loss of erythritol	
	Erythritol	Glycerol	Water		gm./100 ml. solvent	gm./gm. glycerol
16	5.00	7.5	—	4.32	0.68	0.091
17	5.00	10.0	—	4.01	0.99	0.099
18	5.00	12.5	—	3.94	1.06	0.085
19	4.00	0	0	3.45	0.55	
						gm./gm. water
20	4.00	—	2	3.27	0.73	0.36
21	4.00	—	5	3.09	0.91	0.18
22	5.00	—	10	3.39	1.61	0.16
23	5.00	7.5	2	4.02	0.98	—
24	5.00	6.8	4.5	3.57	1.43	—
25	5.00	9.1	1.8	3.92	1.08	—
26	5.00	10.0	5	3.51	1.49	—
27	5.00	12.0	2	3.76	1.24	—
28	5.00	12.0	5	3.38	1.62	—

**Balance ethanol.*

mixtures of ethanol with glycerol as well as water for completeness. The solubility of erythritol in these solvent mixtures at the boiling point varies from 7½% in ethanol alone to over 15% in ethanol containing 10 gm. per 100 ml. of

either glycerol or water. Losses of erythritol shown here are very closely comparable to those found for D-arabitol (Table I).

The six fermentations for which recovery data are shown in Table IV con-

TABLE IV
RECOVERY OF ERYTHRITOL FROM FERMENTATION BROTHS

Sample	Composition			Erythritol recovered, gm.	Predicted loss, gm.	Actual loss, gm.
	Erythritol,* gm.	Water,† gm.	Total‡ volume, ml.			
29A	4.5	5.0	50	2.20	0.8	2.3
29B	4.5	5.0	50	2.21	0.8	2.3
30A	6.1	5.0	50	4.25	0.8	1.8
30B	6.1	5.0	50	4.17	0.8	1.9
31A	4.7	10.0	100	2.30	1.6	2.4
31B	4.7	5.0	50	2.87	0.8	1.8
31C	4.7	5.0	50	2.98	0.8	1.7
32A	7.6	5.0	50	5.9	0.8	1.7
32B	7.6	10.0	100	4.9	1.6	2.7
33A	5.6	5.0	50	3.8	0.8	1.8
33B	5.6	5.0	50	3.2	0.8	2.4
34A	5.5	5.0	50	4.1	0.8	1.4
34B	5.5	5.0	50	3.8	0.8	1.7

*By periodate oxidation.
†Estimated by evaporation under vacuum.
‡Made to these volumes with ethanol.

tained negligibly small amounts of polyhydroxy alcohols other than erythritol. Part of the loss in samples 29A and 29B was mechanical loss in the evaporation, but the uniformly low recoveries in the other samples indicates a real discrepancy between recoveries from synthetic mixtures and fermentation broths. While no other polyhydroxy compound was indicated on the paper chromatograms, not all of the loss could be accounted for on analysis of the mother liquors from the final crystallization. It may be inferred that some interference has occurred and that the initial analyses were high.

The fermentation from which samples 30A and 30B were taken was acidified and boiled before centrifugation, but no increase in yield was obtained. Apparently erythritol either is not present in the cells or cannot be released as D-arabitol can be by this treatment. Recovery of erythritol must be started very shortly after completion of the fermentation. Even at 0° C. losses are apparent after 10 to 12 hr. storage of the whole fermentation or clarified broth. Fermentations containing D-arabitol may be stored for several days under these conditions with little or no loss.

Recovery of Mannitol

The particular fermentations grown specifically for erythritol as described in the previous section were found to contain a small amount of mannitol. In the recovery of erythritol as outlined most of the mannitol crystallizes with the main product, the rest remains in the glycerol–ethanol solution. Because of the small amounts involved no quantitative estimate of the distribution was made.

Erythritol from 6 liters of clarified fermentation broth was recovered as outlined previously, yielding 200 gm. (m.p. 112° C.–114° C.). This was recrystallized from boiling ethanol (3 liters) yielding 160 gm. (m.p. 119° C.). By concentrating the mother liquors from this recrystallization in several steps, cooling to 0° C. after each reduction in volume, a fraction, 5.3 gm. (m.p. 160° C.–161° C.), was obtained, which on recrystallization from 80% ethanol yielded 4.0 gm. (m.p. 167° C.–169° C.) of essentially pure mannitol. The identity was confirmed by infrared spectrum, paper chromatography, and production of the acetate.

While this yield of less than 0.1% is too low to be of real value, the indication is that some strains may be found which will produce more substantial yields of mannitol and that it can be recovered by much the same process as has been used for D-arabitol and erythritol.

REFERENCES

1. GODFREY, T. M. Glycerol. Am. Chem. Soc. Monograph No. 117. Reinhold Publishing Corporation, New York. 1953. p. 76.
2. SCHLACHTER, F. A. and HOFFMAN, H. D. J. Am. Oil Chemists' Soc. 31: 174. 1954.
3. SPENCER, J. F. T., ROXBURGH, J. M., and SALLANS, H. R. In preparation.
4. SPENCER, J. F. T. and SALLANS, H. R. Can. J. Microbiol. 2: 72. 1956.

THE MEASUREMENT OF THE THERMAL INSULATION OF TEXTILES IN WIND[1]

By C. D. Niven

ABSTRACT

Measurement of the thermal insulation of two fabrics was made on a hot plate in a wind parallel to the plate and in a wind approaching the plate at an angle of 45°; also on a cylinder in an air stream at right angles to its axis. The plate test in the parallel wind gave the highest insulation value.

The work described below was undertaken to find out something about the conditions under which samples of textile materials should be measured in order to get a correct estimate of their thermal insulation in wind. Up to the present time in this laboratory samples to be tested in wind have been tested with the wind striking the sample at an angle of 45°. Mr. R. J. Templin of the Canadian National Aeronautical Establishment, who designed the fan for the assembly described below, suggested to the writer that it might make very little difference if the wind were brought across the sample parallel to the surface instead of at an angle. To decide whether or not this was the case was one of the main objectives of the present investigation, because a parallel wind causes little turbulence and simplifies things considerably.

On the other hand there was some doubt as to whether the hot plate was a suitable piece of apparatus for thermal conductivity measurements in wind; it was felt that a cylinder might be better because it presented a piece of surface at every angle to the direction of wind flow, and thus gave a more realistic representation of a garment being worn.

To answer these questions required the construction of a cylinder to compare with the hot plate already in use (2) and also of a wind tunnel which could, by means of a duct system, blow air at 45° or 0° to the surface of the plate and also across the cylinder with axis at right angles to the direction of the wind.

APPARATUS AND METHODS

At the start of the work much time was wasted in trying to get a good agreement between results in still air on the hot plate and those on a cylinder which had been designed and built by a previous experimenter in these laboratories. This cylinder consisted of a cylindrical brass tube around a core of wood and is mentioned here because the failure of this apparatus emphasized the great care which must be taken to guard against end heat-losses. This apparatus had two pieces of guard cylinder which could prevent end losses at the surface of the cylinder but could do little to prevent end loss through the wooden core between the circumference and the axis. It was only after the

[1]*Manuscript received March 8, 1956.*
Contribution from the Division of Applied Physics, National Research Council, Ottawa, Canada. Issued as N.R.C. No. 4013.

hot plate had been checked with a hot plate which the writer had had constructed some years ago for measuring the thermal conductivity of wall board (4), and which is now in the Building Research Division of these laboratories, that it was definitely decided that the error lay in the cylinder and that it would have to be completely redesigned.

Fig. 1 shows the new design. At each end aluminum disks E were separated by rings of bakelite F and held in place by a circular spring K, known as a

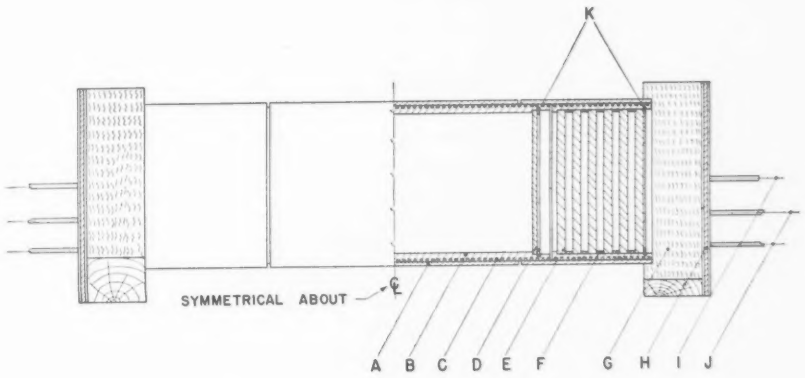

FIG. 1. Drawing of heated cylinder.

"truarc ring". These disks simultaneously insulated the ends by reflection of heat and conducted heat into the axis from the surface of the cylinder. One and one half inches of onazote or expanded ebonite insulation G covered the ends; this was supported by pieces of wood H. The length of guard cylinder at each end was increased from 2 in. to 4 in. and the length of the measured portion of the cylinder A was reduced from 10 in. to $7\frac{1}{2}$ in. The heater element C consisted of No. 19 B and S manganin wire wound on a bakelite cylinder B. The end of the manganin wire was taken to a three-arm bakelite support D and attached to one of the main heater leads I. The guard ends were also wound with the No. 19 B and S manganin wire; the ends of the wire were attached to the leads J.

The wind tunnel is shown diagrammatically in Fig. 2(A) and (B). It had two branches arranged so that the wind could be directed from the fan into either of these by means of a swing door S. The end portion of each of these branches could be disconnected at x or y, thus permitting the use of an alternative end portion. In this way one fan and motor assembly could be used to give four different kinds of air flow. The upper branch of the wind tunnel was used for measurements on the hot plate P. Fig. 2(A) shows the hot plate tilted so that wind at 45° could strike the sample while Fig. 2(B) shows the plate in position for a parallel wind. By means of a cardboard "honeycomb" placed between x and the plate, and by means of some vertical baffles behind x, i.e.

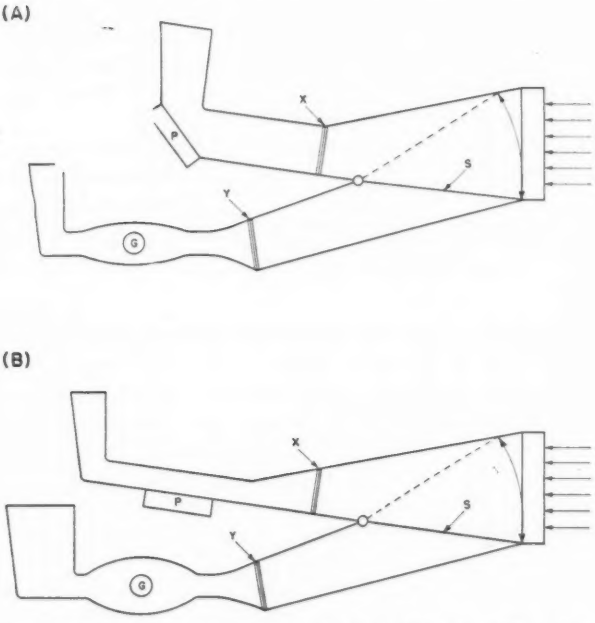

FIG. 2. Diagram showing the arrangement of the ducts giving different air streams.

"up wind", a very even wind could be obtained over the plate using the parallel flow. A honeycomb was also used in the duct for the 45° wind but a perfectly even distribution of velocity from front to back could not be obtained. The lower branch of the wind tunnel was used for measurements on the cylinder G. No honeycomb or baffles were used in this branch. The two end ducts were somewhat similar except that one measured 11 in. and the other 15 in. in depth at the place where the cylinder was located during a test. Since the cylinder was 5 in. in diameter, this implied 3 in. and 5 in. respectively of free air passage including thickness of sample above and below the cylinder.

The "cold side" thermocouple for these thermal conductivity tests in wind was always more than 1.5 in. away from the surface of the sample, because it was necessary to include the insulation of the ambient air in the results. Care was taken to avoid looseness in sewing the sample around the cylinder. On the plate, air pockets were not so likely to occur in still air or in low velocity winds. In high velocity winds parallel to the plate, the sample was lifted, however, and entirely wrong results could thus be obtained. To obviate this a $\frac{1}{2}$ in. wire mesh grid had to be placed over the sample and fixed down at the corners for high wind velocity tests.

The results are given in clo units (1). The values can be converted into conductance values in "B.t.u. per hour per sq. ft. per ° F." units by means of the equation $CR = 1.14$ where C is thermal conductance and R thermal

resistance in clo units. The wind velocities were measured on a vane anemometer. For the plate tests this was placed right on the sample after the thermal conductivity measurement had been completed, while for the cylinder tests it was held 4 in. below the mouth of the duct. Special provision would have been necessary to get the instrument into the duct near the cylinder but in any case an average velocity for the wind flow around the cylinder was considered an adequate estimate. The velocity for the cylinder measurements was calculated by multiplying the anemometer value by the ratio of the area of the duct's cross section 4 in. below the mouth to the area of the free air passage in the duct at the cylinder.

Two pieces of overcoating were used as samples for the tests; these, for purpose of reference, will be designated as Sample A and Sample B. Their thicknesses were measured in a standard thickness measuring apparatus (11.31 oz. over a 3 in. diameter circular disk), the air permeability was measured by the Schiefer and Boyland (5) apparatus using a differential pressure of $\frac{1}{2}$ in. water pressure, and the straight surface to surface thermal conductivity without environmental air was measured on the hot plate using a thin, light, blackened aluminum plate to cover the sample. These three measurements give a fair description of the test samples and are tabulated in Table I.

TABLE I

	Sample A	Sample B
Thickness of sample in thousandths of an inch	173	127
Air permeability in cu. ft./sq. ft./min.	52	37
Thermal resistance in clo units	0.83	0.63

RESULTS

The results of the thermal insulation tests in winds are plotted in Figs. 3 and 4. The general shape of the curves agrees well with that obtained by Miss I. Moote (3) for a pile fabric sample measured in a 45° wind. The parallel plate method gave results which were higher by about 0.13 clo than the cylinder method. The results on the cylinder using the ducts of different depths were so alike that only one curve has been drawn through the two sets of points. This would suggest that the method of calculating the wind velocity at the cylinder was satisfactory. The 45° wind results at low speed differed only slightly from the results with the parallel wind but at high wind velocities the 45° wind results were more like those on the cylinder.

Altogether it appeared from the above results that varying the method of testing in winds caused rather a small but nonetheless quite noticeable difference in insulation value. At 20 m.p.h. the graphs show that a reduction in clo value, compared to the value in still air, ranged from 43% to 50% for the A sample and from 44% to 55% for the B sample depending on how the wind was applied. Since the human body is an exceedingly sensitive "heat loss detector", such differences in percentage would almost certainly be noticed by

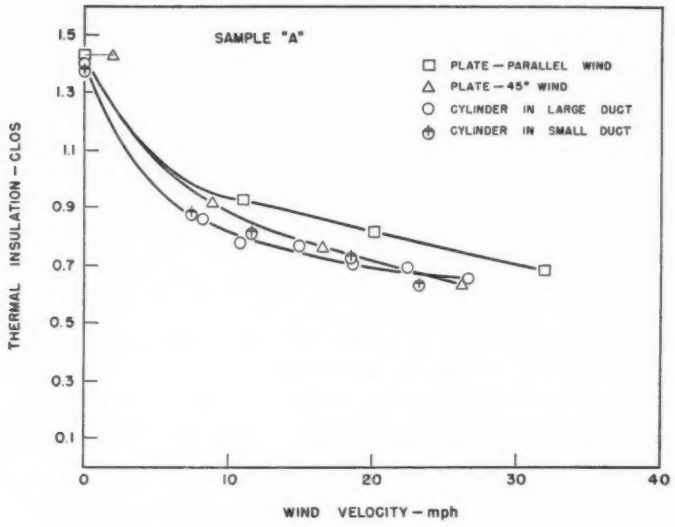

FIG. 3. Insulation vs. wind velocity curves for Sample A.

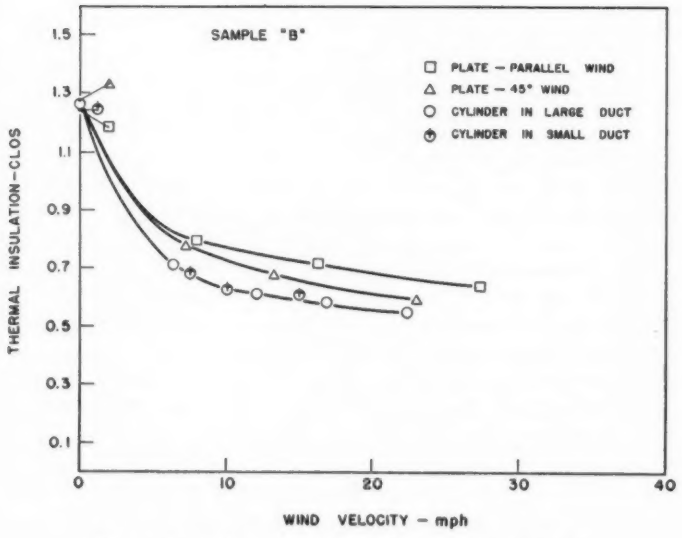

FIG. 4. Insulation vs. wind velocity curves for Sample B.

the wearer of a garment and might well account for an instinctive distrust of Mr. Templin's thesis. Unpublished results indicate furthermore that when there is an air space under the fabric—and this is how clothing is often worn—the parallel wind gives quite markedly higher clo values than the 45° wind; from a standardizing point of view this opens up the whole question as to whether measurements in wind, on overcoatings lying next to the hot plate or cylinder, give a fair assessment of the sample's worth at all, and complicates the whole problem.

However, the present work is concerned merely with the material lying next to the heated body and under these circumstances it is fair to conclude that the plate method with a parallel wind will yield higher results than those obtained on a cylinder, or on a plate with the wind approaching at 45°.

ACKNOWLEDGMENT

The writer wishes to make grateful acknowledgment to Miss M. T. Mitton of the National Research Council's Textiles Laboratory for measuring the air permeability of the samples.

REFERENCES

1. Gagge, A. P., Burton, A. C., and Bazett, H. C. Science, 94: 428. 1941.
2. Larose, P. Can. J. Research, A, 25: 169. 1947.
3. Moote, I. Textile Research J. 25: 832. 1955.
4. Niven, C. D. Can. J. Research, 7: 115. 1932.
5. Schiefer, H. F. and Boyland, P. M. J. Research Natl. Bur. Standards, 28: 637. 1942.

THE EXPLOSIVE CHARACTERISTICS OF ELEVATOR DUSTS[1]

By J. M. Roxburgh

ABSTRACT

An investigation of the effect of several variables on the lower explosive limit of dusts collected in terminal elevators indicates that particle size, and in particular the concentration of material finer than 150 mesh, has the most effect on the explosion hazard engendered by this material. The results suggest that the most effective method of controlling the hazard is efficient control of dust at all stages of grain handling coupled with separation and safe disposal of the finer fraction of the material discharged by the dust control cyclones.

INTRODUCTION

This investigation was instigated as a result of a severe explosion which occurred in a Port Arthur terminal elevator on September 24, 1952. A Dust Problem Committee was formed by the interested parties, and this research represents one aspect of the extensive program instituted under their auspices in an attempt to determine the causes of such explosions and thus to enable elevator owners and operators to avoid future disasters.

An extensive literature on dust explosion research exists, much of it in relation to coal mine explosions. The subject has been effectively reviewed recently by Morse (6) for this same Committee. Little specific information has been published on elevator dusts, but their general characteristics as explosive materials can be surmised by analogy with similar materials which have been studied (1, 3). A lower explosive limit in air of 70 to 100 mgm. per liter would be expected (for dust passing 200 mesh) with an ignition temperature in the region of 300° C.

This investigation was concerned solely with those characteristics of the dust itself which could be conveniently controlled in the terminal elevator in such a way as to reduce the explosion hazard. The lower explosive limits of a large number of samples were therefore determined, and the effect of several variables on this explosive limit was investigated.

EXPERIMENTAL

Since the purpose of this investigation was primarily to suggest practical methods of reducing the explosion hazards in terminal elevators, experiments were made to determine the range of the significant variables likely to be encountered in practice and their effect assessed primarily within this range.

Two explosion chambers were used; both gave consistent and reproducible values for lower explosive limits, but one gave values very much higher than the other. With these chambers the effects of moisture, ash, particle size, and source of dust were tested separately. To conclude the study, a large number

[1]*Manuscript received May 9, 1956.*
Contribution from the National Research Council of Canada, Prairie Regional Laboratory, Saskatoon, Saskatchewan. Issued as Paper No. 223 on the Uses of Plant Products and as N.R.C. No. 4014.

of samples from the discharge of the dust control cyclone of a modern terminal elevator were tested in both chambers to establish the validity of tentative conclusions drawn from the results of the preliminary experiments.

Explosion Chambers

Chamber "A", used in early experiments and again in the final evaluation, was a "Lucite" box 3 in. square and 6 in. high fitted with a loose plastic lid. A 25 watt heater wound from 30 gauge nichrome wire and operated at 20 volts was used to ignite the dust. Samples were held in a plastic weighing boat and dispersed by a metered blast of air. A filter paper diaphragm in the lid retained dust but allowed air to escape without dislodging the lid. An explosion was recorded for a specific test if a flame was observed to travel substantially to all parts of the chamber or if the lid was lifted completely.

The second chamber (chamber "B") followed the general pattern described by Hartmann (5). An aluminum cylinder 3 in. in diameter and 14 in. high was fitted with tungsten electrodes to provide a spark gap adjustable as to both length and position in the cylinder. This cylinder fitted snugly over a dished bottom in which the sample was placed. A metered blast of air dispersed the sample, as before, and was followed after a specific time delay by the igniting spark from a 5000 v. transformer. If the loose lid lifted, or if the paper diaphragm in it scorched indicating that a flame had reached the top, an explosion was recorded. Length and position of the spark gap were adjusted to give minimum values for the lower explosive limit with each type of dust tested.

These chambers were calibrated using vacuum-dried corn starch and a representative pooled sample of elevator dust which passed a 150 mesh standard screen (Table I). Values for the minimum explosive concentration of dry

TABLE I

EFFECT OF EXPLOSION CHAMBER DESIGN AND MOISTURE ON THE DETERMINATION OF LOWER EXPLOSIVE LIMITS

Sample	Moisture, %	Minimum explosive limit, gm./liter	
		Chamber "A"	Chamber "B"
Corn starch	8.0	0.25	0.32
	0	0.035	0.045
Pooled 150 mesh elevator dust	12.5	1.40	0.34
	5.7	1.20	0.34
	0	0.50	0.10

corn starch of 35 and 45 mgm. per liter of air were obtained in chamber "A" and "B", respectively, in good agreement with reported values of 40 mgm. per liter (2) and 45 mgm. per liter (3). Elevator dust showed no such agreement. In chamber "A", which was the one first tested, the lowest value obtainable was 500 mgm. per liter with vacuum-dried dust, rising to 1.4 gm. per liter at higher moisture contents. This dust would be expected to have a true lower

explosive limit in the region of 70 to 100 mgm. per liter by analogy with similar reported dusts (1). As a result, chamber "B" was constructed and tested, and gave the expected value of 100 mgm. per liter with the dried dust.

Effects of Moisture and Humidity

Samples of elevator dusts from various sources were equilibrated at known humidities, and moisture determinations made by drying under vacuum at 105° C. All samples are represented by the single curve shown in Fig. 1 when moisture content is calculated on the basis of ash free sample weight.

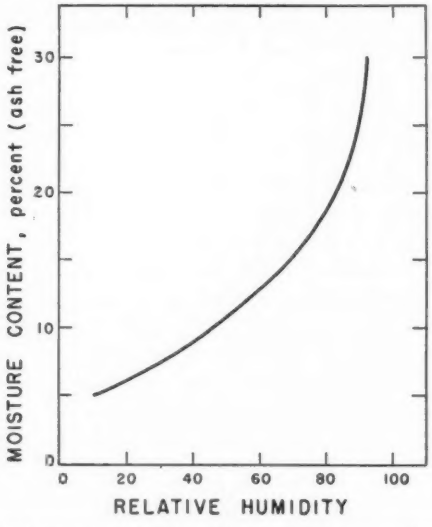

FIG. 1. The relation between relative humidity and moisture content for elevator dusts.

Neither moisture content in the normal "as received" range of 5% to 10% nor relative humidity of the air in the test chamber in the equivalent range of 10% to 50% had any measurable effect on the minimum explosive limit of the dust samples. Explosive limits did decrease markedly as moisture content was lowered below 5% (Table I) but no samples have been received with this little moisture in them.

Effect of Ash

Elevator dusts consist normally of fragments of straw, chaff, and epidermis of grains being handled. With these are associated variable amounts of material of inorganic nature, such as soil and clay particles. Ash content, as determined in a muffle furnace at 900° C., varies from a low of about 8–10% for coarse samples up to 65% for the finest sieve fractions.

Table II indicates that this ash fraction may be considered to be a simple diluent, since consistent results were obtained by calculating minimum explosive limits on the basis of ash free samples.

TABLE II

EFFECT OF ASH CONTENT ON THE LOWER EXPLOSIVE LIMIT OF GRAIN DUSTS PASSING 150 MESH SCREEN

Sample	Ash content, %	Moisture content, %	Explosive limit, gm./liter	
			Whole sample	Ash free sample
1	26.0	4.50	0.70	0.52
2	36.1	7.64	1.00	0.63
3	26.0	5.12	0.75	0.55
4	33.5	3.60	1.0	0.66
5	15.6	4.25	0.70	0.59
6	41.7	0	0.45	0.27
7	23.1	0	0.35	0.25

Effect of Size and Size Distribution

Early experiments indicated the expected relation between decreasing particle size and decreasing explosive limit. For this reason the evaluation of the effect of moisture and ash was determined on fine fractions screened from the generally coarser samples received. Fig. 2 shows the relation between average particle size and minimum explosive limit for closely screened samples of elevator dusts using both explosion chambers. Curve 1 shows a minimum at 200 mesh which disappears when the correction for ash content is applied (Curve 2). Curve 3, using chamber "B" and correcting for ash, is in good

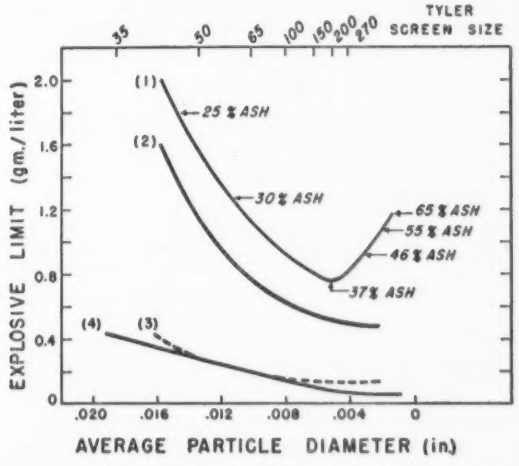

FIG. 2. The relation between average particle size and minimum explosive concentration in air for:
(1) Elevator dusts tested in chamber "A".
(2) Curve 1 calculated on the basis of ash free samples.
(3) Elevator dusts tested in chamber "B" and calculated as ash free samples.
(4) Cellulose acetate resin dusts taken from Hartmann (3).

agreement with Curve 4 for cellulose acetate resin powders taken from Hartmann's work (3).

These curves represent average values from a large number of experiments. Because of the nature of the particles involved, screening is a poor method of classifying elevator dusts. Not only are the particles far from spherical, but the action of screening itself breaks them up and produces more fine material. However, reasonably consistent screen analyses can be obtained by standardizing the technique, and quite reproducible explosive limits are obtained for the resultant fractions.

Effect of the Source of Dust

Dusts were collected from several elevators during the handling of different grains. As has been indicated previously, the moisture–humidity relation for all these dusts was the same. The fractions passing 150 mesh from all these samples were tested for explosive limit with no significant variation in the results which could be attributed to source.

When the samples were tested "as received" without removal of the coarser material, a different picture emerged. Only two classes of samples had minimum explosive limits (chamber "B") less than 1.0 gm. per liter. These were the very fine dusts from high ledges and beams and the discharge from dust control cyclones. All other samples had very much lower content of fine fragments and were much less explosive. The concluding studies were therefore made on a series of samples collected daily from the main dust control cyclone in a terminal elevator with modern dust control equipment.

Experiments on Samples from Dust Control Cyclone Discharge

The range of moisture and fine dust content of all samples tested is shown in Table III. The minimum explosive limit for each sample was obtained in

TABLE III

MOISTURE AND FINES CONTENT OF 25 DAILY SAMPLES FROM DUST CONTROL CYCLONE DISCHARGE

	Maximum	Minimum	Mean	Standard deviation
Moisture, %	10.22	6.56	8.09	±1.10
Passing 150 mesh screen, %	29.2	10.4	18.4	±4.4

both test chambers. In Fig. 3 the regressions determined by the method of least squares for both sets of results are shown. Correlation coefficients of −0.85 and −0.65 were obtained for chamber "A" and "B" results respectively, indicating a high degree of correlation. Regression coefficients for the two lines are −0.080 and −0.020 with mean values of 2.20 and 0.543 gm. per liter, showing almost exactly a four to one relation between values obtained with the two chambers.

The values for the explosive limits used in constructing this plot were not corrected for ash, since no significant increase in correlation was obtained by

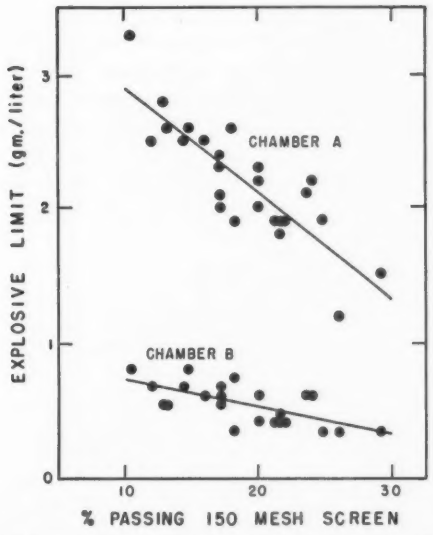

FIG. 3. The effect of the content of fines (passing 150 mesh screen) on the minimum explosive limit of elevator dusts. Not corrected for ash. Daily samples from dust collector cyclone discharge.

including the correction. Similarly no improvement was obtained by including moisture in the calculation.

While it might be concluded that the minimum explosive limit is inversely related to the content of material passing 150 mesh, Table IV showing the

TABLE IV

SELECTED SAMPLES FROM DUST COLLECTOR DISCHARGE

Sample	Moisture, %	Minimum explosive limit, gm./liter
		Chamber "B"
May 18th containing		
(*a*) 18.0% −150 mesh	7.2	0.74
	0.0	0.41
(*b*) −150 mesh removed	7.2	1.5
	0.0	1.0
(*c*) −100 mesh removed	7.2	>2.0
June 5th containing		
(*a*) 18.2% −150 mesh	5.6	0.34
	0.0	0.21
(*b*) −150 mesh removed	5.6	0.75
	0.0	0.50
(*c*) −100 mesh removed	5.6	1.9

results of more complete tests on two selected samples with almost identical fines content shows that the explosive limit of a specific sample cannot be predicted with any useful degree of accuracy on this basis. On the other hand, both samples approximately double their minimum explosive limit on removal of the material passing 150 mesh, and show a further increase at least as great on removal of 100 mesh and finer dust. Thus, although the explosive limit cannot be predicted from screen analysis, the percentage increase in explosive limit obtained by removal of a specified screen fraction can be estimated roughly.

DISCUSSION

The consistent difference between explosive limits determined in the two test chambers indicates the importance of test conditions in investigations of this kind. In this respect it is rather interesting to note that chamber "A" gives a value for the lower explosive limit of corn starch that is lower than values reported in the literature and yet gives values at least four times too high for elevator dusts.

Despite the quantitative difference in values for explosive limits obtained in the two chambers, the relative values can be relied on. That is to say, the ratio between explosive limits of two samples will be roughly the same regardless of the test conditions used. It is probable from comparison with values for other materials reported in the literature that chamber "B" gives values approaching the true explosive limit for these dusts, but tests on a larger scale would be required to confirm this.

The reason for the discrepancy between results in the two chambers is not clear but probably may be attributed to the nature of the dispersion obtained, the less suitable shape of the "Lucite" chamber, and the method of ignition.

The negligible effect of moisture on the explosive limit seems at first rather surprising, but Hartmann (4) recently has reported a similar result with coal dusts. Under these test conditions, using a high-energy high-temperature source of ignition, moisture between 5% and 10% of the dry weight appears to act purely as an inert diluent. Below 5% it is probable that better dispersion is obtained, resulting in lower explosive limits, and above about 15% moisture ignition is suppressed. No investigation of the minimum energy for ignition or the pressures developed by the explosion was made. These would be expected to be affected by moisture content.

The experiments on samples from the dust collector cyclone discharge indicate that statistically speaking the explosive tendencies of elevator dusts are related directly to the content of fine material, which has been arbitrarily defined as material finer than 150 mesh. While individual samples may vary widely from the average in their explosive limit, the removal of this fine material has the same relative effect on all samples. Hartmann (4) has reported that coal dusts coarser than the 150 to 200 mesh fraction cannot be exploded in air by an electric spark. Elevator dusts with this and finer fractions removed can still be exploded, but only at concentrations at least twice that required with the original sample. This behavior, combined with the more

rapid settling in air of the coarse residue, means that the explosion hazard can be very substantially reduced by the removal of this fine material.

The implications of these results on elevator practice are apparent. In the one elevator examined carefully in the course of this investigation the only substantial amounts of very fine dust were found in the dust collector discharge and on high beams and ledges not reached in the routine cleaning procedures. Since more of this fine dust is produced each time grain is handled, efficient dust control equipment is required in all terminal elevator operations. Housekeeping methods designed to keep static dust to an absolute minimum are required to prevent the spread of minor explosions to major proportions. When these precautions have been effected, substantially all of the highly explosive fine dust will appear at the discharge of the dust control cyclones, where it should be separated and disposed of safely.

REFERENCES

1. EDWARDS, P. W. and HARRISON, R. W. Ind. Eng. Chem. Anal. Ed. 2: 344. 1930.
2. HARTMANN, I. *In* Industrial hygiene and toxicology. *Edited by* F. A. Patty. Interscience Publishers, Inc., New York. 1948.
3. HARTMANN, I. Ind. Eng. Chem. 40: 752. 1948.
4. HARTMANN, I. J. Am. Soc. Safety Engrs. 1: 9. 1956.
5. HARTMANN, I. and NAGY, J. U.S. Bur. Mines Rept. Invest. 3751. 1944.
6. MORSE, A. R. Natl. Research Council Can. Bull. No. 3614. 1955.

THE DESIGN OF PRESSURE VESSELS SUBJECTED TO THERMAL STRESS

I. GENERAL THEORY FOR MONOBLOCK VESSELS[1]

By E. Whalley

ABSTRACT

The effect of combined thermal and pressure stresses on the elastic and the plastic behavior of spherical and cylindrical pressure vessels is considered for any arbitrary temperature distribution and for both brittle and ductile materials. A brittle material is assumed to fracture when the maximum principal stress reaches the fracture stress. A ductile material is assumed to yield at constant maximum shear stress. The bursting pressure of a brittle vessel, and the yield and shakedown pressures of a ductile vessel can be either increased or decreased by the presence of thermal stresses. The ultimate pressure of a ductile vessel is not affected. The effect of these considerations on the design of pressure vessels is discussed in general terms.

NOMENCLATURE

The following nomenclature is used in this paper:

a = inside radius.
b = outside radius.
C_1, C_2, C_3 = constants of integration.
E = Young's modulus.
$k = b/a$.
p = pressure.
p_i = inside pressure.
p_o = outside pressure.
$\Delta p = p_i - p_o$.
Δp_s = shakedown pressure difference.
Δp_y = yield pressure difference.
Δp_u = ultimate pressure difference.
r = radius.
r_y = radius at which yield first occurs.
r_s = radius at which shakedown first occurs.
T = temperature at radius r.
T_i = temperature at inside wall.
T_o = temperature at outside wall.
T_s = temperature at radius r_s.
T_y = temperature at radius r_y.
T_ρ = temperature at radius ρ.
T_{ρ_1} = temperature at radius ρ_1.
T_{ρ_2} = temperature at radius ρ_2.
u = radial displacement at radius r.
α = coefficient of thermal expansion.

[1]*Manuscript received October 7, 1955.*
Contribution from the Division of Applied Chemistry, National Research Council of Canada, Ottawa. Issued as N.R.C. No. 4006.

ν = Poisson's ratio.
ρ, ρ_1, ρ_2 = radius of plastic–elastic boundaries.
σ_r = radial stress.
σ_t = tangential stress.
σ_u = fracture stress.
σ_y = tensile yield stress.

1. INTRODUCTION

The design of vessels to withstand high pressures is usually based on either the bursting pressure or the pressure required to cause elastic failure at the inside surface. It has been known for many years that the presence of thermal gradients causes thermal stresses and that these may reach very high values, which may easily be comparable to or greater than the pressure stresses. However, the effect of thermal stresses on the design of pressure vessels has been largely ignored. Both the 1953 ASME Boiler and Unfired Pressure Vessel Code and the British Standard Code 1500 for Fusion-Welded Pressure Vessels say that thermal stresses should be taken account of, but give no details. However, the British Code states that they can become important in vessels with thick walls, with poor conductivity, or with high heat transfer.

In recent years there has been a trend towards using very high heat transfer rates, for example, using liquid metals (10). Higher pressures are being used in both industrial practice and the laboratory and frequently both high pressures and high thermal gradients are used simultaneously. It has become important, therefore, to take account of the presence of thermal stresses in the design of pressure vessels. The behavior of spherical and cylindrical vessels stressed by pressure and temperature is well known if the stresses are everywhere below the elastic limit (12). However, it is not always either practicable or desirable to ensure that the stresses are maintained always below the elastic limit. Indeed the residual stresses left after overstraining a pressure vessel are frequently beneficial and are consciously sought in the process known as autofrettage.

Knowledge is required therefore of the behavior of a vessel subjected to both pressure and temperature stresses when the elastic limit has been exceeded. We must take account not only of the stresses due to steady-state heat flow, but also of those due to the transient temperature field obtained during the warming-up or the cooling-down period. It will frequently happen that there is a maximum allowable rate of heating and cooling consistent with a reasonable life of the equipment. Vessels are frequently subjected to thermal stresses and to either internal or external pressures, or to both simultaneously, for example in thermocouple wells, "cold fingers", and heat exchangers. Thick-walled spherical vessels are sometimes used, particularly in the laboratory, for example in work on explosions. The theory has been developed, therefore, for both spherical and cylindrical vessels subjected to internal and external pressures and to an arbitrary radially symmetrical temperature field. In later papers the more important particular temperature fields will be discussed.

In Section 2 the assumptions of the present treatment will be described. The rest of this section will be devoted to a brief review of previous theoretical investigations of the effect of thermal stress on the design of pressure vessels. Papers on the calculation of thermal stresses in elastic vessels under various temperature distributions, but without considerations of design, have been excluded from this survey. No experimental work appears to have been reported.

Luster (7) considered the effect of combined pressure and thermal stresses on the design of tubular pressure vessels and piping. He calculated the elastic stresses in the walls for internal pressure and steady-state heat transfer. He showed that for a given internal pressure and heat transfer rate there was a value of the ratio of the radii of the outside and inside walls which gave a minimum value of the maximum principal stress at the bore. He proposed that the wall thickness of vessels and piping to be used under creep conditions be determined by the formulae he derived. It is now known that creep conditions require special consideration and that these formulae are not applicable. However, the formulae are still valid for the tangential stresses in an elastic vessel.

Kern (5) has discussed the stresses in hollow cylinders and spheres with internal pressure and steady heat dissipation, particularly in connection with the design of high pressure (100 atm.) lamps. Spherical vessels were treated in most detail. He was concerned with internal pressure combined with heat transfer to the outside and under these conditions the pressure and thermal stresses oppose one another at the inside surface. He proposed the design criterion that the maximum shear stress at the inside wall should be zero. It might be remarked that Equation (17) of Kern's paper is incorrect; Poisson's ratio should be a multiplier for each term within the square brackets. Fig. 3 of Kern's paper is drawn from this equation and is also incorrect; at both the inside and the outside radius the tangential and longitudinal thermal stresses should be equal. A further criticism which may be made of this paper is that the author was concerned primarily with the design of vessels made of quartz, which is brittle. The maximum principal stress criterion would seem more appropriate than the maximum shear stress.

Lenngren (6) considered the stresses in gun barrels with a temperature distribution

$$T = Ar^n + B,$$

where A, n, and B are constants. It was shown that the assumptions of elasticity were not justified, and a numerical solution for the plastic–elastic problem was suggested.

2. THE PRESENT TREATMENT

The following assumptions are made:

(i) A brittle material is perfectly elastic up to the ultimate strength. It then fractures, without appreciable yielding, according to the maximum principal stress theory.

(ii) A ductile material is perfectly elastic up to the yield point. It then yields at constant maximum shear stress, i.e., according to the Tresca theory. No strain hardening occurs.

(iii) The temperature is everywhere low enough that creep is inappreciable.

(iv) The effect of temperature and stress on the elastic moduli, the yield point, and the coefficient of thermal expansion is negligible.

(v) The Bauschinger effect (reduction in yield point due to previous plastic flow in the reverse direction) does not occur in a pressure vessel.

(vi) There are no important stress raisers present.

(vii) The strains are everywhere small compared with the dimensions of the vessel.

We will now discuss how closely a real vessel made of real material might be expected to conform to these assumptions. Assumption (i) appears to be a fairly good approximation to the behavior of a brittle material (9) and agrees quite well with the measurements of Cook and Robertson (2) on the bursting pressure of cast iron cylinders. Assumption (ii) agrees quite well with the behavior of mild steel and of some alloy steels which have a more or less long flat part of the stress–strain curve. Cook (1) and Steele and Young (11) found that the Tresca criterion was adequate to explain the behavior of mild steel vessels though Morrison (8) favored the von Mises theory for low alloy steels. However, the maximum difference between the Tresca and the von Mises criteria is only about 15%, and the use of the Tresca criterion very much simplifies the mathematical treatment of the cylindrical vessel because the controlling stresses are independent of the longitudinal stress. Materials which begin to strain-harden as soon as the yield point is passed will depart from the present theory by an amount dependent on the rate of strain-hardening. Assumption (iii) needs no comment. Assumption (iv) is justifiable in that the temperature and pressure coefficients of the quantities listed are not large. Assumption (v) is based on some experimental evidence (3, 13) which indicates, though not compellingly, that the Bauschinger effect is not so important in pressure vessels as in tensile bars. Assumption (vi) will be discussed in Section 5. Assumption (vii) will be very nearly true in vessels with a radius ratio of less than about five to six and in which the plastic deformation is contained, i.e. which is still partly elastic.

Three important design criteria have been suggested and used for pressure vessels:

(i) The yield load.

(ii) The shakedown load, i.e., that load which if cycled just does not cause repeated plastic deformation.

(iii) The bursting load.

The effect of temperature on each of these three criteria will be discussed in the next two sections. The design of pressure vessels is discussed in Section 5.

3. SPHERICAL VESSELS

1. General Considerations

We consider a spherical hollow vessel of inside radius a and outside radius b. It is subjected to an internal pressure p_i acting uniformly on the inside surface

and to an external pressure p_o acting uniformly on the outside surface. A radially symmetrical temperature distribution exists within the walls and the temperature at any radius r is T. The temperature of the inside wall is T_i and of the outside wall T_o. Also

$$\Delta p = p_i - p_o.$$

The principal stresses are a radial stress σ_r and two equal tangential stresses σ_t.

In the elastic parts of the vessel the stresses and strains are determined from Hooke's law and the equation of equilibrium. The resulting equations are (12, p. 417)

$$[3.1] \qquad \sigma_r = \frac{EC_1}{1-2\nu} - \frac{2EC_2}{1+\nu}\cdot\frac{1}{r^3} - \frac{2\alpha E}{1-\nu}\,\frac{1}{r^3}\int_a^r Tr^2 dr,$$

$$[3.2] \qquad \sigma_t = \frac{EC_1}{1-2\nu} + \frac{EC_2}{1+\nu}\cdot\frac{1}{r^3} + \frac{\alpha E}{1-\nu}\left\{\frac{1}{r^3}\int_a^r Tr^2 dr - T\right\},$$

and the displacement u is

$$[3.3] \qquad \frac{u}{r} = C_1 + \frac{C_2}{r^3} + \frac{1+\nu}{1-\nu}\alpha\,\frac{1}{r^3}\int_a^r Tr^2 dr,$$

where α is the coefficient of thermal expansion, E is Young's modulus, ν is Poisson's ratio, and C_1 and C_2 are constants of integration to be determined from the boundary conditions.

In the plastic region the equation of equilibrium (12, Ch. 2)

$$[3.4] \qquad r\,d\sigma_r/dr = 2(\sigma_t - \sigma_r)$$

holds. The Tresca yield criterion is

$$[3.5] \qquad \sigma_3 - \sigma_1 = \sigma_y,$$

where σ_3 and σ_1 are the major and minor principal stresses respectively and σ_y is the yield stress in tension. The von Mises yield criterion is

$$[3.6] \qquad (\sigma_1-\sigma_2)^2 + (\sigma_2-\sigma_3)^2 + (\sigma_3-\sigma_1)^2 = 2\sigma_y^2.$$

Since the stress system in a spherical vessel is by symmetry (σ_r, σ_t, σ_t), both Equations [3.5] and [3.6] become

$$[3.7] \qquad \sigma_t - \sigma_r = \pm\sigma_y.$$

There are thus two defining equations for plasticity. The positive sign is to be used if plasticity occurs in tension, and the negative sign if plasticity occurs in compression. In the absence of thermal stress this occurs where $p_i > p_o$, and where $p_i < p_o$ respectively. In the development to follow the two values will always be possible, at least in principle. The upper sign associated in the following equations with any σ_y is to be used if plasticity occurs in tension and the lower sign if it occurs in compression. Inserting Equation [3.7] into [3.4] and integrating gives

$$[3.8] \qquad \sigma_r = \pm 2\sigma_y \ln r + C_3,$$

where C_3 is a constant of integration. The stresses in the vessel wall are com-

pletely determined by Equations [3.1], [3.2], [3.7], and [3.8] and the appropriate boundary conditions.

The boundary conditions are

[3.9] (i) at $r = a$, $\sigma_r = -p_i$,

[3.10] (ii) at $r = b$, $\sigma_r = -p_o$,

(iii) the stresses are continuous across the plastic–elastic boundary.

These equations are exactly valid within the limits of assumptions (i)–(iv) and (vi) of Section 2 if the dimensions a, b, and r are those of the strained vessel. If the strains are small little error is introduced by using the original values of a, b, and r. This is true within the elastic region within the usual range of approximation, and is true in the plastic region so long as the vessel is still partly elastic and providing the radius ratio is not too large (<5–6).

The calculation of the plastic strain requires further assumptions, the simplest of which is that the material is incompressible in the plastic region. This will not concern us.

2. The Completely Elastic Vessel

If the whole of the vessel is within the elastic region the boundary conditions required to determine C_1 and C_2 are Equations [3.9] and [3.10]. Inserting these conditions into Equations [3.1] and [3.2] leads to values of C_1 and C_2 and when these are put into Equations [3.1], [3.2], and [3.3] we find that the stresses are

$$[3.11] \qquad \sigma_r = -\frac{p_i}{k^3-1}\left(\frac{b^3}{r^3}-1\right)-\frac{p_o k^3}{k^3-1}\left(1-\frac{a^3}{r^3}\right) + \frac{2\alpha E}{1-\nu}\left\{\frac{1-a^3/r^3}{b^3-a^3}\int_a^b Tr^2dr-\frac{1}{r^3}\int_a^r Tr^2dr\right\},$$

$$[3.12] \qquad \sigma_t = \frac{p_i}{k^3-1}\left(\frac{b^3}{2r^3}+1\right)-\frac{p_o k^3}{k^3-1}\left(1+\frac{a^3}{2r^3}\right) + \frac{2\alpha E}{1-\nu}\left\{\frac{1+a^3/2r^3}{b^3-a^3}\int_a^b Tr^2dr+\frac{1}{2r^3}\int_a^r Tr^2dr-\tfrac{1}{2}T\right\},$$

and the displacement is

$$[3.13] \qquad \frac{u}{r} = \frac{p_i}{E(k^3-1)}\left\{(1-2\nu)+(1+\nu)\frac{b^3}{2r^3}\right\}-\frac{p_o k^3}{E(k^3-1)}\left\{(1-2\nu)+(1+\nu)\frac{a^3}{2r^3}\right\} + \frac{2\alpha}{1-\nu}\left\{\frac{(1-2\nu)+(1+\nu)a^3/2r^3}{b^3-a^3}\int_a^b Tr^2dr+\frac{1+\nu}{2r^3}\int_a^r Tr^2dr\right\},$$

where $$k = b/a.$$

(i) *Failure of Brittle Materials*

The maximum principal stress is the tangential stress, and failure of a brittle vessel will occur when this first reaches the fracture stress σ_u. By putting the right-hand side of Equation [3.12] equal to σ_u, it is seen that the pressures required for failure are dependent on thermal stresses. The thermal stresses may be such as to oppose the pressure stresses and so increase the pressure for failure, or they may reinforce the pressure stresses and so decrease the pressure

for failure. There are of course two values of σ_u, one positive (failure in tension) and one negative (failure in compression). For brittle materials the latter is much higher than the former. Further discussion in terms of an arbitrary temperature distribution is not very profitable. A more detailed treatment is better left to later papers concerned with particular temperature distributions.

(ii) *Failure of Ductile Materials*

For a spherical pressure vessel both the Tresca and the von Mises theories give the same result, namely that yielding will first occur according to Equation [3.7]. From Equations [3.11] and [3.12] $\sigma_t - \sigma_r$ in an entirely elastic vessel is given by

$$[3.14] \quad \sigma_t - \sigma_r = \frac{3}{2}\,\Delta p\,\frac{b^3/r^3}{k^3-1} + \frac{3\alpha E}{1-\nu}\left\{\frac{a^3/r^3}{b^3-a^3}\int_a^b Tr^2dr + \frac{1}{r^3}\int_a^r Tr^2dr - \tfrac{1}{3}T\right\}.$$

In the absence of a temperature gradient the maximum shear stress $\sigma_t - \sigma_r$ is given by the first term of the right-hand side of Equation [3.14]. The maximum always occurs at $r = a$, and yielding will always begin at the inside surface at the yield pressure Δp_y given by

$$[3.15] \quad \frac{\Delta p_y}{\pm\sigma_y} = \frac{k^3-1}{\frac{3}{2}k^3}.$$

In the presence of temperature gradients yielding can occur at any position within the walls depending on the values of the thermal and pressure stresses.

The radius at which yielding begins is determined from the following considerations:

(*a*) If the value of Δp_y for yielding at $r = a$ is numerically less than its value at all other radii, i.e. if

$$[3.16] \quad \pm\frac{3\alpha E}{(1-\nu)\,\sigma_y}\left\{\frac{1}{r^3-a^3}\int_a^r Tr^2dr - \frac{1}{3}\,\frac{r^3T-a^3T_i}{r^3-a^3}\right\} < 1$$

for all values of r, yielding under combined pressure and temperature will first begin at the inside surface. The yield pressure Δp_y is given by

$$[3.17] \quad \pm\frac{\Delta p_y}{\sigma_y} = \frac{k^3-1}{\frac{3}{2}k^3}\left\{1 \mp \frac{3\alpha E}{(1-\nu)\,\sigma_y}\left(\frac{1}{b^3-a^3}\int_a^b Tr^2dr - \tfrac{1}{3}T_i\right)\right\}.$$

(*b*) If the value of Δp_y for yielding at $r = b$ is numerically less than its value at all other radii, i.e. if

$$[3.18] \quad \pm\frac{3\alpha E}{(1-\nu)\,\sigma_y}\left\{\frac{1}{b^3-r^3}\int_r^b Tr^2dr - \frac{1}{3}\,\frac{b^3T_o-r^3T}{b^3-r^3}\right\} > 1$$

for all values of r, yielding will begin at the outside surface. The yield pressure is given by

$$[3.19] \quad \pm\frac{\Delta p_y}{\sigma_y} = \frac{k^3-1}{3/2}\left\{1 \mp \frac{3\alpha E}{(1-\nu)\,\sigma_y}\left(\frac{1}{b^3-a^3}\int_a^b Tr^2dr - \tfrac{1}{3}T_o\right)\right\}.$$

(*c*) Otherwise, yielding will start between the walls at radius r_y at the pressure

$$[3.20] \pm\frac{\Delta p_y}{\sigma_y} = \frac{k^3-1}{\frac{3}{2}b^3/r_y^3}\left\{1 \mp \frac{3\alpha E}{(1-\nu)\sigma_y}\left(\frac{a^3/r_y^3}{b^3-a^3}\int_a^b Tr^2dr + \frac{1}{r_y^3}\int_a^{r_y} Tr^2dr - \tfrac{1}{3}T_y\right)\right\},$$

where T_y is the value of T at r_y. The value of r_y is that at which $\sigma_t - \sigma_r$ is a maximum and is obtained by equating the differential of Equation [3.14] to zero. One obtains

$$[3.21] \qquad \frac{\Delta p_y}{k^3-1}\frac{b^3}{r_y^3} + \frac{2\alpha E}{1-\nu}\left\{\frac{a^3/r_y^3}{b^3-a^3}\int_a^b Tr^2dr + \frac{1}{r_y^3}\int_a^{r_y} Tr^2dr - \tfrac{1}{3}T_y + \frac{1}{6}\left(\frac{dT}{d\ln r}\right)_{r=r_y}\right\} = 0.$$

The solution of Equations [3.20] and [3.21] gives Δp_y and r_y. Substitution of [3.20] into [3.21] gives

$$[3.22] \qquad \mp\frac{1}{3}\frac{\alpha E}{(1-\nu)\sigma_y}\left(\frac{dT}{d\ln r}\right)_{r=r_y} = 1.$$

If the temperature gradient is nowhere high enough to fit this equation, yielding can never begin between the walls. The converse, of course, is not necessarily true.

The conditions for yielding under thermal stress alone, i.e. in the absence of pressure stress, are obtained easily by putting $\Delta p_y = 0$ into the above equations.

Comparison of the yield pressure in the absence of a temperature gradient, Equation [3.15], with that in the presence of a temperature gradient, Equations [3.17], [3.19], [3.20], shows that the temperature gradient has an effect on the yield pressure. It may be either increased or decreased, depending on whether the thermal and pressure stresses reinforce or oppose one another.

3. The Partly Plastic Vessel

If the stresses in a vessel made of a ductile material are increased beyond the yield point, plastic flow will occur, and the stresses will be readjusted. The plastic region will increase as the stresses are increased and eventually the vessel will burst. In this section the stresses in a partly plastic vessel are examined.

The following possible modes of yielding will be considered:

(i) Yielding starting at the inside surface and progressing continuously to the outside.

(ii) Yielding starting at the outside surface and progressing continuously to the inside.

(iii) Yielding occurring in regions starting from both the inside and the outside surfaces.

(iv) Yielding starting within the walls.

The stresses for each of these conditions will be examined. However, one can obtain information of considerable value without detailed analysis of each possible mode of yielding.

The maximum pressure that the vessel can withstand can be obtained from the following considerations. If the vessel is completely plastic Equation [3.8] holds with the boundary conditions [3.9] and [3.10]. One obtains easily

$$[3.23] \qquad \Delta p_u = \pm 2\sigma_y \ln k.$$

The pressure required to cause the whole wall just to become plastic is thus independent of the presence of any thermal stress. This pressure is the maximum pressure the vessel will withstand since subsequent expansion will cause k to decrease and hence Δp_u will decrease.

The shakedown load will be calculated assuming that the load cycle is from maximum load to zero. After at most a few applications of the loading cycle, no more plastic flow occurs, and the loading and unloading is completely elastic. The stress in the region in which plastic flow has occurred is

$$\sigma_t - \sigma_r = \pm\sigma_y.$$

If the unloading is completely elastic the residual stress $(\sigma_t-\sigma_r)_{res}$ is given by

$$(\sigma_t-\sigma_r)_{res} = \pm\sigma_y - (\sigma_t-\sigma_r)_{el},$$

where $(\sigma_t-\sigma_r)_{el}$ is the stress caused by the load, calculated assuming the vessel to be elastic. Under shakedown conditions the maximum residual stress is the yield stress so that

$$\max(\sigma_t-\sigma_r)_{el} = \pm 2\sigma_y. \tag{3.24}$$

If the position at which the maximum occurs is the same as that at which yielding began on loading, then the shakedown load is twice the load for initial yield.

If the position at which $|(\sigma_t-\sigma_r)_{el}|$ is maximum is not that at which yielding began, a more detailed analysis is required. If shakedown occurs at radius r_s, the shakedown pressure Δp_s is given by

$$\frac{3}{2}\Delta p_s \frac{b^3/r_s^3}{k^3-1} + \frac{3\alpha E}{1-\nu}\left(\frac{a^3/r_s^3}{b^3-a^3}\int_a^b Tr^2dr + \frac{1}{r_s^3}\int_a^r Tr^2dr - \tfrac{1}{3}T_s\right) = \pm 2\sigma_y, \tag{3.25}$$

where T_s is the temperature at radius r_s. It can be easily shown in a manner similar to that used in discussing initial yielding that:

(*a*) If

$$\pm\frac{\frac{3}{2}\alpha E}{(1-\nu)\sigma_y}\left\{\frac{1}{r^3-a^3}\int_a^r Tr^2dr - \frac{1}{3}\frac{r^3T-a^3T_i}{r^3-a^3}\right\} < 1 \tag{3.26}$$

for all values of r, shakedown occurs at the inside surface, and the shakedown load is

$$\frac{\Delta p_s}{\pm\sigma_y} = \frac{k^3-1}{\frac{3}{4}k^3}\left\{1-\frac{3\alpha E}{(1-\nu)\sigma_y}\left(\frac{1}{b^3-a^3}\int_a^b Tr^2dr - \tfrac{1}{3}T_i\right)\right\}. \tag{3.27}$$

(*b*) If

$$\pm\frac{\frac{3}{2}\alpha E}{(1-\nu)\sigma_y}\left\{\frac{1}{b^3-r^3}\int_r^b Tr^2dr - \frac{1}{3}\frac{b^3T_o-r^3T}{b^3-a^3}\right\} > 1 \tag{3.28}$$

for all values of r, shakedown will occur at the outside surface, and the shakedown load is

$$\frac{\Delta p_s}{\pm\sigma_y} = \frac{k^3-1}{3/4}\left\{1 \mp \frac{3\alpha E}{(1-\nu)\sigma_y}\left(\frac{1}{b^3-a^3}\int_a^b Tr^2dr - \tfrac{1}{3}T_o\right)\right\}. \tag{3.29}$$

(*c*) Otherwise shakedown will occur at radius r_s at the load

$$[3.30]\quad \frac{\Delta p_s}{\pm\sigma_y} = \frac{k^3-1}{\frac{3}{4}b^3/r_s^3}\left\{1 \mp \frac{3\alpha E}{(1-\nu)\sigma_y}\,\frac{a^3/r_s^3}{b^3-a^3}\int_a^b Tr^2dr+\frac{1}{r_s^3}\int_a^{r_s} Tr^2dr-\tfrac{1}{3}T_s\right\},$$

where T_s is the temperature at radius r_s. The radius r_s is that at which $|(\sigma_t-\sigma_r)_{el}|$ is maximum and is given by Equation [3.21] if Δp_s, r_s, and T_s are written for Δp_y, r_y, and T_y. Substituting [3.21] into [3.30] gives

$$\mp\frac{1}{6}\frac{\alpha E}{(1-\nu)\sigma_y}\left(\frac{dT}{d\ln r}\right)_{r=r_s} = 1.$$

If the temperature gradient is nowhere high enough to satisfy this equation, shakedown will not occur within the walls. The converse is of course not necessarily true.

We will now consider the various modes of yielding.

(i) *Plasticity Starts from the Inside Wall*

If a vessel has yielded at the inside surface, then increase in pressure will cause the plastic region to extend into the wall. For symmetrical reasons the radius ρ of the plastic–elastic boundary is constant at constant pressure and thermal stresses. The stresses and displacements in the elastic region are obtained from Equations [3.1], [3.2], and [3.3] and the boundary conditions [3.10] and

$$\text{at } r = \rho, \qquad \sigma_t-\sigma_r = \pm\sigma_y.$$

One obtains

$$[3.31]\quad \sigma_r = -p_o \mp \frac{2}{3}\sigma_y\frac{\rho^3}{b^3}\left(\frac{b^3}{r^3}-1\right) + \frac{2\alpha E}{1-\nu}\left\{\frac{1}{b^3}\int_\rho^b Tr^2dr-\frac{1}{r^3}\int_\rho^r Tr^2dr-\frac{1}{3}T_\rho\frac{\rho^3}{b^3}\left(\frac{b^3}{r^3}-1\right)\right\},$$

$$[3.32]\quad \sigma_t = -p_o \pm \frac{2}{3}\sigma_y\frac{\rho^3}{b^3}\left(\frac{b^3}{2r^3}+1\right) + \frac{2\alpha E}{1-\nu}\left\{\frac{1}{b^3}\int_\rho^b Tr^2dr+\frac{1}{2r^3}\int_\rho^r Tr^2dr+\frac{1}{3}T_\rho\frac{\rho^3}{b^3}\left(\frac{b^3}{2r^3}+1\right)-\tfrac{1}{2}T\right\},$$

$$[3.33]\quad \frac{u}{r} = -\frac{p_o}{E}(1-2\nu) \pm \frac{2}{3}\frac{\sigma_y}{E}\frac{\rho^3}{b^3}\left\{(1-2\nu)+\frac{b^3}{2r^3}(1+\nu)\right\} + \frac{2\alpha}{1-\nu}\left\{\frac{1-2\nu}{b^3}\int_\rho^b Tr^2dr+\frac{1+\nu}{r^3}\int_\rho^r Tr^2dr + \frac{1}{3}T_\rho\frac{\rho^3}{b^3}\left((1-2\nu)+\frac{b^3}{2r^3}(1+\nu)\right)\right\},$$

$$\rho < r < b.$$

In the plastic region Equation [3.8] holds with the boundary condition [3.9]. One obtains readily

$$[3.34]\quad \sigma_r = \pm 2\sigma_y\ln(r/a)-p_i,$$
$$\sigma_t = \sigma_r \pm \sigma_y.$$

To determine the position of ρ we use the boundary condition that the radial stress is continuous across the plastic–elastic boundary. Equating Equations [3.31] and [3.34] at $r = \rho$ one obtains that the pressure required to maintain the plastic–elastic boundary at radius ρ is

$$[3.35]\quad \frac{\Delta p}{\pm\sigma_y} = 2\ln\frac{\rho}{a}+\frac{2}{3}\left(1-\frac{\rho^3}{b^3}\right) \mp \frac{2\alpha E}{(1-\nu)\sigma_y}\left\{\frac{1}{b^3}\int_\rho^b Tr^2dr-\frac{1}{3}T_\rho\left(1-\frac{\rho^3}{b^3}\right)\right\}.$$

The condition for the maximum pressure is obtained by setting $\partial\Delta p/\partial\rho = 0$ and one obtains

$$[3.36]\quad \left\{1-\frac{\rho^3}{b^3}\right\}\left\{1 \pm \frac{1}{3}\frac{\alpha E}{(1-\nu)\sigma_y}\left(\frac{dT}{d\ln r}\right)_{r=\rho}\right\} = 0.$$

The condition

$$\mp\frac{1}{3}\frac{\alpha E}{(1-\nu)\sigma_y}\left(\frac{dT}{d\ln r}\right)_{r=\rho} = 1$$

corresponds to a point of inflection. A maximum is obtained when

$$\rho = b,$$

i.e., the plastic–elastic radius extends to the outside wall. The maximum pressure is

$$\Delta p_u = \pm 2\sigma_y \ln k,$$

as obtained in Equation [3.23].

If plastic flow does not occur on unloading, i.e. if the whole unloading is elastic, the residual stress is obtained by subtracting from the stresses in the partly plastic vessel the stresses due to the thermal and pressure loading calculated assuming complete elasticity. One obtains that in the region that was elastic the residual stresses are

$$[3.37]\quad \sigma_r = -\left(\pm\frac{2}{3}\sigma_y\frac{\rho^3}{b^3}-\frac{\Delta p}{k^3-1}\right)\left(\frac{b^3}{r^3}-1\right) - \frac{2\alpha E}{1-\nu}\left\{\frac{1-a^3/r^3}{b^3-a^3}\int_a^b Tr^2dr-\frac{1}{r^3}\int_a^\rho Tr^2dr - \frac{1}{b^3}\int_\rho^b Tr^2dr+\frac{1}{3}T_\rho\frac{\rho^3}{b^3}\left(\frac{b^3}{r^3}-1\right)\right\},$$

$$[3.38]\quad \sigma_t = \left(\pm\frac{2}{3}\sigma_y\frac{\rho^3}{b^3}-\frac{\Delta p}{k^3-1}\right)\left(\frac{b^3}{2r^3}+1\right) - \frac{2\alpha E}{1-\nu}\left\{\frac{1+a^3/2r^3}{b^3-a^3}\int_a^b Tr^2dr-\frac{1}{2r^3}\int_a^\rho Tr^2dr + \frac{1}{b^3}\int_\rho^b Tr^2dr-\frac{1}{3}T_\rho\frac{\rho^3}{b^3}\left(\frac{b^3}{2r^3}+1\right)\right\},$$

$$[3.39]\quad \frac{u}{r} = \frac{1}{E}\left(\pm\frac{2}{3}\sigma_y\frac{\rho^3}{b^3} - \frac{\Delta p}{k^3-1}\right)\left((1-2\nu)+\frac{b^3}{2r^3}(1+\nu)\right) - \frac{2\alpha}{1-\nu}\left\{\frac{(1-2\nu)+(1+\nu)\,a^3/2r^3}{b^3-a^3}\int_a^b Tr^2dr - \frac{1-2\nu}{b^3}\int_\rho^b Tr^2dr + \frac{1+\nu}{2r^3}\int_a^\rho Tr^2dr - \frac{1}{3}T_\rho\frac{\rho^3}{b^3}\left((1-2\nu)+\frac{b^3}{2r^3}(1+\nu)\right)\right\},$$

$$\rho \leqslant r \leqslant b.$$

In the region which was plastic the residual stresses are

$$[3.40]\quad \sigma_r = \pm 2\sigma_y \ln\frac{r}{a} - \frac{\Delta p\, k^3}{k^3-1}\left(1-\frac{a^3}{r^3}\right) - \frac{2\alpha E}{1-\nu}\left\{\frac{1-a^3/r^3}{b^3-a^3}\int_a^b Tr^2dr - \frac{1}{r^3}\int_a^r Tr^2dr\right\},$$

$$[3.41]\quad \sigma_t = \pm 2\sigma_y \ln\frac{r}{a} \pm \sigma_y - \frac{\Delta p\, k^3}{k^3-1}\left(1+\frac{a^3}{2r^3}\right) - \frac{2\alpha E}{1-\nu}\left\{\frac{1+a^3/2r^3}{b^3-a^3}\int_a^b Tr^2dr + \frac{1}{2r^3}\int_a^r Tr^2dr - T\right\},$$

$$a \leqslant r \leqslant \rho.$$

(ii) *Plasticity Starts from the Outside Wall*

In the elastic region $r = a$ to $r = \rho$ Equations [3.1] and [3.2] hold with the boundary conditions [3.9] and

$$\text{at } r = \rho, \quad \sigma_t - \sigma_r = \pm\sigma_y.$$

The solution is

$$[3.42]\quad \sigma_r = -p_i \pm \frac{2}{3}\sigma_y\frac{\rho^3}{a^3}\left(1-\frac{a^3}{r^3}\right) - \frac{2\alpha E}{1-\nu}\left\{\frac{1}{a^3}\int_a^\rho Tr^2dr - \frac{1}{r^3}\int_r^\rho Tr^2dr - \frac{1}{3}T_\rho\frac{\rho^3}{a^3}\left(1-\frac{a^3}{r^3}\right)\right\},$$

$$[3.43]\quad \sigma_t = -p_i \pm \frac{2}{3}\sigma_y\frac{\rho^3}{a^3}\left(1+\frac{a^3}{2r^3}\right) - \frac{2\alpha E}{1-\nu}\left\{\frac{1}{a^3}\int_a^\rho Tr^2dr - \frac{1}{2r^3}\int_r^\rho Tr^2dr - \frac{1}{3}T_\rho\frac{\rho^3}{a^3}\left(1+\frac{a^3}{2r^3}\right) + \tfrac{1}{2}T\right\},$$

$$a \leqslant r \leqslant \rho.$$

In the plastic region $r = \rho$ to $r = b$ Equation [3.8] with the boundary condition [3.10] holds. The stresses are

$$[3.44]\quad \sigma_r = \mp 2\sigma_y \ln(b/r) - p_o,$$

$$[3.45]\quad \sigma_t = \mp 2\sigma_y \ln(b/r) - p_o + \sigma_y,$$

$$\rho \leqslant r \leqslant b.$$

The load required to cause the plastic–elastic radius to extend to ρ is obtained from the condition that σ_r is continuous across the plastic boundary. One obtains by equating [3.42] and [3.44] at $r = \rho$ that

$$[3.46] \quad \frac{\Delta p}{\pm\sigma_y} = 2\ln\frac{b}{\rho}+\frac{2}{3}\left(\frac{\rho^3}{a^3}-1\right) \mp \frac{2\alpha E}{(1-\nu)\sigma_y}\left\{\frac{1}{a^3}\int_a^\rho Tr^2dr-\frac{1}{3}T_\rho\left(\frac{\rho^3}{a^3}-1\right)\right\}.$$

Differentiating this with respect to ρ and equating to zero in order to obtain the maximum pressure gives

$$[3.47] \quad \left(\frac{\rho^3}{a^3}-1\right)\left(1 \pm \frac{1}{3}\frac{\alpha E}{(1-\nu)\sigma_y}\left(\frac{dT}{d\ln r}\right)_{r=\rho}\right) = 0.$$

The condition

$$\mp\frac{1}{3}\frac{\alpha E}{(1-\nu)\sigma_y}\left(\frac{dT}{d\ln r}\right)_{r=\rho} = 1$$

is again a point of inflection of Δp and the maximum pressure is obtained when

$$[3.48] \quad \rho = a,$$

and is

$$\Delta p_u = \pm 2\sigma_y \ln k,$$

again verifying [3.23].

The residual stresses are easily calculated from the appropriate equations if required.

(iii) *Yielding Occurring Simultaneously in Regions Extending from Both the Inside and the Outside Surface*

When yielding has occurred from both walls, let the plastic regions extend from a to ρ_1 and from ρ_2 to b. Proceeding in the same manner as above, the equations for the stresses in the inner plastic region are

$$[3.49] \quad \sigma_r = \pm 2\sigma_y \ln(r/a) - p_i,$$

$$[3.50] \quad \sigma_t = \sigma_r \pm \sigma_y, \qquad a \leqslant r \leqslant \rho_1.$$

In the outer plastic region

$$[3.51] \quad \sigma_r = \pm 2\sigma_y \ln(b/r) - p_o,$$

$$[3.52] \quad \sigma_t = \sigma_r \pm \sigma_y, \qquad \rho_2 \leqslant r \leqslant b.$$

In the elastic region from ρ_1 to ρ_2 the Equations [3.1] and [3.2] hold, with the boundary conditions that σ_r is continuous across both ρ_1 and ρ_2.

It is readily shown from these conditions that the relation

$$[3.53] \quad \pm\frac{3\alpha E}{(1-\nu)\sigma_y}\left\{\frac{1}{\rho_2^3-\rho_1^3}\int_{\rho_1}^{\rho_2} Tr^2dr-\frac{1}{3}\frac{\rho_2^3T_{\rho_2}-\rho_1^3T_{\rho_1}}{\rho_2^3-\rho_1^3}\right\} = 1$$

must hold, where T_{ρ_1} and T_{ρ_2} are the temperatures at radii ρ_1 and ρ_2 respectively, and that

[3.54] $$\frac{\Delta p}{\pm\sigma_y} = 2(\ln k - \ln \rho_2/\rho_1) \mp \frac{2\alpha E}{(1-\nu)\sigma_y}(T_{\rho_2} - T_{\rho_1}).$$

The maximum pressure difference the vessel will withstand is obtained when

$$\frac{\partial \Delta p}{\partial \rho_1} = \frac{\partial \Delta p}{\partial \rho_2} = 0,$$

i.e. when

$$\left\{1 \pm \frac{\alpha E}{(1-\nu)\sigma_y}\left(\frac{dT}{d\ln r}\right)_{r=\rho_1}\right\} = \left\{1 \pm \frac{\alpha E}{(1-\nu)\sigma_y}\left(\frac{dT}{d\ln r}\right)_{r=\rho_2}\right\} = 0.$$

This occurs when

$$\rho_1 = \rho_2,$$

and the temperature gradient at $r = \rho_1 = \rho_2$ is given by

$$\left(\frac{dT}{d\ln r}\right)_{r=\rho_1=\rho_2} = \mp\frac{(1-\nu)\sigma_y}{\alpha E},$$

and the maximum pressure is again

$$\Delta p_u = \pm 2\sigma_y \ln k.$$

(iv) *Yielding Starting between the Walls*

Yielding first occurs according to Equations [3.20] and [3.21], and progresses so that the material between radii ρ_1 and ρ_2 is plastic.

In the inner elastic region $r = a$ to $r = \rho_1$ the stresses and strains are those given in Equations [3.42] and [3.43] with ρ_1 substituted for ρ. In the outer elastic region $r = \rho_2$ to $r = b$ the stresses are those given by Equations [3.31], [3.32], and [3.33] with ρ_2 written for ρ. The plastic stresses in the region $r = \rho_1$ to $r = \rho_2$ are given by Equation [3.8] with the boundary condition that σ_r is continuous across the elastic–plastic boundaries ρ_1 and ρ_2. One obtains

[3.55] $$\frac{\Delta p}{\pm\sigma_y} = 2\ln\frac{\rho_2}{\rho_1} + \frac{2}{3}\left(\frac{\rho_1^3}{a^3} - \frac{\rho_2^3}{b^3}\right) \mp \frac{2\alpha E}{(1-\nu)\sigma_y}\left\{\frac{1}{a^3}\int_a^{\rho_1} Tr^2 dr + \frac{1}{b^3}\int_{\rho_2}^{b} Tr^2 dr - \frac{1}{3}T_{\rho_1}\left(\frac{\rho_1^3}{a^3} - 1\right) - \frac{1}{3}T_{\rho_2}\left(1 - \frac{\rho_2^3}{b^3}\right)\right\}.$$

The maximum pressure is obtained when

$$\frac{\partial \Delta p}{\partial \rho_1} = \frac{\partial \Delta p}{\partial \rho_2} = 0.$$

One obtains

$$\left(\frac{\rho_1^3}{a^3} - 1\right)\left(1 \pm \frac{1}{3}\frac{\alpha E}{(1-\nu)\sigma_y}\left(\frac{dT}{d\ln r}\right)_{r=\rho_1}\right) = \left(\frac{\rho_2^3}{b^3} - 1\right)\left(1 \pm \frac{1}{3}\frac{\alpha E}{(1-\nu)\sigma_y}\left(\frac{dT}{d\ln r}\right)_{r=\rho_2}\right) = 0.$$

As before the conditions

$$\mp\frac{1}{3}\frac{\alpha E}{(1-\nu)\sigma_y}\left(\frac{dT}{d\ln r}\right)_{r=\rho_1} = \mp\frac{1}{3}\frac{\alpha E}{(1-\nu)\sigma_y}\left(\frac{dT}{d\ln r}\right)_{r=\rho_2} = 1$$

correspond to points of inflection. The maximum pressure is obtained when

$$\rho_1 = a, \qquad \rho_2 = b,$$

and is

$$\Delta p_u = \pm 2\sigma_y \ln k.$$

4. THE CYLINDRICAL VESSEL

1. General Considerations

The principal stresses in a cylindrical vessel are a radial σ_r, a tangential σ_t, and a longitudinal σ_l. The accurate calculation of the stresses and strains in a partly plastic cylinder is very much more difficult than for a sphere (4). The equation of equilibrium,

[4.1] $$r\, d\sigma_r/dr = \sigma_t - \sigma_r,$$

is independent of the longitudinal stress, and to obtain this stress a stress–strain relation in the plastic region must be assumed. If only pressure stresses are present it can be shown (4) that the longitudinal stress is always the intermediate principal stress, and if one assumes the Tresca yield criterion the plastic–elastic radius is independent of the longitudinal stress and is readily calculated as a function of pressure.

In the following treatment of a vessel subjected to both pressure and thermal stresses we have assumed that the thermal stresses are not sufficiently high relative to the pressure stresses that the longitudinal stress is promoted to the major or demoted to the minor principal stress. Under this condition, the treatment is accurately valid. If the thermal stresses are high enough to make the longitudinal stress not the intermediate stress, the treatment will not be accurate. Nevertheless if the longitudinal stress is not the intermediate stress it might be expected that the differences between the correct and the approximate theories would not be very large and that the approximate theory presented here would be suitable for design purposes.

The general equations for the stresses in the elastic region of the tube are (12, p. 409)

[4.2] $$\sigma_r = C_1 - \frac{C_2}{r^2} - \frac{\alpha E}{1-\nu}\frac{1}{r^2}\int_a^r Tr\,dr,$$

[4.3] $$\sigma_t = C_1 + \frac{C_2}{r^2} + \frac{\alpha E}{1-\nu}\left\{\frac{1}{r^2}\int_a^r Tr\,dr - T\right\},$$

where C_1 and C_2 are constants. The longitudinal stress is not determined, and the displacements cannot be calculated without it.

In the plastic region the equation of equilibrium [4.1] holds, together with the plasticity equation

[4.4] $$\sigma_t - \sigma_r = \pm\sigma_y.$$

Inserting [4.4] into [4.1] and integrating one obtains

[4.5] $$\sigma_r = \pm\sigma_y \ln r + C_3,$$

where C_3 is a constant of integration.

The constants C_1, C_2, and C_3 are to be determined from the boundary conditions

[4.6] (i) at $r = a$, $\sigma_r = -p_i$,

[4.7] (ii) at $r = b$, $\sigma_r = -p_o$,

(iii) the stresses are continuous across the plastic–elastic boundary.

2. The Completely Elastic Vessel

For a tube which is stressed wholly within the elastic region the boundary conditions are Equations [4.6] and [4.7]. Inserting these conditions into Equation [4.2], evaluating C_1 and C_2, and inserting these values in [4.2] and [4.3] gives

$$[4.8]\quad \sigma_r = -\frac{p_i}{k^2-1}\left(\frac{b^2}{r^2}-1\right)-\frac{p_o k^2}{k^2-1}\left(1-\frac{a^2}{r^2}\right) + \frac{\alpha E}{1-\nu}\left\{\frac{1-a^2/r^2}{b^2-a^2}\int_a^b Trdr-\frac{1}{r^2}\int_a^r Trdr\right\},$$

$$[4.9]\quad \sigma_t = \frac{p_i}{k^2-1}\left(\frac{b^2}{r^2}+1\right)-\frac{p_o k^2}{k^2-1}\left(1+\frac{a^2}{r^2}\right) + \frac{\alpha E}{1-\nu}\left\{\frac{1+a^2/r^2}{b^2-a^2}\int_a^b Trdr+\frac{1}{r^2}\int_a^r Trdr-T\right\}.$$

(i) *Failure of Brittle Materials*

A brittle material fails elastically and fractures when the maximum principal stress reaches a limiting value σ_u. The maximum principal stress is the tangential stress and failure will occur when the right-hand side of Equation [4.9] becomes equal to σ_u. The compressive ultimate stress is very much higher than the tensile ultimate stress so the value of σ_u will depend upon the sign of the stress. The thermal stresses may either reinforce or oppose the pressure stresses, and so weaken or strengthen the vessel. Detailed discussion of the failure of brittle vessels for an arbitrary temperature gradient is not very profitable, and further consideration will be left to later papers concerned with particular temperature distributions.

(ii) *Failure of Ductile Materials*

According to the maximum shear stress theory, elastic failure will occur when

$$\sigma_t-\sigma_r = \pm\sigma_y,$$

i.e., substituting σ_t and σ_r from [4.8] and [4.9], when

$$[4.10]\quad \frac{2\Delta p}{k^2-1}\frac{b^2}{r^2}+\frac{2\alpha E}{1-\nu}\left\{\frac{a^2/r^2}{b^2-a^2}\int_a^b Trdr+\frac{1}{r^2}\int_a^r Trdr-\tfrac{1}{2}T\right\} = \pm\sigma_y.$$

If only pressure stresses are present the maximum stress difference $(\sigma_t-\sigma_r)$ is at the inside wall, and yielding will begin there at the pressure

$$\frac{\Delta p_y}{\pm\sigma_y} = \frac{k^2-1}{2k^2}.$$

If both pressure and thermal stresses are present, yielding may occur anywhere within the walls. It can readily be shown from Equation [4.10] that:

(*a*) If the value of Δp_y for yielding at $r = a$ is numerically less than its value for all other radii, i.e. if

$$[4.11] \qquad \pm\frac{2\alpha E}{(1-\nu)\sigma_y}\left\{\frac{1}{r^2-a^2}\int_a^r Trdr-\frac{1}{2}\frac{r^2T-a^2T_i}{r^2-a^2}\right\} < 1$$

for all values of r, then yielding will commence at the inside surface when the pressure is increased to the yield value

$$[4.12] \qquad \frac{\Delta p_y}{\pm\sigma_y} = \frac{k^2-1}{2k^2}\left\{1 \mp \frac{2\alpha E}{(1-\nu)\sigma_y}\left(\frac{1}{b^2-a^2}\int_a^b Trdr-\tfrac{1}{2}T_i\right)\right\}.$$

(*b*) If the value of Δp_y for yielding at $r = b$ is numerically less than its value at all other radii, i.e. if

$$[4.13] \qquad \pm\frac{2\alpha E}{(1-\nu)\sigma_y}\left\{\frac{1}{b^2-r^2}\int_r^b Trdr-\frac{1}{2}\frac{b^2T_o-r^2T}{b^2-r^2}\right\} > 1$$

for all values of r, yielding will first begin at the outside surface when the pressure is increased to the value

$$[4.14] \qquad \frac{\Delta p_y}{\pm\sigma_y} = \frac{(k^2-1)}{2}\left\{1 \mp \frac{2\alpha E}{(1-\nu)\sigma_y}\left(\frac{1}{b^2-a^2}\int_a^b Trdr-\tfrac{1}{2}T_o\right)\right\}.$$

(*c*) Otherwise yielding will start between the walls at radius r_y at the pressure

$$[4.15] \qquad \frac{\Delta p_y}{\pm\sigma_y} = \frac{k^2-1}{2b^2/r_y^2}\left\{1 \mp \frac{2\alpha E}{(1-\nu)\sigma_y}\left(\frac{a^2/r_y^2}{b^2-a^2}\int_a^b Trdr-\frac{1}{r_y^2}\int_a^{r_y} Trdr-\tfrac{1}{2}T_y\right)\right\}.$$

The value of r_y is that at which $|\sigma_t-\sigma_r|$ is a maximum and is obtained by equating to zero the differential with respect to r of Equation [4.10]. One obtains

$$[4.16] \qquad \frac{\Delta p_y}{k^2-1}\frac{b^2}{r_y^2}+\frac{\alpha E}{1-\nu}\left\{\frac{a^2/r_y^2}{b^2-a^2}\int_a^b Trdr+\frac{1}{r_y^2}\int_a^{r_y} Trdr-\tfrac{1}{2}T_y+\frac{1}{4}\left(\frac{dT}{d\ln r}\right)_{r=r_y}\right\}=0.$$

Substituting [4.15] into [4.16] gives

$$\mp\frac{1}{2}\frac{\alpha E}{(1-\nu)\sigma_y}\left(\frac{dT}{d\ln r}\right)_{r=r_y} = 1.$$

A temperature gradient satisfying this equation is required for yielding to begin within the walls, but its presence does not necessarily lead to yielding.

3. The Partly Plastic Vessel

The possible modes of yielding of the cylindrical vessel are the same as those of the spherical vessel, q.v.

The maximum pressure which the vessel can hold is easily obtained. If the vessel is completely plastic, Equation [4.5] with the boundary conditions [4.6] and [4.7] holds and gives

$$[4.17] \qquad \Delta p_u = \pm\sigma_y \ln k.$$

As with the spherical vessel, this is the maximum pressure the vessel will

withstand and is independent of the thermal stresses. The shakedown load is obtained by the same arguments as used for the spherical vessel, and is twice the pressure required to just cause yielding, providing the position of maximum shear stress calculated assuming elastic conditions occurs at the same place as that at which yielding first begins.

If the position at which $|(\sigma_t-\sigma_r)_{el}|$ is a maximum is not that at which yielding began a more detailed analysis is required. The shakedown load occurs at a radius r_s and is given by

$$[4.18] \qquad \Delta p_s \frac{b^2/r_s^2}{k^2-1}+\frac{\alpha E}{1-\nu}\left\{\frac{a^2/r_s^2}{b^2-a^2}\int_a^b Trdr+\frac{1}{r_s^2}\int_a^{r_s} Trdr-\tfrac{1}{2}T_s\right\} = \pm\sigma_y,$$

where T_s is the temperature at radius r_s.

(*a*) If

$$[4.19] \qquad \pm\frac{\alpha E}{(1-\nu)\sigma_y}\left\{\frac{1}{r^2-a^2}\int_a^r Trdr-\frac{1}{2}\frac{r^2T-a^2T_i}{r^2-a^2}\right\} < 1$$

for all values of r, shakedown occurs at the inside surface, and the shakedown load is

$$[4.20] \qquad \frac{\Delta p_s}{\pm\sigma_y} = \frac{k^2-1}{k^2}\left\{1 \mp \frac{2\alpha E}{(1-\nu)\sigma_y}\left(\frac{1}{b^2-a^2}\int_a^b Trdr-\tfrac{1}{2}T_i\right)\right\}.$$

(*b*) If

$$[4.21] \qquad \pm\frac{\alpha E}{(1-\nu)\sigma_y}\left\{\frac{1}{b^2-r^2}\int_r^b Trdr-\frac{1}{2}\frac{b^2T_o-r^2T}{b^2-r^2}\right\} > 1$$

for all values of r, shakedown will occur at the outside surface and the shakedown load is

$$[4.22] \qquad \frac{\Delta p_s}{\pm\sigma_y} = (k^2-1)\left\{1 \mp \frac{2\alpha E}{(1-\nu)\sigma_y}\left(\frac{1}{b^2-a^2}\int_a^b Trdr-\tfrac{1}{2}T_o\right)\right\}.$$

(*c*) Otherwise shakedown will occur at a radius r_s under the load

$$[4.23] \qquad \frac{\Delta p_s}{\pm\sigma_y} = (k^2-1)\left\{1 \mp \frac{2\alpha E}{(1-\nu)\sigma_y}\left(\frac{a^2/r_s^2}{b^2-a^2}\int_a^b Trdr+\frac{1}{r_s^2}\int_a^{r_s} Trdr-\tfrac{1}{2}T_s\right)\right\}.$$

The value of r_s is that at which $|(\sigma_t-\sigma_r)_{el}|$ is a maximum. One obtains Equation [4.16] with Δp_s, r_s, and T_s substituted for Δp_y, r_y, and T_y. Combining this with [4.23] one obtains that at r_s

$$\mp\frac{1}{4}\frac{\alpha E}{(1-\nu)\sigma_y}\left(\frac{dT}{d\ln r}\right)_{r=r_s} = 1.$$

A temperature gradient satisfying this equation is required for shakedown to occur between the walls, but its presence does not necessarily lead to shakedown.

We will now consider the various modes of yielding.

(i) *Plasticity Starts from the Inside Wall*

In the elastic region the stresses are given by Equations [4.2] and [4.3] with the boundary conditions [4.6] and

$$\text{at } r = \rho, \quad \sigma_t-\sigma_r = \sigma_y.$$

One obtains

$$[4.24]\qquad \sigma_r = -p_o \mp \frac{1}{2}\sigma_y \frac{\rho^2}{b^2}\left(\frac{b^2}{r^2}-1\right)+\frac{\alpha E}{1-\nu}\left\{\frac{1}{b^2}\int_\rho^b Trdr - \frac{1}{r^2}\int_\rho^r Trdr - \frac{1}{2}T_\rho \frac{\rho^2}{b^2}\left(\frac{b^2}{r^2}-1\right)\right\},$$

$$[4.25]\qquad \sigma_t = -p_o \pm \frac{1}{2}\sigma_y \frac{\rho^2}{b^2}\left(\frac{b^2}{r^2}+1\right)+\frac{\alpha E}{1-\nu}\left\{\frac{1}{b^2}\int_\rho^b Trdr + \frac{1}{r^2}\int_\rho^r Trdr + \frac{1}{2}T_\rho \frac{\rho^2}{b^2}\left(\frac{b^2}{r^2}+1\right) - T\right\},$$

$$\rho \leqslant r \leqslant b.$$

In the plastic region Equation [4.5] holds with the boundary condition [4.6] giving

$$[4.26]\qquad \sigma_r = \pm\sigma_y \ln(r/a) - p_i,$$
$$\sigma_t = \sigma_r \pm \sigma_y,$$
$$a \leqslant r \leqslant \rho.$$

To determine the radius ρ of the plastic–elastic boundary we use the condition that σ_r is continuous across the plastic–elastic boundary and obtain from [4.24] and [4.26]

$$[4.27]\qquad \frac{\Delta p}{\pm\sigma_y} = \ln\frac{\rho}{a}+\frac{1}{2}\left(1-\frac{\rho^2}{b^2}\right) \mp \frac{\alpha E}{(1-\nu)\sigma_y}\left\{\frac{1}{b^2}\int_\rho^b Trdr - \frac{1}{2}T_\rho\left(1-\frac{\rho^2}{b^2}\right)\right\}.$$

The ultimate pressure is obtained by equating $\partial\Delta p/\partial\rho$ to zero. We obtain

$$\left(1-\frac{\rho^2}{b^2}\right)\left(1 \pm \frac{1}{2}\frac{\alpha E}{(1-\nu)\sigma_y}\left(\frac{dT}{d\ln r}\right)_{r=\rho}\right) = 0.$$

The condition

$$1 \pm \frac{1}{2}\frac{\alpha E}{(1-\nu)\sigma_y}\left(\frac{dT}{d\ln r}\right)_{r=\rho} = 0$$

is an inflection point, and a maximum is obtained only when

$$\rho = b.$$

The ultimate pressure is then

$$\Delta p_u = \pm\sigma_y \ln k,$$

verifying Equation [4.17].

On unloading elastically the residual stresses are obtained by subtracting from [4.24] and [4.25] the stresses calculated assuming elasticity. In the region which was plastic the residual stresses are

$$[4.28]\qquad \sigma_r = \pm\sigma_y \ln\frac{r}{a} - \frac{\Delta p k^2}{k^2-1}\left(1-\frac{a^2}{r^2}\right) - \frac{\alpha E}{1-\nu}\left\{\frac{1-a^2/r^2}{b^2-a^2}\int_a^b Trdr - \frac{1}{r^2}\int_a^r Trdr\right\},$$

$$[4.29]\qquad \sigma_t = \pm\sigma_y \ln\frac{r}{a} - \frac{\Delta p k^2}{k^2-1}\left(1+\frac{a^2}{r^2}\right) - \frac{\alpha E}{1-\nu}\left\{\frac{1+a^2/r^2}{b^2-a^2}\int_a^b Trdr + \frac{1}{r^2}\int_a^r Trdr - T\right\},$$

$$a \leqslant r \leqslant \rho.$$

In the region which was elastic the residual stresses are

$$[4.30]\quad \sigma_r = -\left(\pm\frac{1}{2}\sigma_y\frac{\rho^2}{b^2}-\frac{\Delta p}{k^2-1}\right)\left(\frac{b^2}{r^2}-1\right) - \frac{\alpha E}{1-\nu}\left\{\frac{1-a^2/r^2}{b^2-a^2}\int_a^b Trdr-\frac{1}{b^2}\int_\rho^b Trdr-\frac{1}{r^2}\int_a^\rho Trdr+\frac{1}{2}T_\rho\frac{\rho^2}{b^2}\left(\frac{b^2}{r^2}-1\right)\right\},$$

$$[4.31]\quad \sigma_t = \left(\pm\frac{1}{2}\sigma_y\frac{\rho^2}{b^2}-\frac{\Delta p}{k^2-1}\right)\left(\frac{b^2}{r^2}+1\right) - \frac{\alpha E}{1-\nu}\left\{\frac{1+a^2/r^2}{b^2-a^2}\int_a^b Trdr-\frac{1}{b^2}\int_\rho^b Trdr-\frac{1}{r^2}\int_a^\rho Trdr-\frac{1}{2}T_\rho\frac{\rho^2}{b^2}\left(\frac{b^2}{r^2}+1\right)\right\},$$

$$\rho \leqslant r \leqslant b.$$

(ii) *Plasticity Starts from the Outside Wall*

In the elastic region $r = a$ to $r = \rho$ the stresses are given by Equations [4.2] and [4.3] with the boundary conditions [4.6] and

$$\text{at } r = \rho, \qquad \sigma_t-\sigma_r = \pm\sigma_y.$$

One obtains

$$[4.32]\quad \sigma_r = -p_i \pm \frac{1}{2}\sigma_y\frac{\rho^2}{a^2}\left(1-\frac{a^2}{r^2}\right) - \frac{\alpha E}{1-\nu}\left\{\frac{1}{a^2}\int_a^\rho Trdr-\frac{1}{r^2}\int_r^\rho Trdr-\frac{1}{2}T_\rho\frac{\rho^2}{a^2}\left(1-\frac{a^2}{r^2}\right)\right\},$$

$$[4.33]\quad \sigma_t = -p_i \pm \frac{1}{2}\sigma_y\frac{\rho^2}{a^2}\left(1+\frac{a^2}{r^2}\right) - \frac{\alpha E}{1-\nu}\left\{\frac{1}{a^2}\int_a^\rho Trdr-\frac{1}{r^2}\int_r^\rho Trdr-\frac{1}{2}T_\rho\frac{\rho^2}{a^2}\left(1+\frac{a^2}{r^2}\right)+T\right\},$$

$$a \leqslant r \leqslant \rho.$$

The stresses in the plastic region are obtained from the plasticity equation [4.5] and the boundary condition [4.7]. One obtains

$$[4.34]\quad \sigma_r = -p_o \mp \sigma_y \ln(b/r),$$
$$\sigma_t = \sigma_r \pm \sigma_y,$$
$$\rho \leqslant r \leqslant b.$$

The pressure required to maintain the plastic–elastic radius at a value ρ is obtained from the condition that σ_r is continuous across the plastic–elastic boundary. Equating [4.32] and [4.34] at $r = \rho$ one obtains

$$[4.35]\quad \frac{\Delta p}{\pm\sigma_y} = \ln\frac{b}{r}+\frac{1}{2}\left(\frac{\rho^2}{a^2}-1\right) \mp \frac{\alpha E}{(1-\nu)\sigma_y}\left\{\frac{1}{a^2}\int_a^\rho Trdr-\frac{1}{2}T_\rho\left(\frac{\rho^2}{a^2}-1\right)\right\}.$$

The maximum pressure is obtained by differentiating this equation with respect to ρ and equating to zero. We obtain

$$\left(\frac{\rho^2}{a^2}-1\right)\left(1 \pm \frac{1}{2}\frac{\alpha E}{(1-\nu)\sigma_y}\left(\frac{dT}{d\ln r}\right)_{r=\rho}\right) = 0.$$

The condition

$$\mp\frac{1}{2}\frac{\alpha E}{(1-\nu)\sigma_y}\left(\frac{dT}{d\ln r}\right)_{r=\rho} = 1$$

is a point of inflection. The maximum pressure is obtained when

$$\rho = a,$$

and is

$$\Delta p_u = \pm\sigma_y \ln k,$$

again verifying Equation [4.17].

(iii) *Yielding Occurring Simultaneously in Regions Extending from Both the Inside and the Outside Surface*

The regions $r = a$ to $r = \rho_1$ and $r = \rho_2$ to $r = b$ are plastic, and the region $r = \rho_1$ to $r = \rho_2$ is elastic. In the inner plastic region Equation [4.26] holds and in the outer plastic region Equation [4.34] holds. In the elastic region Equations [4.2] and [4.3] hold with the boundary conditions that σ_r and σ_t are continuous across ρ_1 and ρ_2. The stresses are readily calculated and it can be shown that the condition

$$[4.36] \qquad \pm\frac{2\alpha E}{(1-\nu)\sigma_y}\left\{\frac{1}{\rho_2^2-\rho_1^2}\int_{\rho_1}^{\rho_2} Tr\,dr - \frac{1}{2}\frac{T_{\rho_2}\rho_2^2 - T_{\rho_1}\rho_1^2}{\rho_2^2-\rho_1^2}\right\} = 1$$

holds and that

$$[4.37] \qquad \frac{\Delta p}{\pm\sigma_y} = \ln k - \ln\frac{\rho_2}{\rho_1} \mp \frac{1}{2}\frac{\alpha E}{(1-\nu)\sigma_y}(T_2 - T_1).$$

The maximum value of Δp is obtained when

$$\partial\Delta p/\partial\rho_1 = \partial\Delta p/\partial\rho_2 = 0,$$

i.e., when

$$\left\{1 \pm \frac{1}{2}\frac{\alpha E}{(1-\nu)\sigma_y}\left(\frac{dT}{d\ln r}\right)_{r=\rho_1}\right\} = \left\{1 \pm \frac{1}{2}\frac{\alpha E}{(1-\nu)\sigma_y}\left(\frac{dT}{d\ln r}\right)_{r=\rho_2}\right\} = 0.$$

This occurs only when

$$\rho_1 = \rho_2,$$

and

$$\pm\frac{1}{2}\frac{\alpha E}{(1-\nu)\sigma_y}\left(\frac{dT}{d\ln r}\right)_{r=\rho_1=\rho_2} = -1.$$

The maximum pressure is

$$\Delta p_u = \pm\sigma_y \ln k.$$

(iv) *Yielding Starting between the Walls*

The regions $r = a$ to $r = \rho_1$ and $r = \rho_2$ to $r = b$ are elastic and the region $r = \rho_1$ to $r = \rho_2$ is plastic. In the inner elastic region the stresses are given by Equations [4.32] and [4.33] when ρ_1 is written for ρ. In the outer elastic region the stresses are given by Equations [4.24] and [4.25] when ρ_2 is written for ρ.

The stresses in the plastic region $r = \rho_1$ to $r = \rho_2$ are obtained from Equation [4.5] and the boundary conditions that the stresses are continuous across the plastic–elastic boundaries. The pressure required to extend the plastic region to radii ρ_1 and ρ_2 is

$$[4.38] \quad \frac{\Delta p}{\pm\sigma_y} = \ln\frac{\rho_2}{\rho_1}+\frac{1}{2}\left(\frac{\rho_1^2}{a^2}-\frac{\rho_2^2}{b^2}\right) \mp \frac{\alpha E}{(1-\nu)\sigma_y}\left\{\frac{1}{a^2}\int_a^{\rho_1} Tr\,dr+\frac{1}{b^2}\int_{\rho_2}^{b} Tr\,dr-\frac{1}{2}T_{\rho_1}\left(\frac{\rho_1^2}{a^2}-1\right)-\frac{1}{2}T_{\rho_2}\left(1-\frac{\rho_2^2}{b^2}\right)\right\}.$$

The maximum value of Δp is obtained by putting

$$\frac{\partial \Delta p}{\partial \rho_1} = \frac{\partial \Delta p}{\partial \rho_2} = 0,$$

and one obtains

$$\left(\frac{\rho_1^2}{a^2}-1\right)\left(1 \pm \frac{1}{2}\frac{\alpha E}{(1-\nu)\sigma_y}\left(\frac{dT}{d\ln r}\right)_{r=\rho_1}\right) = \left(1-\frac{\rho_1^2}{b^2}\right)\left(1 \pm \frac{1}{2}\frac{\alpha E}{(1-\nu)\sigma_y}\left(\frac{dT}{d\ln r}\right)_{r=\rho_2}\right) = 0.$$

The conditions

$$\mp\frac{1}{2}\frac{\alpha E}{(1-\nu)\sigma_y}\left(\frac{dT}{d\ln r}\right)_{r=\rho_1} = 1, \quad \mp\frac{1}{2}\frac{\alpha E}{(1-\nu)\sigma_y}\left(\frac{dT}{d\ln r}\right)_{r=\rho_2} = 1$$

are points of inflection only. The maximum pressure is obtained when

$$\rho_1 = a, \qquad \rho_2 = b,$$

and is

$$\Delta p_u = \pm\sigma_y \ln k.$$

5. SUMMARY AND DISCUSSION

The main conclusions of the foregoing theory are as follows:

(i) The bursting pressure of a brittle vessel is affected by thermal stresses.

(ii) The ultimate pressure of a ductile vessel is independent of the presence of thermal stresses, and is given by

$$\Delta p_u = \pm 2\sigma_y \ln k, \quad \text{and} \quad \Delta p_u = \pm\sigma_y \ln k,$$

for spherical and cylindrical vessels respectively.

(iii) The onset of yielding, the early stages of plastic flow, and the residual stresses on unloading of a ductile vessel are affected by thermal stresses.

As we have already stated there are no experimental results to compare these conclusions with. However, a similar treatment applied to rotating disks leads to similar conclusions, namely that while the bursting speed of a ductile disk is independent of the thermal stresses the early stages of plastic flow are strongly affected. These conclusions have been confirmed experimentally by the work of Manson *et al.* (14) on the behavior of rotating disks containing a temperature gradient. The experiments were performed on disks made of a strongly strain-hardening material, so quantitative comparison cannot be made.

As remarked above the three most important criteria which are used for the design of pressure vessels are:

(i) initial yield,

(ii) bursting,

(iii) shakedown.

For brittle materials criterion (i) using the maximum principal stress theory is probably the most useful because when elastic failure occurs the material cracks.

The criterion to be used for ductile materials depends partly on how the vessel is to be used. A small amount of plastic flow when pressure is first applied will be intolerable only when the original dimensions of the vessel must be maintained; then criterion (i) using either the Tresca or the von Mises theory should be used with an appropriate safety factor. If the vessel is to be used only a very few times there is no need to take account of the fatigue caused by successive plastic deformations on loading and unloading, and only the bursting pressure need be considered; in this case thermal stresses will have no effect on design. If the vessel is to be loaded many times, the maximum allowable load should be based on the required factor of safety for either bursting or shakedown, whichever gives the smaller load. A vessel loaded thermally and with internal and external pressure will usually be required to withstand any two of these acting together, or any one of them alone. The strengthening effect obtained when the thermal and the pressure stresses tend to cancel one another at the point of maximum stress should therefore not be taken into account.

It will be noticed that two important factors have been omitted from this discussion.

(i) Stress raisers can increase considerably the stresses due to pressure and temperature and if any are present they should be taken into account.

(ii) Fatigue due to stressing below the elastic limit has not been taken account of, partly because of the complexity of the problem, and partly because little is known about the effects of fatigue on pressure vessels.

REFERENCES

1. Cook, G. Proc. Inst. Mech. Engrs. (London), 126: 407. 1934.
2. Cook, G. and Robertson, A. Engineering, 92: 786. 1911.
3. Faupel, J. H. J. Franklin Inst. 259: 405. 1955.
4. Hill, R. The mathematical theory of plasticity. Oxford at the Clarendon Press. 1950.
5. Kern, J. Z. angew. Phys. 3: 321. 1951.
6. Lenngren, C. E. Artill. Tidskr. 80: 87. 1951; Appl. Mechanics Rev. 5: 187. 1952.
7. Luster, E. W. Trans. Am. Soc. Mech. Engrs. 53: 161. 1931.
8. Morrison, J. M. C. Proc. Inst. Mech. Engrs. (London), 159: 81. 1948.
9. Nadai, A. Theory of flow and fracture of solids. 2nd ed. McGraw-Hill Book Company, Inc., New York. 1950.
10. Poppendiek, H. F. Heat transfer. Engineering Research Institute, University of Michigan.
11. Steele, M. C. and Young, J. Trans. Am. Soc. Mech. Engrs. 74: 355. 1952.
12. Timoshenko, S. and Goodier, J. N. Theory of elasticity. 2nd ed. McGraw-Hill Book Company, Inc., New York. 1951.
13. Warren, A. G. Symposium on Internal Stresses in Metals and Alloys. Inst. Metals (London), Monograph and Rept. Ser. No. 5: 209. 1948.
14. Wilterdink, P. I., Holms, A. G., and Manson, S. S. Natl. Advisory Committee for Aeronautics Note 2803. 1952.

THE DESIGN OF PRESSURE VESSELS SUBJECTED TO THERMAL STRESS

II. STEADY STATE TEMPERATURE DISTRIBUTION[1]

By E. Whalley

ABSTRACT

The general equations derived in the preceding paper for the behavior of pressure vessels under thermal and pressure stresses have been specialized for steady state heat flow. Design curves are presented for both brittle and ductile cylindrical vessels.

NOMENCLATURE

The nomenclature used in Part I is retained in Part II, and the following symbols are also used:

p_{iu} = ultimate inside pressure.
Q = heat conducted through the vessel wall divided by either (a) the diameter if the vessel is spherical, or (b) the length if it is cylindrical.
$\Delta T = T_o - T_i$.
$\beta = \alpha E \Delta T/(1-\nu)$.
$\gamma = \alpha EQ/[2\pi\lambda(1-\nu)]$.
λ = coefficient of thermal conductivity.

1. INTRODUCTION

In the first paper in this series (2) (Part I) the behavior under both pressure and thermal stresses of spherical and cylindrical vessels was discussed in some detail for any arbitrary temperature distribution. In this paper the application of the results of Part I to a steady state temperature distribution is considered.

The following assumptions were made:

(i) Ductile materials have a well-defined yield point and yield at constant maximum shear stress without strain hardening. Brittle materials fracture when the maximum principal stress reaches a limiting value.

(ii) The plastic strains are everywhere small.

(iii) The mechanical properties of the material, such as the thermal conductivity, the coefficient of linear expansion, the yield stress, the elastic moduli, are independent of temperature.

(iv) In discussing the behavior of a cylindrical vessel it was assumed that the longitudinal stress is everywhere the intermediate principal stress.

(v) The temperature is everywhere sufficiently low that creep is not important.

(vi) The Bauschinger effect is negligible.

A discussion of these assumptions has been given in Section 2 of Part I.

[1]*Manuscript received October 7, 1955.*
Contribution from the Division of Applied Chemistry, National Research Council of Canada, Ottawa, Canada. Issued as N.R.C. No. 4017.

2. SPHERICAL VESSELS

The temperature T at radius r in the walls of a spherical vessel subjected to a steady state temperature gradient is readily calculated thus. If bQ is the rate of loss of heat from the sphere and λ the coefficient of thermal conductivity, then

$$\frac{bQ}{4\pi r^2} = -\lambda \frac{dT}{dr}. \tag{2.1}$$

By integrating this with Q constant we obtain

$$T - T_i = -\frac{kQ}{4\pi\lambda}\left(1-\frac{a}{r}\right). \tag{2.2}$$

At $r = b$, $T = T_o$ and

$$Q = -4\pi\lambda\Delta T/(k-1), \tag{2.3}$$

where

$$\Delta T = T_o - T_i. \tag{2.4}$$

From [2.2] and [2.3]

$$T = T_i + \frac{k\Delta T}{k-1}\left(1-\frac{a}{r}\right). \tag{2.5}$$

The thermal variable of primary interest may be either the temperature difference between the outside and inside walls, or the rate of heat transfer between the walls. It is convenient to define the variables

$$\beta = \alpha E \Delta T/(1-\nu), \tag{2.6}$$

$$\gamma = \alpha E Q/[2\pi\lambda(1-\nu)]. \tag{2.7}$$

The functions β and γ will be used in discussing both spherical and cylindrical vessels. Q is the total amount of heat conducted through the wall of the vessel, divided by the outer radius if the vessel is spherical or by its length if it is cylindrical. From [2.3], [2.6], and [2.7] it is easily shown that for spherical vessels

$$\beta = \gamma(k-1). \tag{2.8}$$

1. The Completely Elastic Vessel

The stresses in the completely elastic vessel are from Equations [I 3.9],* [I 3.10], [2.5], and [2.6]

$$\sigma_r = -\frac{p_i}{k^3-1}\left(\frac{b^3}{r^3}-1\right) - \frac{p_o k^3}{k^3-1}\left(1-\frac{a^3}{r^3}\right) + \beta\frac{k}{k^3-1}\left\{(k+1)\left(1-\frac{b}{r}\right) - \frac{a}{r}\left(1-\frac{b^2}{r^2}\right)\right\}, \tag{2.9}$$

**References to the numbers of equations in Part I are preceded by the figure* I.

[2.10] $$\sigma_t = \frac{p_i}{k^3-1}\left(\frac{b^3}{2r^3}+1\right)-\frac{p_o k^3}{k^3-1}\left(1+\frac{a^3}{2r^3}\right) + \beta\frac{k}{k^3-1}\left\{(k+1)\left(1-\frac{b}{2r}\right)-\frac{a}{2r}\left(1+\frac{b^2}{r^2}\right)\right\}.$$

If the stresses are required in terms of the heat transfer instead of the temperature difference, $\gamma(k-1)$ can be written for β.

2. Fracture of Brittle Materials

Brittle materials are assumed to fail when the maximum principal stress reaches the ultimate tensile strength σ_u. To simplify the discussion we will restrict it to a vessel subjected to internal pressure only, i.e.

$$p_o = 0.$$

From Equations [2.9] and [2.10] the maximum principal pressure stress is always the bore tangential stress; and the maximum principal thermal stress is also the bore tangential stress. If fracture first occurs at the inside surface, it will do so at the internal pressure p_{iu} such that the tangential stress at $r = a$ (Equation [2.10]) is equal to the fracture stress σ_u, i.e. when

[2.11] $$\sigma_u = p_{iu}\frac{\frac{1}{2}k^3+1}{k^3-1}-\frac{1}{2}\beta\frac{k(2k^2-k-1)}{k^3-1}.$$

On rearrangement this gives

$$\frac{p_{iu}}{\sigma_u} = \frac{k^3-1}{\frac{1}{2}k^3+1}+\frac{\beta}{\sigma_u}\frac{k(2k^2-k-1)}{k^3+2}$$

[2.12] $$= \frac{k^3-1}{\frac{1}{2}k^3+1}+\frac{\gamma}{\sigma_u}\frac{k(k-1)(2k^2-k-1)}{k^3+2}.$$

The first term on the right-hand side of [2.12] gives the ultimate pressure in the absence of a temperature gradient. If β and γ are positive the ultimate pressure is increased by the temperature gradient. It will, however, usually be unwise to use this strengthening in design, and the maximum pressure of a vessel should be a chosen fraction of the ultimate pressure in the absence of temperature gradients, i.e.

[2.13] $$\frac{p_{iu}}{\sigma_u} = \frac{k^3-1}{\frac{1}{2}k^3+1}.$$

If the thermal stresses weaken the vessel, i.e. if β and γ are negative, the maximum allowable pressure should be based on Equations [2.12]. The maximum possible values of β and γ are those which will just cause fracture in the absence of internal pressure. This is obtained by putting $p_{iu} = 0$ in equation [2.12] to give

[2.14] $$\max\frac{\beta}{\sigma_u} = -\frac{2(k^3-1)}{k(2k^2-k-1)},$$
$$\max\frac{\gamma}{\sigma_u} = -\frac{2(k^3-1)}{k(k-1)(2k^2-k-1)}.$$

It can easily be shown that if the maximum pressure is given by Equation [2.13] and the maximum temperature difference by Equation [2.14] the stress at the outside surface can never rise to the ultimate stress, so verifying the assumption that fracture occurs at the bore.

3. Yielding of a Ductile Vessel

From Equations [I 3.15], [I 3.16], and [2.5], if

$$\beta/\sigma_y < 3(k-1)/k, \tag{2.15}$$

yielding will begin at the inside surface as the pressure is increased at constant thermal stress, at a pressure

$$\begin{aligned}\frac{\Delta p_y}{\sigma_y} &= \frac{k^3-1}{\frac{3}{2}k^3}+\frac{\beta}{\sigma_y}\frac{2k^2-k-1}{3k^2} \\ &= \frac{k^3-1}{\frac{3}{2}k^3}+\frac{\gamma}{\sigma_y}\frac{(k-1)(2k^2-k-1)}{3k^2}.\end{aligned} \tag{2.16}$$

The yield pressure in the absence of temperature gradients is

$$\frac{\Delta p_y}{\sigma_y} = \frac{k^3-1}{\frac{3}{2}k^3}. \tag{2.17}$$

The maximum temperature difference and heat transfer in the absence of pressure are given by the same equations as for a brittle vessel [2.14]. If these are not exceeded, it is easy to show that Equation [2.15] will always hold and yielding will always begin at the bore.

4. Shakedown

As shown in Part I the shakedown load for a load cycle from full load to zero load is twice the yield load, i.e.

$$\Delta p_s/\sigma_y = 2\Delta p_y/\sigma_y. \tag{2.18}$$

Δp_s is easily obtained from [2.16] and [2.18].

3. CYLINDRICAL VESSELS

If Q is the rate of flow of heat per unit length from the cylinder, then

$$Q/2\pi r = -\lambda dT/dr. \tag{3.1}$$

On integrating with Q constant,

$$T = T_i-\frac{Q}{2\pi\lambda}\ln\frac{r}{a}. \tag{3.2}$$

At $r = b$, $T = T_o$ and

$$Q = -2\pi\lambda\Delta T/\ln k. \tag{3.3}$$

From [3.2] and [3.3]

$$T = T_i-\Delta T\frac{\ln r/a}{\ln k}. \tag{3.4}$$

From the definitions of β and γ, Equations [2.6] and [2.7], and Equation [3.3], β and γ are related for cylindrical vessels by the equation

$$\beta = y \ln k. \tag{3.5}$$

1. The Completely Elastic Vessel

The elastic stresses due to pressure and thermal gradients are obtained from Equations [I 4.8], [I 4.9], and [3.3], and are

$$\sigma_r = -\frac{p_i}{k^2-1}\left(\frac{b^2}{r^2}-1\right)-\frac{p_o k^2}{k^2-1}\left(1-\frac{a^2}{r^2}\right)+\tfrac{1}{2}\beta\left\{\frac{k^2}{k^2-1}\left(1-\frac{a^2}{r^2}\right)-\frac{\ln r/a}{\ln k}\right\}, \tag{3.6}$$

$$\sigma_t = \frac{p_i}{k^2-1}\left(\frac{b^2}{r^2}+1\right)-\frac{p_o k^2}{k^2-1}\left(1+\frac{a^2}{r^2}\right)-\tfrac{1}{2}\beta\left\{\frac{k^2}{k^2-1}\left(1+\frac{a^2}{r^2}\right)-\frac{\ln r/a}{\ln k}-\frac{1}{\ln k}\right\}. \tag{3.7}$$

The longitudinal stress is

$$\sigma_l = \frac{p_i-p_o k^2}{k^2-1}-\beta\left\{\frac{k^2}{k^2-1}-\frac{\ln r/a}{\ln k}-\frac{1}{2\ln k}\right\}. \tag{3.8}$$

2. Fracture of Brittle Materials

Brittle materials are assumed to fail when the maximum principal stress reaches the fracture value σ_u. To simplify the following discussion we restrict it to a vessel with internal pressure only, i.e.

$$p_o = 0.$$

It is readily seen from [3.6], [3.7], and [3.8] that the maximum principal pressure stress is always the bore tangential stress and the maximum principal thermal stress is also the bore tangential stress. If the stress first reaches the fracture stress at the bore, fracture will occur at the pressure p_{iu} given by

$$\sigma_u = p_{iu}\frac{k^2+1}{k^2-1}-\beta\left\{\frac{k^2}{k^2-1}-\frac{1}{2\ln k}\right\}. \tag{3.9}$$

This rearranges to give

$$\begin{aligned}\frac{p_{iu}}{\sigma_u} &= \frac{k^2-1}{k^2+1}+\frac{\beta}{\sigma_u}\left\{\frac{k^2}{k^2+1}-\frac{k^2-1}{2(k^2+1)\ln k}\right\} \\ &= \frac{k^2-1}{k^2+1}+\frac{\gamma}{\sigma_u}\left\{\frac{k^2\ln k}{k^2+1}-\frac{k^2-1}{2(k^2+1)}\right\}.\end{aligned} \tag{3.10}$$

If the pressure and thermal stresses at the bore act in opposite directions the vessel may withstand a greater pressure if thermal stresses are present than if they are absent. However, it will usually be unwise to make use of this in design, because the vessel may have to withstand both pressure and temperature stresses separately as well as together. In the absence of thermal stresses the bursting pressure is

$$\frac{p_{iu}}{\sigma_u} = \frac{k^2-1}{k^2+1}. \tag{3.11}$$

The maximum values of β and γ are those which will cause fracture. These are obtained by putting $p_{iu} = 0$ in Equations [3.10] and one obtains that

$$\max \frac{\beta}{\sigma_u} = -\left\{\frac{k^2}{k^2-1} - \frac{1}{2 \ln k}\right\}^{-1}, \tag{3.12}$$

$$\max \frac{\gamma}{\sigma_u} = -\left\{\frac{k^2 \ln k}{k^2-1} - \frac{1}{2}\right\}.$$

If the stresses are of opposite sign at the inside surface they will have the same sign at the outside surface. The possibility that a vessel designed according to the above principles will fail by fracture at the outside surface has to be considered. The maximum stress at the outside surface is, from [3.6], [3.7], and [3.8], the tangential stress

$$\sigma_t = \frac{2p_i}{k^2-1} - \beta\left\{\frac{1}{k^2-1} - \frac{1}{2 \ln k}\right\}. \tag{3.13}$$

The maximum pressure is given by Equation [3.11]. The maximum temperature is obtained from [3.12]. Putting these into [3.13] we find that the maximum principal stress at the outside surface is

$$\max \sigma_t = \sigma_u\left\{\frac{2}{k^2+1} - \frac{k^2-1-2 \ln k}{k^2-1-2k^2 \ln k}\right\}. \tag{3.14}$$

The quantity in the curly brackets is always less than unity for real values of k, so that failure will not occur at the outside surface. We have here assumed that the maximum allowable thermal stress is computed from Equation [3.12] assuming σ_u to be the tensile strength.

In Figs. 1 to 3 the ultimate pressures obtained from Equations [3.10] for various values of β/σ_u and γ/σ_u are plotted against the radius ratio. It will be noticed that the maximum bursting pressure obtainable according to these equations does not occur for an infinitely thick wall, but for a vessel with a definite wall ratio. Increase in the wall ratio beyond this value makes the vessel weaker.

3. The Yield Pressure for Ductile Materials

It was shown in Part I that the ultimate pressure of a ductile vessel is unaffected by thermal stresses, but the yield pressure and the shakedown pressure are strongly affected.

Substituting the steady state temperature distribution Equation [3.4] into Equations [I 4.11] to [I 4.14], it is easily shown that if

$$\beta/\sigma_y < 2 \ln k, \tag{3.15}$$

yielding will first occur at the inside wall at the pressure

$$\frac{\Delta p_y}{\sigma_y} = \frac{k^2-1}{2k^2} + \frac{\beta}{\sigma_y}\left\{\frac{1}{2} - \frac{k^2-1}{4k^2 \ln k}\right\} \tag{3.16}$$

$$= \frac{k^2-1}{2k^2} + \frac{\gamma}{\sigma_y}\left\{\tfrac{1}{2} \ln k - \frac{k^2-1}{4k^2}\right\}.$$

If

$$\beta/\sigma_y > 2 \ln k, \tag{3.17}$$

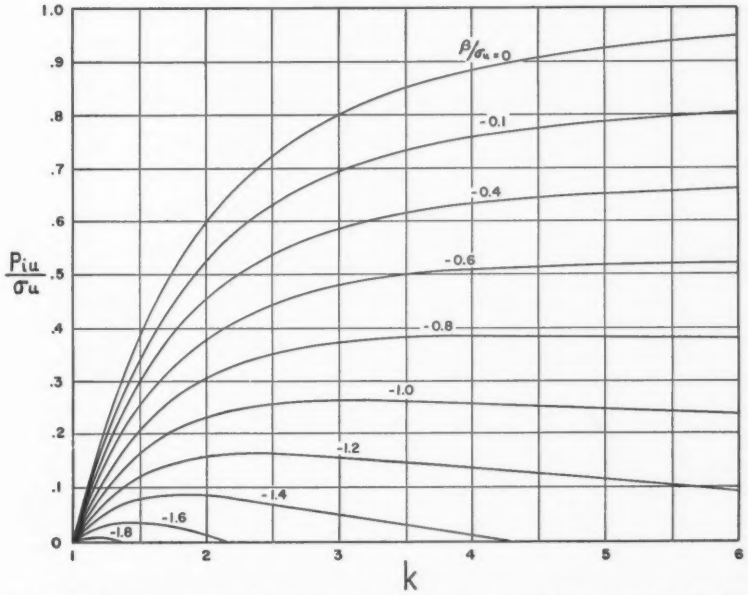

FIG. 1. Bursting pressures of cylindrical vessels made of brittle materials with known steady temperature difference according to Equations [3.10].

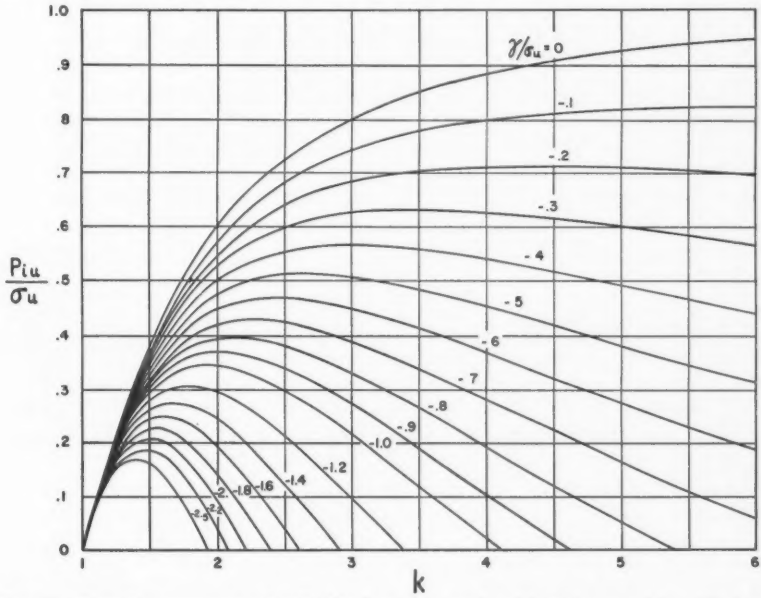

FIG. 2. Bursting pressures of cylindrical vessels made of brittle materials with known steady rate of heat transfer according to Equations [3.10].

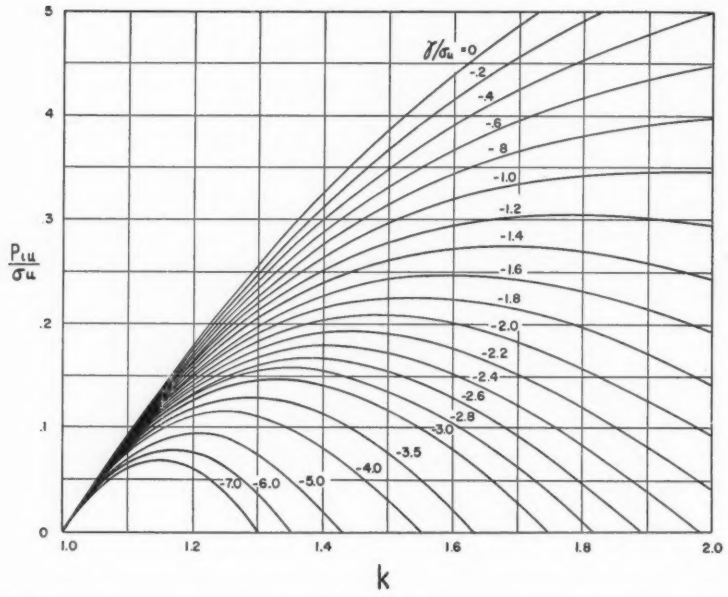

FIG. 3. Bursting pressures of cylindrical vessels made of brittle materials with known steady rate of heat transfer according to Equations [3.10].

yielding will first occur at the outside wall at a pressure

$$\frac{\Delta p_y}{\sigma_y} = \frac{k^2-1}{2} - \frac{\beta}{\sigma_y}\left\{\frac{k^2-1}{4\ln k} - \frac{1}{2}\right\}. \qquad [3.18]$$

Thick-walled high pressure vessels are frequently designed using the yield pressure as the design criterion. The vessel should be able to withstand the effect of both pressure and temperature separately as well as together. In the absence of thermal stress the yield pressure is

$$\frac{\Delta p_y}{\sigma_y} = \frac{k^2-1}{2k^2}. \qquad [3.19]$$

The maximum temperature gradient the vessel will withstand without yielding in the absence of pressure is given by the same Equations [3.12] as for a brittle vessel.

The maximum shear stress at the outside surface occurs when Δp is given by [3.19] and when β is given by [3.12]. The shear stress at the outside surface is, at $r = b$,

$$\sigma_t - \sigma_r = \sigma_y\left\{\frac{1}{k^2} - \frac{k^2-1-2\ln k}{2k^2\ln k - k^2 1+}\right\}. \qquad [3.20]$$

The quantity in brackets on the right-hand side is always less than unity for real values of k so the stress at the outside surface never reaches the yield stress providing conditions [3.12] and [3.19] are met.

4. The Stresses in a Partly Plastic Vessel

The stresses in a vessel which has started yielding from the inside surface, and has yielded to a radius ρ, are easily shown from Equations [I 4.24], [I 4.25], [I 4.26], and [3.4] to be, in the elastic region,

$$[3.21] \qquad \sigma_r = -\frac{1}{2}\sigma_y \frac{\rho^2}{b^2}\left(\frac{b^2}{r^2}-1\right)+\frac{\beta}{2\ln k}\left\{\frac{1}{2}\frac{\rho^2}{b^2}\left(\frac{b^2}{r^2}-1\right)-\ln\frac{b}{r}\right\}-p_o,$$

$$[3.22] \qquad \sigma_t = \frac{1}{2}\sigma_y \frac{\rho^2}{b^2}\left(\frac{b^2}{r^2}+1\right)-\frac{\beta}{2\ln k}\left\{\frac{1}{2}\frac{\rho^2}{b^2}\left(\frac{b^2}{r^2}+1\right)+\ln\frac{b}{r}-1\right\}-p_o,$$

$$\rho \leqslant r \leqslant b,$$

and, in the plastic region,

$$[3.23] \qquad \sigma_r = \sigma_y \ln r/a - p_i,$$

$$[3.24] \qquad \sigma_t = \sigma_r + \sigma_y,$$

$$a \leqslant r \leqslant \rho.$$

By equating at $r = \rho$ the values of σ_r from Equations [3.21] and [3.23], the pressure required to extend the plastic–elastic radius to ρ is shown to be given by

$$\frac{\Delta p}{\sigma_y} = \ln\frac{\rho}{a}+\frac{1}{2}\left(1-\frac{\rho^2}{b^2}\right)-\frac{\beta}{2\sigma_y \ln k}\left\{\frac{1}{2}\left(1-\frac{\rho^2}{b^2}\right)-\ln\frac{b}{\rho}\right\}.$$

This is easily arranged for ease of computation to

$$[3.25] \qquad \frac{\Delta p/\sigma_y - \ln k}{1-\frac{1}{2}\beta/\sigma_y \ln k} = \frac{1}{2}\left(1-\frac{\rho^2}{b^2}\right)+\ln\frac{\rho}{b}.$$

A graph of the right-hand side of Equation [3.25] against ρ/b readily enables the left-hand side to be obtained for any value of ρ/b, or ρ/b to be obtained for any value of the thermal and pressure stresses. Such a graph is given by Prager and Hoge (1). The ultimate pressure is obtained by putting

$$\partial \Delta p/\partial \rho = 0,$$

and one obtains

$$[3.26] \qquad \Delta p_u = \sigma_y \ln k.$$

5. The Shakedown Conditions

A better design criterion than the yield stress is the ultimate pressure and the shakedown load. The shakedown load is that for which unloading occurs completely elastically and leaves a residual stress just equal to the yield stress. The maximum load would be given by either the ultimate pressure or the shakedown pressure whichever is the smaller. The bursting pressure is unaffected by the presence of thermal stress (see Part I). The shakedown load is obtained by applying the results of Part I with a temperature distribution given by Equation [3.4]. From Equations [I 4.19]–[I 4.22], if

$$\beta/\sigma_y < 4 \ln k,$$

shakedown will occur at the bore under the load

[3.27]
$$\frac{\Delta p_s}{\sigma_y} = \frac{k^2-1}{k^2}+\frac{\beta}{\sigma_y}\left\{1-\frac{k^2-1}{2k^2 \ln k}\right\}$$
$$= \frac{k^2-1}{k^2}+\frac{\gamma}{\sigma_y}\left\{\ln k-\frac{k^2-1}{2k^2}\right\}.$$

If
$$\beta/\sigma_y > 4 \ln k,$$

shakedown will occur at the outside radius under the load

[3.28]
$$\frac{\Delta p_s}{\sigma_y} = (k^2-1)+\frac{\beta}{\sigma_y}\left\{1-\frac{k^2-1}{2 \ln k}\right\}$$
$$= (k^2-1)+\frac{\gamma}{\sigma_y}\left\{\frac{1}{\ln k}-\frac{k^2-1}{2}\right\}.$$

Equations [3.27] and [3.28] describe the conditions for shakedown under both thermal and pressure stresses. A vessel will usually have to withstand the thermal and the pressure stresses separately. This sets the maximum pressure as the shakedown pressure in the absence of thermal stress,

[3.29]
$$\frac{\Delta p_s}{\sigma_y} = \frac{k^2-1}{k^2},$$

and the maximum temperature difference as that in the absence of pressure stresses

[3.30]
$$\max \frac{\beta}{\sigma_y} = \left\{\frac{k^2}{k^2-1}-\frac{1}{2 \ln k}\right\}^{-1},$$
$$\max \frac{\gamma}{\sigma_y} = \left\{\frac{k^2 \ln k}{k^2-1}-\frac{1}{2}\right\}^{-1}.$$

If these conditions are fulfilled, the shear stress at the outside surface, if the outer part is elastic, is

$$\sigma_t-\sigma_r = \sigma_y\left\{\frac{2}{k^2}-\frac{k^2-1-2 \ln k}{2k^2 \ln k-k^2-1}\right\}.$$

The quantity in brackets on the right-hand side never reaches unity, so yielding never occurs on the outside for a vessel designed according to the above principles.

In Figs. 4 to 6 the shakedown pressure according to Equation [3.27] is plotted against k for various values of β/σ_y and γ/σ_y. The ultimate pressure given by Equation [3.26] is also plotted. For the smaller values of k the shakedown pressure is greater than the ultimate pressure, and so has no real meaning. However, the values have been drawn in dotted lines because the same graph can be used to calculate the yield pressure from the relation

[3.31]
$$\Delta p_y/\sigma_y = \tfrac{1}{2}\Delta p_s/\sigma_y.$$

4. SUMMARY AND DISCUSSION

The equations derived in Part I for the elastic and plastic behavior of a spherical and a cylindrical pressure vessel subjected to pressure and to an

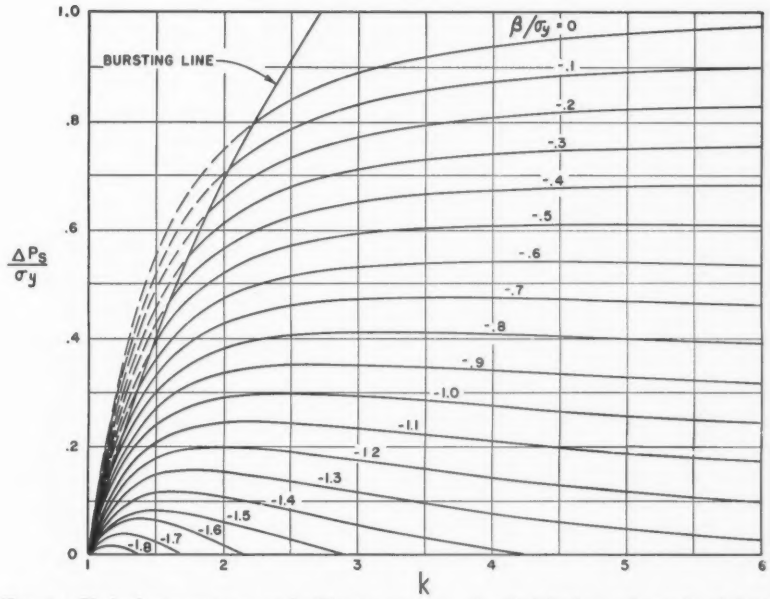

FIG. 4. Shakedown pressure and ultimate pressure of cylindrical vessels made of ductile materials with known steady temperature difference according to Equations [3.27] and [3.26].

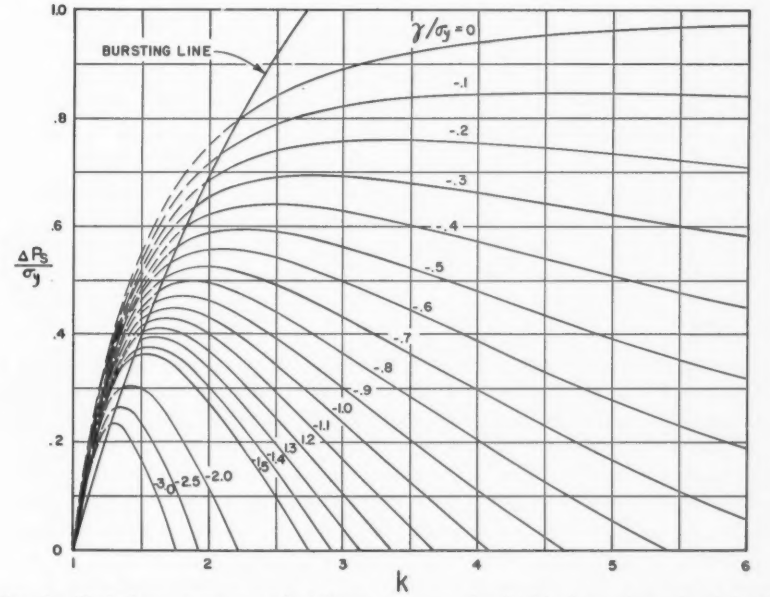

FIG. 5. Shakedown pressure and ultimate pressure of cylindrical vessels made of ductile materials with known steady rate of heat transfer according to Equations [3.27] and [3.26].

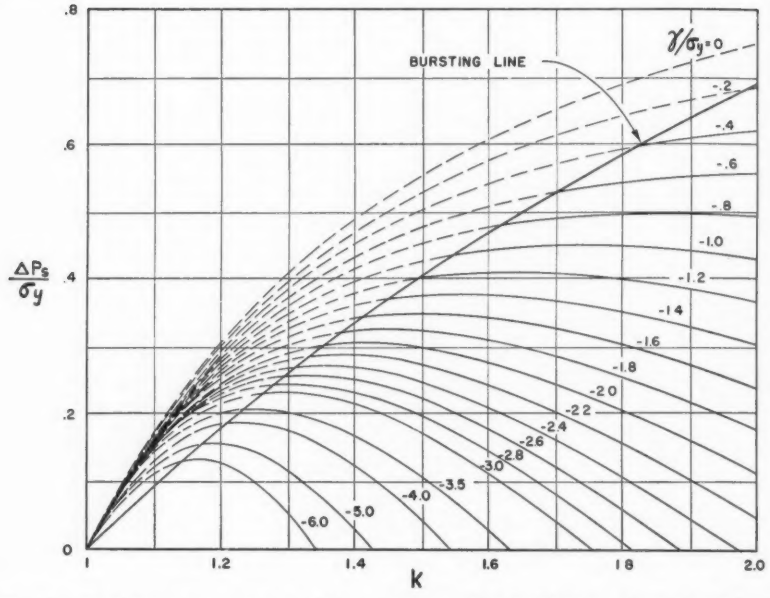

FIG. 6. Shakedown pressure and ultimate pressure of cylindrical vessels made of ductile materials with known steady rate of heat transfer according to Equations [3.27] and [3.26].

arbitrary temperature gradient have been specialized for the temperature gradient obtained in steady state heat flow. The assumptions made in the theory have been listed in Section 1 and discussed in Section 2 of Part I. A general discussion of the problem of design has been given in Section 5 of Part I.

To give an indication of the magnitude of β/σ_y and γ/σ_y we calculate that for a material which has $E = 30\times10^6$ p.s.i., $\sigma_y = 30\times10^3$ p.s.i., $\nu = 1/3$, $\alpha = 20\times10^{-6}$ ° F.$^{-1}$, $\lambda = 0.09$ B.t.u. ft.$^{-2}$ sec.$^{-1}$ for a temperature gradient of 1° F. in.$^{-1}$, then $\beta/\sigma_y = 0.030$ ° F.$^{-1}$, $\gamma/\sigma_y = 0.0319$ B.t.u. ft.$^{-1}$ sec.$^{-1}$.

1. Brittle Vessels

The bursting pressure of vessels made of brittle materials is given by Equations [2.12] and [3.10] for spherical and cylindrical vessels respectively. The bursting pressure of cylindrical vessels is presented graphically in Figs. 1–3. The bursting pressure is greatly affected by the thermal stresses, and it is important to take account of these, particularly in relatively thick walled vessels. Figs. 1–3 will readily enable this to be done. Increasing the wall ratio indefinitely does not make the vessel hold greater pressure for a given temperature difference or rate of heat transfer. There is, for each value of β or γ, a wall ratio which gives the highest value of p_{iu}. This occurs because for a given β or γ the thermal stresses increase as k increases.

2. Ductile Vessels

The ultimate pressure of vessels made of ductile materials is not affected by thermal stresses within the limits of the theory. For vessels which are to be used only a few times and which are not required to have very stable dimensions no account need be taken of thermal stresses. This assumes that the material is perfectly ductile, and since no material is so, the usual precautions for preventing cracking during rapid heating and cooling should be observed.

The yield pressure and shakedown pressure, on the contrary, are strongly affected by thermal stresses. The appropriate equations for spherical and cylindrical vessels are respectively [2.16] and [2.18], and [3.16] and [3.27]. Equations [3.27] are presented graphically in Figs. 4–6, together with the ultimate pressure [3.26]. The yield pressure can be obtained from Figs. 4–6 and Equation [3.31].

Probably the most serious assumption made in this theory is the omission of strain hardening. Most engineering materials strain harden, particularly those such as the stainless steels and monels which are frequently used in making laboratory vessels, and it is certainly conservative to neglect its effect in design. But until the theory is worked out for a strain hardening material any allowance can be only a guess. The theory has neglected also the presence of stress raisers, and possible failure by fatigue caused by stressing below the elastic limit. These may be important in any particular vessel.

It is recommended that in designing a pressure vessel the following conditions should hold.

1. The maximum pressure shall be less than the bursting pressure by an appropriate factor of safety. This safety factor will depend on a number of conditions, and will usually be in the range 3–5.

2. The maximum pressure shall be less than the shakedown pressure by an appropriate factor of safety. This safety factor may be close to unity, but should be somewhat greater to allow for a possible Bauschinger effect.

ACKNOWLEDGMENT

The author's thanks are due to Mr. G. Kell for help in computing and drawing graphs.

REFERENCES

1. PRAGER, W. and HOGE, P. G. Theory of perfectly plastic solids. John Wiley & Sons, Inc., New York. 1951. p. 106.
2. WHALLEY, E. Can. J. Technol. 34: 268. 1956.

PROPERTIES OF VACUUM AS A SWITCHING AMBIENT[1]

By Mohamed Khalifa[2]

ABSTRACT

Recommendations for the manufacture of vacuum circuit breakers are given based on the study of the dielectric strength of vacuum, its effect on the amount of arc erosion, and its rate of dielectric recovery after arc interruption. A practicable method for raising the dielectric strength of vacuum is described and the arc erosion in vacuum is for the first time compared with that in atmospheric air. Also a new circuit for synthetic testing of vacuum circuit breakers and similar types of breakers is described.

INTRODUCTION

Vacuum switches have shown an impressive performance in the handling of low ranges of power up to the order of 10 amperes and hundreds of volts (9, 14, 15, 24, 25). In the higher ranges, however, the life of vacuum switches and circuit breakers has been limited to a few thousand operations (5, 10, 14). Therefore, a systematic study of the properties of vacuum as a switching ambient was undertaken to compare the rate of arc erosion in vacuum with that in atmospheric air. Also, the rate of dielectric recovery of vacuum after arc interruption was assessed, and a believed new method for improving its dielectric strength was evolved.

DIELECTRIC BREAKDOWN OF VACUUM

Several authors have accounted for the initiation of the dielectric breakdown of vacuum by the electron field emission from the microscopic protuberances on the cathode surface (4). On the other hand, Janitzky proposed that the electrons and positive ions contributing to the discharge in vacuum are liberated from the gases occluded in the surface layers of the electrodes (12). Also, Cranberg postulated that a clump of metal loosely adhering to either electrode, but in electrical contact with it, might be detached by electrostatic repulsion, traverse the high voltage gap, and impinge on the other electrode. The immense pulse of energy delivered to the limited area would result in raising the temperature of the area high above the boiling point and ultimately lead to the breakdown of the gap in the form of a metal vapor arc (7).

It is thus noticed that the dielectric breakdown of vacuum depends upon the microroughness of the electrode surfaces, and the gases occluded in their surface layers. The breakdown voltage also depends upon the electrodes' material, shape, and separation (7). A relation that was proposed for the breakdown voltage V as a function of the distance d between parallel plane electrodes is:

$$V = kd^{\frac{1}{2}}$$

where k is a constant depending upon the electrode material and surface conditions.

[1]*Manuscript received March 20, 1956.*
Contribution from the Department of Electrical Engineering, University of Toronto, Toronto, Ontario.
[2]*Now at Faculty of Engineering, University of Cairo, Cairo, Egypt.*

Conditioning of the Electrode Surfaces

To achieve a higher breakdown voltage for the same electrode material, shape, and separation, the surface conditions of the electrodes may be improved by heating the electrodes at high temperatures under vacuum (8, 11, 21), allowing a glow discharge between them in a rarefied hydrogen atmosphere (1, 3, 8, 11), or simply by running a series of sparks between them at a suitable voltage under vacuum (2, 16, 26). Each of these methods of conditioning has its relative merits. The repeated sparking between the electrodes needs the minimum extra facilities. It is not, however, as effective in improving the dielectric strength of vacuum as the other two methods. Further, its improvement usually decays in a short time of about 24 hours (20, 22). The glow discharge in hydrogen gives satisfactory results only if the hydrogen is very pure. Moreover, this treatment may lead to injurious embrittlement of the metal and an increase in its electrical resistance (23). Heating the electrodes in vacuum has shown good results almost devoid of these objections. The method of heating in vacuum that has hitherto been adopted is to heat the electrodes in position after assembly and evacuation of their container. This requires special connections and leads through the container's walls, which may not be needed any more after the electrodes are conditioned. Further, this method heats all the metal parts to about the same temperature and period, which will lead to deterioration of the mechanical and electrical properties of some parts of the mechanism which are made of different metals.

A Practicable Method for Conditioning the Electrodes

After the electrodes are polished and thoroughly cleaned, they are put into a commercial induction furnace, which is then evacuated to the hardest possible vacuum, better than 10^{-2} mm. of mercury. After the vacuum is achieved, the electrodes are heated up to a specified temperature for a specified period, according to their nature. When the electrodes have cooled to the room temperature while the vacuum is maintained, a dry air leak is introduced into the furnace, and the electrodes are transferred to their permanent container, care being taken to keep them clean.

This method of conditioning was investigated with parallel electrodes made of ordinary machine steel. This material has previously shown almost the highest breakdown voltage for a given vacuum gap (1, 7). In the present work, the electrodes were heated for one hour in a vacuum of 10^{-2} mm. of mercury at temperatures of 600, 700, 800, 900, and 1000° C. After they were transferred to their permanent container, which was then evacuated down to 8×10^{-6} mm. of mercury, a few sparks were allowed between them at a gradually increasing d-c. voltage. For the same electrode separation, the breakdown first occurred at a relatively low voltage and then gradually increased until a ceiling breakdown voltage was reached. The results obtained for gaps of 0.25 and 0.5 mm. are compared with the ceiling voltages achieved without conditioning in Fig. 1.

It is noticed that heating the electrodes up to 1000° C. for one hour under vacuum according to the present method improved the dielectric strength of the vacuum gap more than four times. This may be ascribed to the smoothing

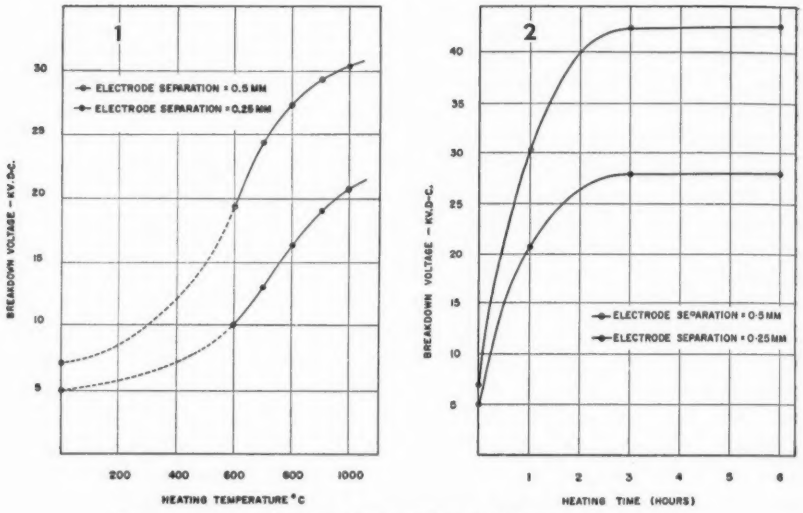

FIG. 1. Effect of heating the electrodes at different temperatures.
FIG. 2. Effect of the heating time at 1000° C.

down of the microscopic protuberances of the electrode surfaces (11, 21), as well as to partial denuding of their surface layers of occluded gases (12). The rate of rise of the dielectric strength with temperature increased appreciably between the temperatures of 700 and 900° C., Fig. 1. This is probably due to the increase in the rate of diffusion of the occluded gases in this temperature range, which corresponds to the transition from the body centered α-phase to the face centered γ-phase of iron. The subsequent reduction in the rate of rise of the dielectric strength for temperatures higher than 900° C. probably occurred because the degassed surface layer of the electrodes became thicker than that penetrated by the arc roots during the breakdowns. The slight increase in the dielectric strength may have been only due to the improvement of the surface microroughness and the further reduction of the residual gas content in the surface layer.

A further increase in the dielectric strength of the vacuum gap was achieved by heating the electrodes at 1000° C. for longer periods, Fig. 2. With the present electrode dimensions of the order of 3 in., three hours showed almost the full improvement that could be achieved by this conditioning method. The breakdown voltage for the same gap was increased to about six times its value before conditioning.

To study the decay of this conditioning effect, the breakdown voltage was measured for the same gap at intervals of about two hours over a period of 54 hr. This test was carried out just after the electrodes were conditioned at 1000° C. for periods of one and six hours, Fig. 3. It is noticed that the decay is much slower than was previously anticipated (16, 20, 22). Both curves show mainly two superimposed exponential functions, which implies that two main

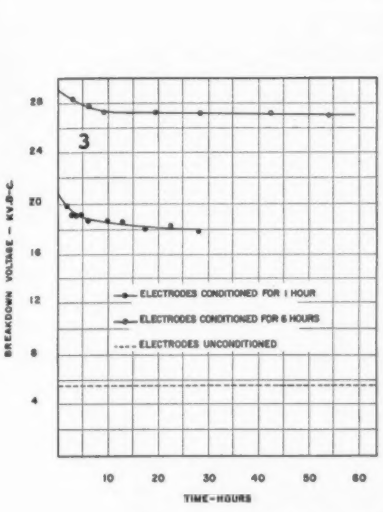

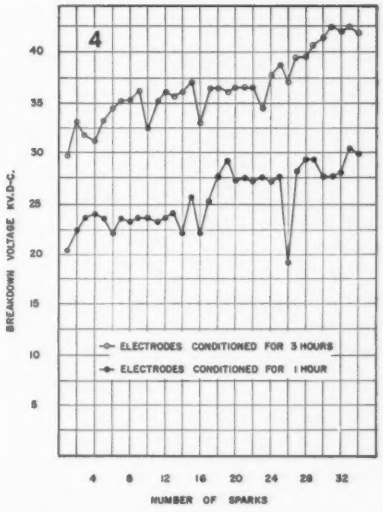

FIG. 3. Decay of the conditioning effect.
FIG. 4. The dielectric strength of a vacuum gap 0.5 mm. long.

phenomena contribute to the reduction in the breakdown voltage with time. These probably are:

(1) Contamination of the surface monomolecular layers of the electrodes with the gases that might have been adsorbed while the electrodes were being transferred from the furnace to the container. This chemical process is likely to have the shorter time constant.

(2) Diffusion of the absorbed gases from the interior of the electrodes to the surface layers, which probably has the longer time constant.

While these decay curves were being plotted, the vacuum in the container of the electrodes was maintained at about 10^{-2} mm. of mercury, and was improved to 8×10^{-6} mm. of mercury only when the readings were taken. This procedure of noncontinuous maintenance of a hard vacuum in the container probably caused the improvement in the dielectric strength to decay faster than is anticipated in practice. Nevertheless, the observed rate of decay of the improvement achieved by six-hour conditioning was about 0.37% per day. This rate might have been considerably reduced by extending the period of conditioning. Furthermore, to compensate for this decay, a series of about 100 sparks may be run between the electrodes at intervals of one or two months. Thus, the dielectric strength may be maintained at a fairly constant value.

Consistency of the Dielectric Strength of Vacuum

The dielectric strength of any medium is the maximum voltage that can be imposed between two electrodes set a unit length apart and immersed in the medium. For most dielectrics other than vacuum, the breakdown voltage for a certain gap is a fairly definite value. In vacuum, however, the breakdown

criterion primarily depends upon the electrode materials and surface conditions. The magnitude of the breakdown voltage for a certain gap is sensitive to variation in the surface microroughness. As each spark results in the melting of a part of a protuberance and a change in the contamination and the amount of adsorbed gases in its area, the magnitude of the breakdown voltage is not expected to be identical for each spark. Generally, successive sparks do not occur at the same pair of points on the surfaces of the parallel plane electrodes. They take place at the points having the most favorable conditions for breakdown.

The curves in Fig. 4 display the breakdown voltages for successive sparks between the electrodes 0.5 mm. apart after they are conditioned for one and three hours. It is noticed that the inconsistency in the breakdown voltage was reduced with repeated sparking, and also with the longer period of conditioning. Sometimes a spark occurred at a lower voltage than did the previous sparks. This was probably due to a clump as proposed by Cranberg (7).

On the other hand, the application of a suitable voltage across the vacuum gap will not result in its breakdown even if the voltage is maintained for a very long time. A gap of 0.5 mm. could stand a voltage of 29.7 kv. (d-c. and peak value a-c.) without breakdown for more than 30 min. A further safety factor of about 2 may be suitable in assessing the working voltages of vacuum switches. This factor of safety may cater for the time effect on the dielectric strength of vacuum. It may be inferred from this that a contact separation of 6 mm. in a vacuum circuit breaker may be suitable for a working voltage of 115 kv., as compared to 100 mm. in compressed air circuit breakers and 700 mm. in air load-interrupters.

ARC EROSION IN VACUUM AND IN ATMOSPHERIC AIR

It has been generally accepted that arc erosion is considerably greater in vacuum than in atmospheric air (1, 5), although it has not been checked. In this work, the same arrangement of the test equipment was employed in measuring the amount of arc erosion in vacuum and in atmospheric air, Fig. 5.

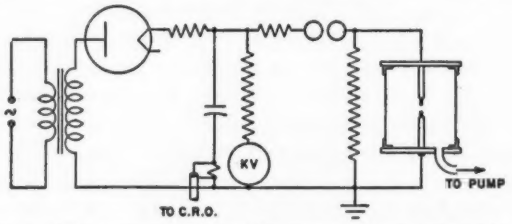

FIG. 5. The arrangement used for measuring the arc erosion.

A current wave, Fig. 11, was generated with an adjustable peak and duration for the same generator voltage of 40 kv. This voltage was maintained constant to eliminate any effect on the erosion that might have taken place because of the discharge of the capacitance between the electrodes at the beginning of the arc (18).

From measurements made at various currents, it was found that erosion could be expressed as a function of the charge flowing through the arc discharge. Fig. 6 shows the amount of erosion per arcing between steel electrodes 0.25 mm. apart, in both vacuum and atmospheric air.

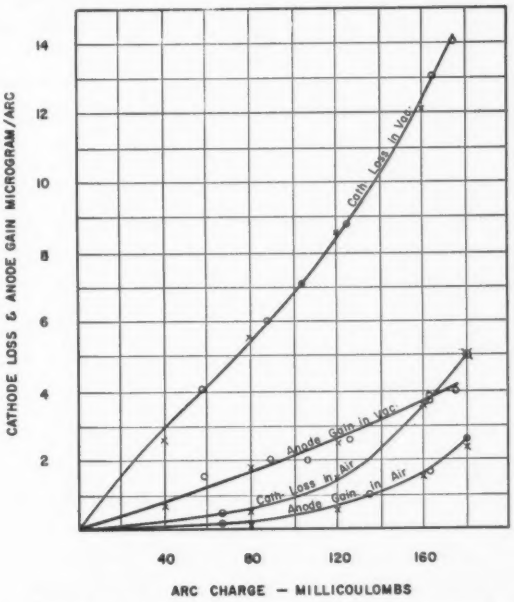

FIG. 6. Arc erosion in vacuum as compared to that in atmospheric air.

Although the anode spot was boiling and the anode metal was evaporating from it during the arc discharge, there was a net gain in the weight of the anode, observed both in vacuum and in atmospheric air. This may be due to the condensation of the metal vapor on the relatively cool parts of the anode.

Over the range of arc current and duration studied, i.e. up to 217 amp. and 4 msec., the following empirical relations were noticed to agree fairly closely with the measurements:

$$\begin{aligned}
&\text{cathode loss in vacuum} = 5.02\times10^{-2}\ C^{1.074}\ \mu\text{gm./arcing},\\
&\text{anode gain in vacuum} = 2.91\times10^{-2}\ C^{0.94}\ \mu\text{gm./arcing},\\
&\text{cathode loss in air} = 2.48\times10^{-6}\ C^{2.8}\ \mu\text{gm./arcing},\\
&\text{anode gain in air} = 1.15\times10^{-6}\ C^{2.8}\ \mu\text{gm./arcing},
\end{aligned}$$

where C = the arc charge in millicoulombs measured as the area under the curve in the current oscillograms.

The calculated points are shown as x on the curves in Fig. 6. These relations show that the cathode loss in vacuum is considerably greater than in atmospheric air only in the low ranges of arc charges, up to about 40 millicoulombs. With increase of the arc charge, however, the ratio of the arc erosion in vacuum

to that in air decreases rapidly from 11 at 40 millicoulombs to about 3 at 170 millicoulombs. Equal amounts of erosion in vacuum and atmospheric air are anticipated by the above relations for arc charges higher than about 350 millicoulombs. This may be because the arc will then be occurring almost entirely in an atmosphere of metal vapor in both cases. This corroborates what was previously concluded regarding equal arc erosions in oil and atmospheric air (27).

The amount of arc erosion is greater in vacuum than in atmospheric air at the lower arc charges, probably because, in the latter, the ionization of the arc column is partially provided by the air molecules, the arc column is cooled by the surrounding air, and the rate of lateral diffusion of the arc products is considerably less than in vacuum.

It is of interest to state that the rates of arc erosion in the vacuum cited above were measured from steel electrodes conditioned according to the aforementioned method. It was observed that this conditioning reduced the rates of arc erosion to about 50%. This may be due to degassing of the electrodes and consequent minimizing of the amount of gases evolved at the cathode spot during the arc. These gases may augment the metal loss in the form of molten drops and solid chunks.

DIELECTRIC RECOVERY OF VACUUM AFTER ARC INTERRUPTION

The dielectric recovery of vacuum was studied by means of a vacuum circuit breaker, Fig. 7, and a new synthetic-testing circuit developed for the purpose.

The main contacts of the circuit breaker were made of copper. A pair of arcing contacts made of steel were set in parallel with the main contacts. Such an arrangement may considerably extend the life of vacuum circuit breakers

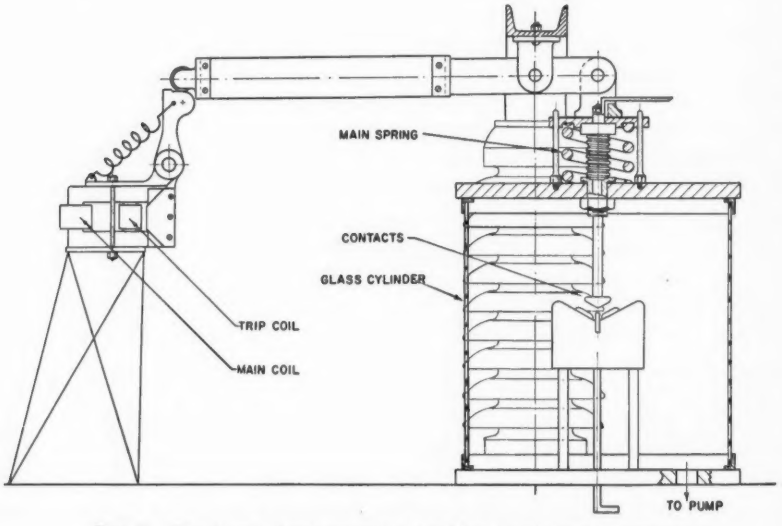

FIG. 7. The circuit breaker used in studying the dielectric recovery.

by releasing the main contacts from pitting caused by the arcs, and thus maintaining a low contact resistance between their surfaces. The breaker was held in the closed position by means of an electromagnet, Fig. 7. To trip the breaker, a tripping signal was applied to an exciting coil in the magnetic circuit of the electromagnet. When the breaker was fully opened, the separation between the arcing contacts was 0.35 cm. and that between the main contacts was 0.75 cm. The weight of the moving parts of the breaker's mechanism was minimized, and the friction was reduced by using a ball bearing at each fulcrum. This resulted in a speed of contact separation of 121 cm. per sec., at the instant when the arcing contacts separated. The dead time between the application of the tripping signal to the exciting coil and the instant of separation of the arcing contacts was 16 msec.

The testing circuit provided the circuit breaker with a current wave in the form of half a cycle of 52 c.p.s. followed by a voltage wave in the form of a decaying cosine curve of a frequency 5140 c.p.s., as shown in Fig. 12, *a* and *b*. The corresponding relations are:

$$i = Ie^{-55.3t}\sin(328t),$$
$$v = Ve^{-325t}\cos(3.23\times10^4t),$$

where t is the time in seconds.

The amplitude of the current wave could be varied up to 217 amp., and the first peak of the voltage wave could be adjusted up to 40 kv. The instant of contact separation of the circuit breaker was so adjusted as to precede the end of the current wave by 2.8 msec. This part of the current wave flowed in the form of an arc between the arcing contacts. The instant of application of the voltage wave followed the end of the current wave after a period that was varied between 1.25 and 96 μsec.

For each setting of the current amplitude and the delay of the voltage wave, the first voltage peak was adjusted to the value at which about 10 shots were taken and arc reignition occurred in 50% of them. Such a voltage magnitude was considered as the recovery voltage of the breaker after the corresponding delay. The results obtained are displayed in Figs. 8, 9. The deviation between the voltages corresponding to 100% breakdown and 100% nonbreakdown was about 1 kv.

It is noticed that the rate of dielectric recovery of vacuum in the first few microseconds after arc interruption is of the order of 1 kv./μsec. for arc currents of the order of 100 amp., as compared with the order of 50 v./μsec. in the case of atmospheric air (19). Moreover, the effective deionization of the vacuum gap seems to take place in a period of the order of 1 msec., after which the breakdown voltage may be considered as solely dependent upon the speed of contact separation. This deionization period is about one order of magnitude less than that of the air blast.

The rate of dielectric recovery of vacuum was higher when the voltage and current waves had opposite polarities than when they were of the same polarity. The former case is the one which takes place in the field when an a-c. inductive current is interrupted. The subsequent rate of rise of the restriking voltage imposed by the power network upon the interrupting breaker usually ranges

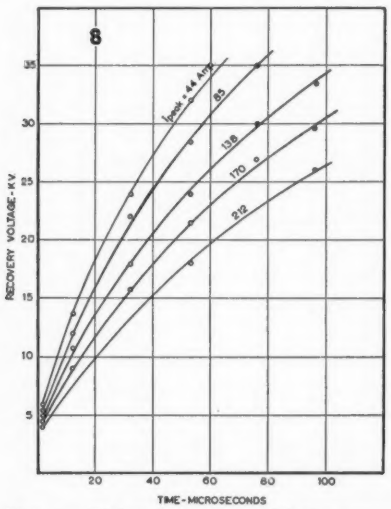

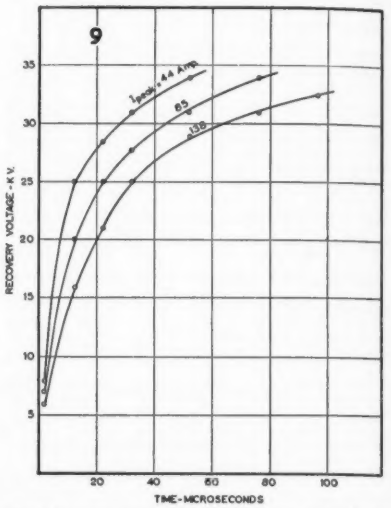

FIG. 8. Dielectric recovery with the current and voltage waves having the same polarity.
FIG. 9. Dielectric recovery with the current and voltage waves having opposite polarities.

between 300 and 1500 v./μsec. (17), with an average of about 500 v./μsec. (6, 13). Therefore, the vacuum circuit breakers should be capable of interrupting a-c. inductive currents of the above order of magnitude under the conditions usually envisaged in practice without arc restriking. On the other hand, these breakers may not be recommended for switching heavy d-c. currents, because their high rates of deionization and the corresponding rapid arc extinction might result in voltage stresses injurious to the system insulation. The rapid effective deionization of the vacuum gap qualifies the vacuum circuit breaker for interrupting a-c. capacitive currents such as those encountered in dropping long lines and capacitor banks. In the case of heavy short circuits, however, the rate of dielectric recovery of vacuum may be reduced as implied by Figs. 8, 9, unless special arrangements are made, as discussed subsequently.

PROPOSALS FOR COMMERCIAL VACUUM CIRCUIT BREAKERS

To maximize the life of vacuum circuit breakers in the high current ranges, the deleterious effects of the arc may be considerably reduced by the following measures:

(1) The main contacts may be supplemented with arcing contacts, thus releasing the main contacts from arc pitting.

(2) The contact materials are to be chosen judiciously. To minimize the temperature rise of the breaker, the material for the main contacts should be chosen such that $\rho/(\delta\lambda\alpha)$ is to be minimum, where:

ρ = the volume resistivity of the contact material,
δ = its density,
λ = its specific heat,
α = its thermal conductivity.

According to this criterion, the best material for the main contacts is copper. To reduce its surface resistance, silver plating may be used.

For the arcing contacts, the breakdown voltage for a certain vacuum gap should be maximum, and the metal's total heat of evaporation should be maximum. The metals recommended are steel, tungsten, and molybdenum.

(3) When more than one metal is used for the contacts, the contact separations must be coordinated so that at any position of the breaker's contacts, the breakdown voltage of the gap between the arcing contacts should be less than that of the gap between the main contacts. This may be readily achieved by the aid of the corresponding breakdown characteristics.

(4) The arc roots may be moved over the surfaces of the arcing contacts by means of a magnetic field. The field may be produced by introducing a coil in series with the contacts and incorporating it in the breaker, or by embedding a permanent magnet inside the contacts.

(5) The different elements of the breaker should be rigorously degassed just before assembly and during the evacuation before the container is sealed. Also a getter may be used to achieve and help in maintaining a hard vacuum.

(6) The arcing encountered in the different switching operations usually carried out in the field may be enough to compensate for the decay envisaged in the dielectric strength of the gap between the arcing contacts. If these switching operations were not sufficiently frequent, however, more operations may be necessary to keep the dielectric strength almost at its initial value.

(7) The speed of contact separation should be increased to the highest practicable value by minimizing the weights of the moving parts and by arranging a number of breaks in series per pole.

(8) The life of vacuum circuit breakers may be further extended by arranging the container with a vacuum-tight window. After the end of the life of the arcing contacts, the contacts may thus possibly be changed. This particular item of the maintenance needs special facilities not readily available in the field. Therefore, the pole out of order might then be replaced by a standby unit.

(9) Because of the small contact separations in vacuum circuit breakers, the sizes of the containers may be so small that their external flashover distances may not be adequate for the working voltages. Therefore, the containers may have to be immersed in an insulating medium such as transformer oil.

CONCLUSIONS

A practicable method for improving the dielectric strength of a vacuum gap has been developed, and is believed to be new.

The arc erosion in vacuum is much higher than that in atmospheric air for small arc charges. The ratio, however, decreases rapidly with increase in the arc charges and ultimately approaches unity.

The rate of dielectric recovery of vacuum is much higher than that of atmospheric air. The former is of the same order of magnitude as the rates of rise of restriking voltages usually experienced in practice.

ACKNOWLEDGMENT

The author is indebted to Professor G. F. Tracy, Professor V. G. Smith, and Dr. G. R. Slemon for their advice and stimulation during the different stages of the work and in the preparation of this paper. He also appreciates the encouraging supervision of Dr. A. Greenwood during the first year of the work.

APPENDIX. A NEW CIRCUIT FOR SYNTHETIC TESTING OF CIRCUIT BREAKERS

The circuit employed in assessing the dielectric recovery of vacuum may be modified and used for synthetic testing of any circuit breaker which can interrupt its arc at the first current zero. The current and voltage sources are simple L–C circuits, Fig. 10. The thyratron Th_1 causes only one half-cycle of the current to flow through the breaker to be tested.

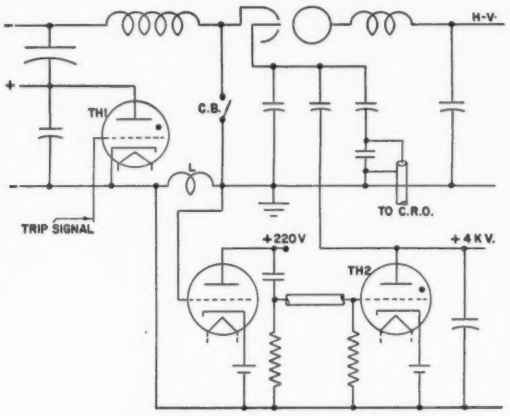

FIG. 10. The circuit arranged for synthetic testing.

To trip the voltage source at the end of the current wave, the voltage that appears across the pickup coil L, Fig. 13a, is introduced into a class C amplifier of which the output, Fig. 13b, is differentiated to the form shown in Fig. 13c. The positive peak, which occurs at the end of the current wave, is employed to trigger the thyratron Th_2, which sends the tripping signal to the trigation of the voltage source. The total delay time between the end of the current wave and the initiation of the voltage wave was measured to be 1.25 ± 0.25 μsec. Possibly ionizing irradiation of the trigation might decrease this delay.

For synthetic testing of breakers, the voltage source is connected as shown in Fig. 10 and thus the generated wave will have the form:

$$v = V(1 - \cos \omega.t)e^{-dt},$$

which has a definite rate of rise of the front and can be adjusted to the values anticipated in practice.

PLATE I

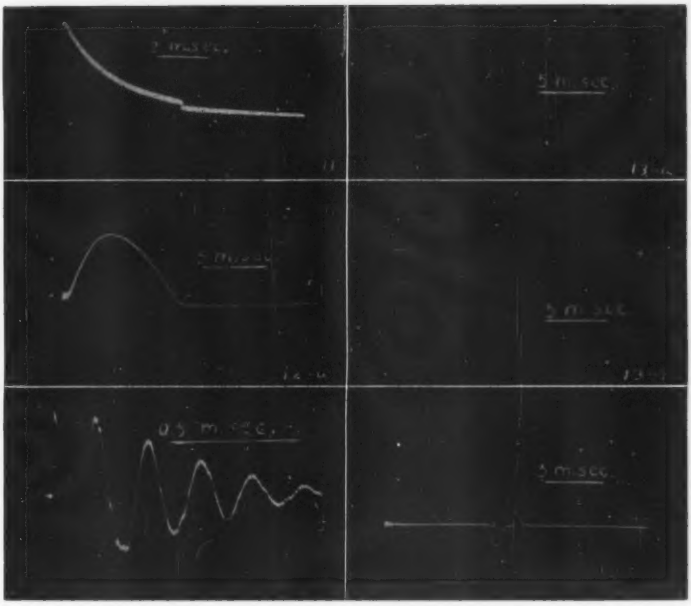

FIG. 11. The current wave used in measuring the arc erosion.
FIG. 12. The waves used in studying the dielectric recovery.
(*a*) The current wave.
(*b*) The voltage wave.
FIG. 13. The signals used for synchronizing the current and voltage sources.
(*a*) The voltage across the pickup coil *L*.
(*b*) The output of the amplifier.
(*c*) The output after being differentiated.

REFERENCES

1. ANDERSON, H. Elec. Eng. 54: 1315. 1935.
2. BEAMS, J. Phys. Rev. 43: 382. 1933.
3. BENNETT, W. Phys. Rev. 37: 582. 1931.
4. BOYLE, W., KISLIUK, P., and GERMER, L. J. Appl. Phys. 26: 720. 1955.
5. BROWNE, T. Westinghouse Research Rept. July, 1946.
6. CHRISTIE, J., LEYBURN, H., and FENN, R. Proc. Inst. Elec. Eng. (London), A, 709. 1955.
7. CRANBERG, W. J. Appl. Phys. 23: 518. 1952.
8. DENHOLM, A. Ph.D. Thesis, University of Glasgow, Glasgow, Scotland. 1954.
9. ELECTRICAL WEST, 78. August, 1955.
10. ELECTRICAL WEST, 72. July, 1955.
11. EYRING, C., MACKEOWN, S., and MILLIKAN, R. Phys. Rev. 31: 900. 1928.
12. JANITZKY, A. Z. Physik, 31: 277. 1925.
13. JOHANSEN, O. CIGRE Rept. No. 104. 1952.
14. JUBITZ, W. Siemens-Z. 10: 420. 1930.
15. KLING, W. Gen. Elec. Rev. 38: 525. 1935.
16. KOLLER, R. Trans. Am. Inst. Elec. Engrs. 65: 597. 1946.
17. KURTH, F. CIGRE Rept. No. 128. 1948.
18. LLEWELLYN JONES, F. Proc. Inst. Elec. Eng. (London), I, 96: 305. 1949.
19. MCCANN, G. and CLARK, J. Trans. Am. Inst. Elec. Engrs. 62: 45. 1943.
20. MILLIKAN, R. and EYRING, C. Phys. Rev. 27: 51. 1926.
21. MILLIKAN, R. A. and SHACKELFORD, B. E. Phys. Rev. 15: 239. 1920.
22. MYERS, C. and RAATZ, W. Report by California Institute of Technology. February, 1955.
23. NORTON, F. and MARSHALL, A. Trans. Am. Inst. Mining Met. Engrs. 156: 351. 1944.
24. RANKIN, W. and HAYWARD, C. Elec. World, 103: 552. 1934.
25. TEARE, W. Gen. Elec. Rev. 41: 280. 1938.
26. TRUMP, J. and VAN DE GRAAFF, R. J. Appl. Phys. 18: 327. 1947.
27. WILSON, W. Am. Inst. Elec. Engrs. Paper No. 215. 1955.

THE OXIDATION, DECOMPOSITION, IGNITION, AND DETONATION OF FUEL VAPORS AND GASES

XXIX. THE ROLE OF NUCLEI IN THE IGNITION BY COMPRESSION OF GASEOUS HEPTANE–AIR MIXTURES: FIRST PAPER[1]

By R. O. King[2] and A. B. Allan[3]

ABSTRACT

The temperature of a special plug protruding into the combustion chamber of a C.F.R. carburetor engine was adjustable to provide a surface at temperatures higher, lower, or equal to that of the exhaust valve whether it was uncooled or sodium cooled. Compression ratio was always adjusted for maximum power output. This optimum value varied with the temperature of the exhaust valve as well as with mixture strength. These factors are dependent variables. The experimental results support the view that mixtures richer than 25% weak were ignited by nuclei of finely divided carbon derived from pyrolysis of the heptane and that the inflammability of the nuclei increased over the mixture range 25% to 40% weak owing to their absorption of aldehydes. The rate of formation of aldehydes increased as mixture strength was further reduced and it appears that nuclei of ignition then became resinous substances, formed of the condensation products. Further experiments with weak mixtures are to be described in a second paper on the subject of this Part.

INTRODUCTION

Hydrogen in mixtures with air was used as the fuel for experiments with a C.F.R. engine described in Part XXVII (7) and ignition by compression did not occur even at values of compression ratio rising to 12: 1 unless nuclei of finely divided carbon were provided by the decomposition of lubricating oil vapor.

Paraffin fuels differ from hydrogen in that they provide nuclei of ignition at values of the compression ratio which, if speed is constant, depend mainly on the factors of mixture strength and the temperature attained by the exhaust valve. Experiments carried out with the C.F.R. engine in the conditions required to determine the effect of these factors are described in this Part. The fuel used was heptane as supplied by Phillips Petroleum Company for the ASTM method of knock rating. Operating conditions were as adopted for the experiments with acetaldehyde and diethyl ether Part XX (2), and the subsequent experiments with heptane, hexane, and pentane, Part XXI (6) and Part XXIV (3), namely: engine speed 400 r.p.m., air supply temperature 50° F.; engine coolant water 100° F. at the outlet from the cylinder head jacket and approximately 97° F. at the entrance to the jacket of the cylinder barrel; a subnormal charge density, 64% of normal was used.

[1]*Manuscript received May 9, 1956.*
Contribution from Defence Research Board, Ottawa, Canada, in association with the Department of Mechanical Engineering, University of Toronto, Toronto, Canada.
[2]*Scientific Officer-in-Charge, Combustion Research, Defence Research Board, Ottawa, Canada, and Special Lecturer, Mechanical Engineering, University of Toronto.*
[3]*Scientific Officer, Defence Research Board.*

I. EXPERIMENTAL ARRANGEMENTS

The standard shrouded inlet valve of the engine was replaced by an exhaust valve in order to eliminate a swirl in the mixture entering the cylinder. The engine was direct connected to a d-c. generator arranged as a swinging field dynamometer. Speed was maintained at 400 r.p.m. by adjustment of load.

The air supply was refrigerated to remove excess moisture in order to avoid ice formation in the carburetor. The temperature of the air was then raised to 50° F. prior to its supply to the carburetor. Engine cooling was by a thermostatically controlled water circulation.

The subnormal charge density was used in order to enable the engine to tolerate the degree of detonation caused by the compression ignition of mixtures richer than 25% weak. It was obtained by fitting a choke tube to the standard C.F.R. carburetor, as described in Part XIX (5, pp. 31 and 40). The choke tube required for a reduction of charge density to 64% of normal was $\frac{1}{4}$ in. only in inside diameter because of the low engine speed of 400 r.p.m. The pressure in the choke tube during the induction stroke was found by a separate experiment to be approximately half an atmosphere. Vaporization of the fuel was promoted accordingly and further by the heat of compression, by that of the residual gas, and by heat absorbed from hot surfaces in the combustion chamber.

Abbreviations used in subsequent text are: C.R. for compression ratio, M.S. for mixture strength, I.T.E. for indicated thermal efficiency, and t.d.c. for top dead center. Stoichiometric mixtures are described as "correct" in the text and as C.C.M. on graphs. Mixture strength is described as per cent weak or rich according to the percentage by which the concentration of fuel in the mixture with air is less or more than is required for a correct mixture.

II. METHOD OF EXPERIMENT

The method was based on the use of the "temperature plug" illustrated by Fig. 1. This device will be described as a "T.P". It was of mild steel machined from solid stock and contained an air cooling device and the leads to a thermocouple for the measurement of the temperature of the rounded end, which protruded slightly into the combustion chamber. The temperature attained by that end when not cooled was from 300° to 400° F. higher than that of the exhaust valve, depending on the variation of heat load with mixture strength. Cooling air was supplied from a high pressure source and provision was made for regulation of the flow in a manner to maintain the temperature of the rounded end at any particular value lower than that attained when it was not cooled.

The C.R. required for ignition was always adjusted to the value at which maximum combustion pressure occurred at the time necessary for the development of maximum power output. This time, taken in degrees of crank angle, varied little from 10° after t.d.c. The corresponding C.R. is the optimum value and is described in subsequent text as the Opt. C.R. Thus the end of the "delay period" required for nuclear ignition was fixed and consequently the

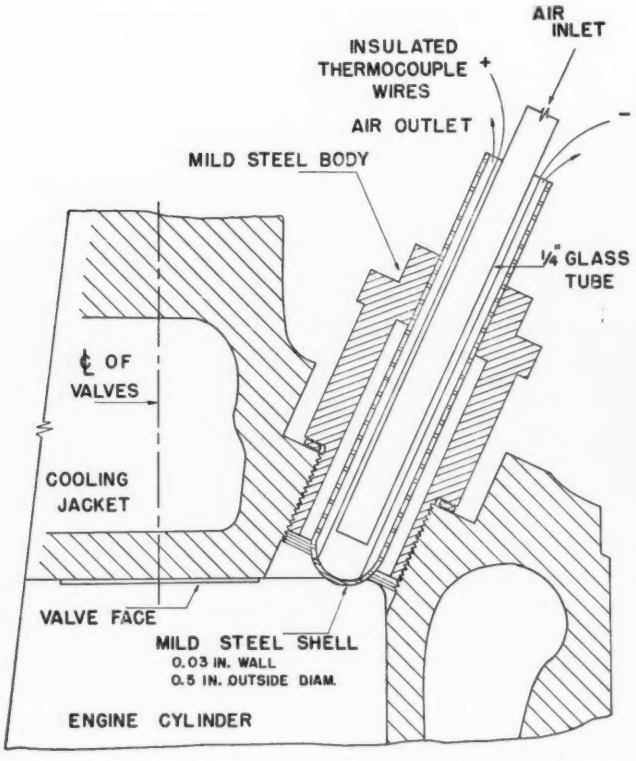

FIG. 1. Illustration of the air-cooled temperature plug as fitted in place of the bouncing pin.

values obtained for I.H.P. and I.T.E. were always consistent with particular values of M.S.

Preliminary Experiments

These were carried out in order to illustrate by indicator diagrams the method of using the T.P. Heptane was used as the fuel and the mixture with air was adjusted to be nearly correct; as measured it was 2.3% weak. Pressure–time and rate of pressure change diagrams were taken simultaneously by a Dumont dual beam oscilloscope. The cylinder was provided with three spark plug holes in the wall. One was used for a "Sunbury" magnetic flux pressure pickup to obtain rate of pressure change diagrams. A "Photocon" capacitance type pickup was used in another hole to obtain pressure–time diagrams. The third hole was fitted with a mild steel blank plug. Timing blips were fed into the electronic circuit at t.d.c. and at 10° intervals before and after. The blips

PLATE I

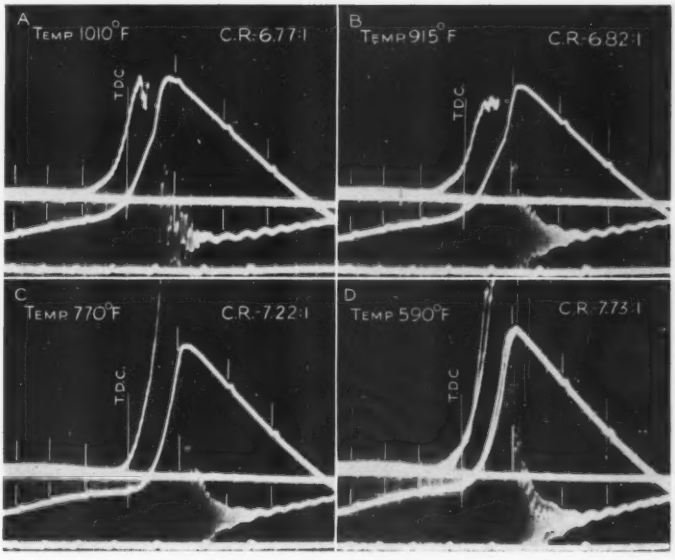

FIG. 2. Pressure–time and rate of pressure change diagrams taken simultaneously to show the increase in the Opt. C.R. at which ignition occurs as plug temperature is reduced to be equal to or less than that of the exhaust valve, nearly correct heptane–air mixtures.

are not always plainly visible on the photographic copies of the diagrams and short vertical lines have been added to mark their positions.

Four of the double diagrams taken during the experiments are reproduced as Fig. 2 and numbered A to D.

A Diagrams

These were taken with the T.P. uncooled. It then attained a temperature of 1010° F. and the Opt. C.R. was 6.77. It is shown by the pressure–time diagram that maximum combustion pressure occurred at 8° after t.d.c. and it is evident from the initially low rate of pressure rise that combustion was initiated by surface ignition. However, before it was completed by the normal thermal process of flame propagation, nuclear ignition accompanied by detonation occurred in the mixture ahead of the flame front (the end gas) and combustion was completed in 2° of crank revolution. Thus detonation was a consequence of nuclear ignition of the end gas.

B Diagrams

The T.P. was cooled to 915° F. A small increase of C.R. to 6.82 only was then required in order to obtain the optimum value. The characteristics of combustion were as described in respect of the A diagrams. The occurrence of both maximum combustion pressure and nuclear ignition about 4° of crank revolution later than shown by the No. 1 diagrams is without significance because it represents the variation that may occur in successive cycles.

C Diagrams

The T.P. was cooled to 770° F. and the Opt.C.R. then became 7.22. Both diagrams show that the T.P. ceased to initiate surface ignition when its temperature had been reduced to 770° F. The rate of heat liberation by the oxidation reaction proceeding on its surface was then too low to raise the adjacent mixture to the temperature required for an igniting effect. The ignition that did occur is attributed to the nuclei formed during compression. The absorption of heat by the decomposition reaction accounts in part for the failure of compression pressure to rise in the normal manner during the latter part of the compression stroke, as is shown by the rate of pressure change diagram.

D Diagrams

The T.P. was cooled to 590° F. and a relatively large increase in C.R. to 7.73 was then required for an optimum value. The diagrams differ from the C pair in showing that an increased rate of combustion followed the initiation of nuclear ignition at the higher value of Opt.C.R. The temperature of the plug appears to have been reduced to be lower than that of the exhaust valve because Opt.C.R. remained constant as plug temperature was further reduced to 520° F. and then to 420° F. if mixture strength were maintained constant as shown by diagrams not reproduced.

Mechanical and Gas Vibrations

Low frequency vibrations which appear in the expansion stroke and extend into the high frequency gas vibrations set up by nuclear ignition are mechanical vibrations of the engine. They were reproduced by holding a small vibrating engraving tool in contact with the outer end of the pressure pickup. The high frequency gas vibrations shown by the A diagrams are confused because pressure rise due to surface ignition began 10° before t.d.c. A single set of high frequency pressure vibrations appears on the B diagrams when plug temperature was reduced by nearly 100° F. and there was a consequent delay in the occurrence of surface ignition. A double set of high frequency pressure waves appear on the D diagrams because they include parts of two cycles which differed slightly in timing.

Exhaust Valve Temperature and Opt.C.R. as Affected by Mixture Strength

An experiment with a particular mixture strength was begun with the T.P. uncooled and values were obtained for its temperature and the corresponding Opt.C.R. The T.P. was then cooled to successively lower temperatures and corresponding values for Opt.C.R. determined as described at the beginning of this section. The experiment was continued until a constant value for Opt.C.R. was obtained for successively lower plug temperatures. It was indicated accordingly that the plug temperature had become equal to and then lower than that of the exhaust valve. The temperature of equality could then be determined from a graph for the relation between plug temperature and Opt.C.R. provided great care had been taken to maintain constancy of operating conditions.

Examples of the graphs obtained when mixtures were 7.7% weak, 24% weak, and chemically correct are given by Fig. 3. Graphs obtained when mixtures were 10%, 20%, 56%, and 102.5% rich are given by Fig. 4. It will

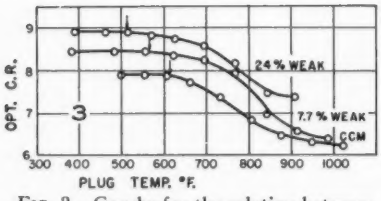

FIG. 3. Graphs for the relation between Opt. C.R. and plug temperature, heptane–air mixtures correct and weaker. The temperature at which that of the plug was the same as the temperature of the exhaust valve is indicated by small arrows.

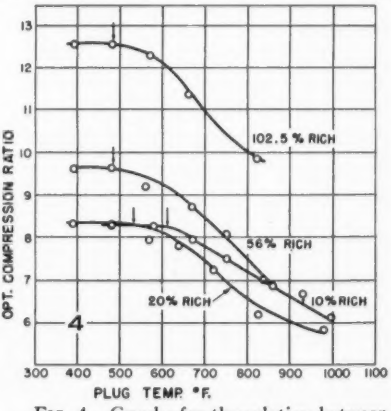

FIG. 4. Graphs for the relation between Opt. C.R. and plug temperature for rich heptane–air mixtures. The temperature at which that of the plug was the same as the temperature of the exhaust valve is indicated by small arrows.

be seen by reference to the graphs that the temperature at which the T.P. ceases to affect the value of Opt.C.R., by becoming equal to that of the exhaust valve, is shown with a fair degree of accuracy by the small arrows on the graphs.

It is of interest that Opt.C.R. tended to become dependent on M.S. only, as that factor was increased to be greater than 20% rich. Thus the temperature of the exhaust valve was 530° F. for a mixture 20% rich. It diminished only to 480° F. for a mixture 56% rich and remained at that temperature as M.S. was increased to be 102% rich.

The Relation between Opt.C.R. and Plug Temperature for Heptane–Air Mixtures Leaner than 37½% Weak

The measurement of exhaust valve temperature by the T.P. method is based on a variation of Opt.C.R. with plug temperature when M.S. has particular values, as illustrated by the graphs of Figs. 3 and 4. When however the values of M.S. were less than 37½ weak, a nearly constant value of Opt.C.R. was obtained for a particular value of mixture strength while the temperature of the plug was varied over a wide range. Experimental results obtained for particular values of M.S. ranging from 40.5% weak to 72% weak are given by the graphs of Fig. 5. They afford an explanation for the failure of the T.P.

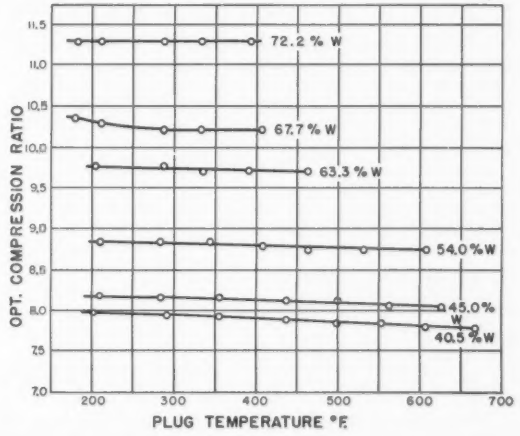

FIG. 5. Graphs showing that the relation between Opt. C.R. and plug temperature remains nearly constant at particular values of mixture strength ranging from 40.5% weak to 72% weak.

method to measure the temperature of the exhaust valve when mixtures were leaner than 37½% weak. The experimental results are of even more interest in showing that for any particular mixture within the range 40.5% weak or weaker, Opt.C.R. remains substantially constant while plug temperature is increased from 200° F. to higher temperatures ranging from 400° F. for a mixture 72% weak to 675° F. for a mixture 40.5% weak. If the plug temperature remained constant at 400° F., Opt.C.R. would vary with M.S. only over the range 40.5% weak to 72% weak.

III. EXPERIMENTAL RESULTS OBTAINED WHEN THE C.F.R. ENGINE WAS OPERATED WITH IGNITION BY COMPRESSION

Compression ignition experiments described in this Section were carried out over a wide range of heptane–air mixtures, while the temperature of the exhaust valve was measured by the T.P. method and then by a direct thermocouple method. Further experiments were then carried out with the T.P. method used to measure the temperature attained by a sodium cooled exhaust valve. C.R. was always adjusted to an optimum value and corresponding values for I.H.P. and I.T.E. were determined.

Exhaust Valve Temperature Measured by the T.P. Method; Heptane–Air Mixtures

The solid C.F.R. exhaust valve used for the experiments, and for those described earlier, was of nichrome steel with a stellite seating. The heptane–air mixtures ranged from 70% weak to 90% rich. The experimental results are given by the graphs of Fig. 6. Significant features are as follows:

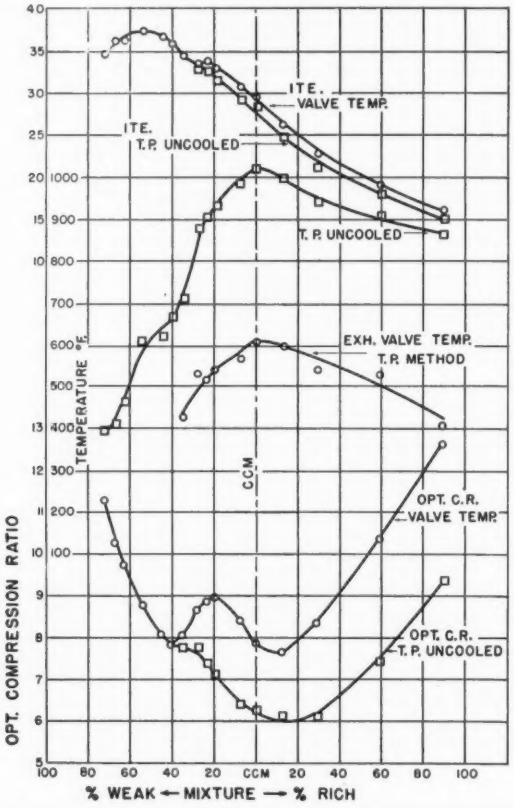

FIG. 6. Graphs for experimental results obtained when the temperature of the standard C.F.R. exhaust valve was determined by the temperature plug method, heptane–air mixtures.

When a correct mixture was used, the uncooled T.P. attained a temperature of 1020° F., the corresponding values for Opt.C.R. and I.T.E. being 6.2 and 27.5% respectively. The temperature of the exhaust valve at the same mixture strength was found to be 610° F. by the indirect T.P. method; the corresponding values for Opt.C.R. and I.T.E. being 7.9 and 29% respectively. The exhaust valve temperature decreased to 440° F. as M.S. was increased from correct to 90% rich, while corresponding values for Opt.C.R. increased to 12.6.

The characteristics of the compression ignition of weak mixtures differed in a striking manner from those for rich mixtures. Thus as M.S. was decreased from the correct value, the temperature of the uncooled T.P. and that of the exhaust valve diminished rapidly and the corresponding value of Opt.C.R. increased in a normal manner until M.S. was 20% weak. Significant events then occurred as M.S. was further reduced to 40% weak. Thus the value for Opt.C.R. diminished from 9.0 to 7.8 instead of increasing, and I.T.E. tended to remain constant at 33⅓%. The leanest mixture for which the exhaust valve temperature could be determined was 37½% weak and identical values were obtained for Opt.C.R. and I.T.E. when the temperature of the plug was 700° F. and that of the exhaust valve 420° F. The values of Opt.C.R. increased in a normal manner as M.S. was further reduced and the corresponding values for I.T.E. increased to a maximum of 37½% when the mixture became 55% weak, although Opt.C.R. had increased to 8.8 only. The experiment was continued until M.S. was reduced to 72% weak. The I.T.E. had then fallen to 35% and Opt.C.R. had risen to 11.3. The relatively low value of 37½% for maximum I.T.E. was shown by experiments described in Part XXIV (3, p. 240) to be due to the excessive proportion of the heat of the compressed mixture that is lost to the combustion chamber wall when extremely weak mixtures are used at a subnormal charge density in the conditions of the experiments.

Exhaust Valve Temperature Measured by Thermocouple; Heptane–Air Mixtures

The drilling of a small hole through the ⅜ in. diameter stem of the C.F.R. nichrome steel exhaust valve in order to provide for thermocouple wires leading to a junction in the valve face was not attempted. The exhaust valve used for the experiments was therefore lathe turned from a bar of cold rolled mild steel. It was a replica of the standard C.F.R. valve except that the stem was made the same diameter as that of the C.F.R. sodium cooled valve, namely 7/16 in. A hole ⅛ in. diameter was drilled through the stem nearly to the valve face and then reduced to 1/16 in. diameter. The ⅛ in. hole was large enough to take iron and constantin wires insulated with fiber glass. The junction was brazed into the 1/16 in. hole to be flush with the face of the valve. The end of the rocker arm which operates the valve was altered to provide a fork through which the thermocouple wires were carried to the temperature indicator. The mild steel valve has been used frequently for more than a year in the low heat load conditions of the experiments without showing any sign of deterioration even on the seating.

The T.P. was replaced by a blank steel plug and the experimental results then obtained are given by the graphs of Fig. 7. It will be noted that a graph

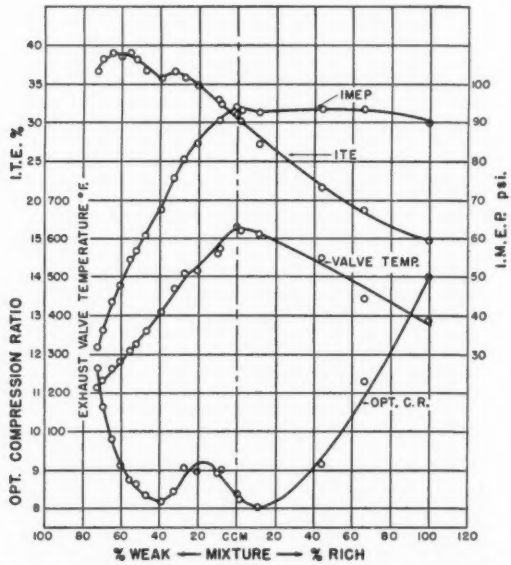

FIG. 7. Graphs for experimental results obtained when the temperature of a mild steel exhaust valve was measured by a thermocouple, heptane–air mixture.

for values obtained for I.M.E.P. is given. Similar I.M.E.P. values were obtained when the T.P. was used but were not shown on Fig. 6, in order to avoid confusion. It will be seen that the relation between Opt.C.R. and I.T.E. was the same as that obtained when the T.P. was used, see Fig. 6, within the limits of experimental error. The graphs for the relation between Opt.C.R. and M.S., Figs. 6 and 7, illustrate the effect of the increase in mixture temperature caused by the extra area of heated surface introduced into the combustion chamber by the T.P. Thus over the mixture range 44% weak to 25% rich, the Opt.C.R. required when the T.P. was used was from 0.1 C.R. to 0.3 C.R. lower than when the exhaust valve temperature was measured by the thermocouple.

The exhaust valve temperatures obtained by the two methods are plotted on a base of mixture strength (Fig. 8). It will be seen that the values fall closely on a single graph. The inconsistencies shown for values of M.S. exceeding 10% rich are not greater than would be expected in view of the irregularity of combustion that occurs in the operation of an engine by compression ignition in the circumstances. The irregularity may be due in part to incomplete vaporization of heptane in rich mixtures with air.

The Temperature of a Sodium Cooled Exhaust Valve as Measured by the T.P. Method; Heptane–Air Mixtures

The direct measurement of the temperature of a sodium cooled exhaust valve involves difficult experimental technique. It is a simple matter when the indirect T.P. method can be used. Temperature measurements were made

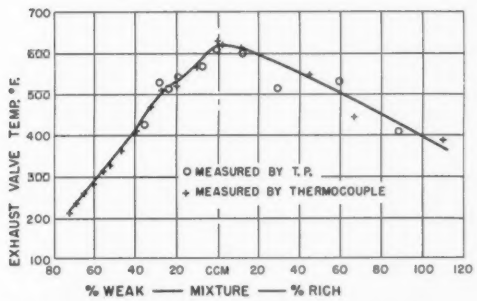

FIG. 8. Graph for a comparison of exhaust valve temperature as measured by the direct and indirect methods.

accordingly when a sodium cooled exhaust valve was fitted in the C.F.R. engine. The valve was of the type in which the hole drilled through the oversize stem extends into the head nearly to the crown. This type was used for hydrogen engine experiments and its design is illustrated by Fig. 15 of Part XXVII (7).

The results of experiments carried out with heptane–air mixtures ranging from 72% weak to 90% rich are given by the graphs of Fig. 9, which include a broken line graph for the temperature of the standard C.F.R. exhaust valve taken from Fig. 6.

It will be seen by reference to the relevant graphs that the temperature attained by the sodium cooled valve was the lower by 290° F. when the mixture was correct. Its temperature diminished more slowly than that of the solid valve as M.S. was increased and Opt.C.R. raised as required. This is attributed to the sodium cooling remaining effective, because I.M.E.P. and the consequent heat load remained nearly constant as shown earlier by Fig. 7.

I.M.E.P. and heat load decreased rapidly as M.S. was reduced from correct, with the result that the length of valve stem enclosed by the guide approached the temperature of solidification of the sodium and the rate of heat transfer from the head of the valve to the relatively cool guide was reduced. Thus the temperature of the sodium cooled valve was 100° F. only lower than that of the solid valve when mixtures ranged from 30% weak to the 40% weak at which the T.P. method of measurement became ineffective. Nevertheless the sodium cooled valve would continue to attain the lower temperature when still weaker mixtures were used even if the sodium solidified, because of its larger stem diameter.

The most significant effect shown to be due to a change from the solid to the sodium cooled valve was the consequent change in the combination of mixture strength and Opt.C.R. required for the initiation of nuclear ignition, as shown by the graphs of Fig. 9, which include a broken line graph for the temperatures attained by the C.F.R. standard solid exhaust valve. It will be seen that higher values for Opt.C.R. were required for mixtures ranging from 40% weak to 50% rich when the valve was sodium cooled. The maximum

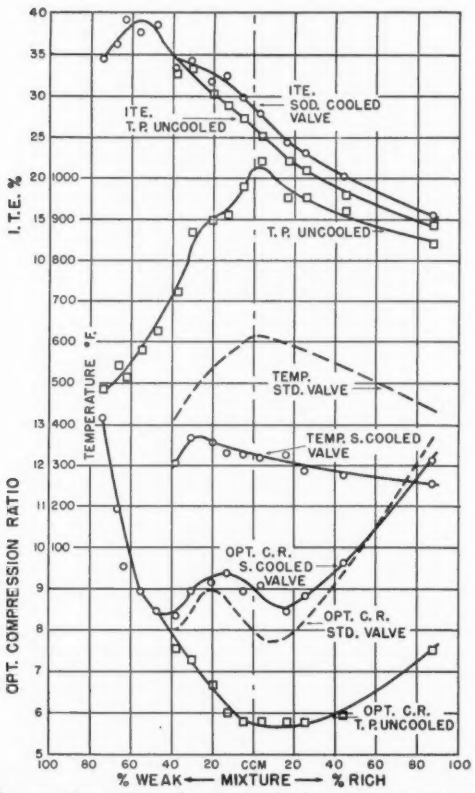

FIG. 9. Graphs for experimental results obtained when the temperature of a sodium cooled exhaust valve was determined by the temperature plug method, heptane–air mixtures.

difference occurred when the mixture was correct. Opt.C.R. was then 7.9 when the solid valve was used and 9.0 after a change was made to the sodium cooled valve.

The value of 28% was obtained for I.T.E. when the solid exhaust valve was used and the Opt.C.R. was 7.9 (see Fig. 6). When a change was made to the sodium cooled valve I.T.E. decreased to 27% although Opt.C.R. was higher at 9.0. The reduction of exhaust valve temperature by 290° F. at correct mixture, caused by sodium cooling, would be accompanied by a reduction in the temperature of the mixture at the end of compression. The observed increase in Opt.C.R. to 9.0 is regarded as having been required for the formation of an igniting concentration of nuclei in the cooler mixture.

IV. FLAME COLOR, LUBRICATING OIL EFFECT, KNOCK INTENSITY, COLD STARTING

Flame Color

A short length of polished Pyrex rod was used as a window. It was set in a mild steel mounting adapted to replace an 18 mm. spark plug in the cylinder

wall. The inner end of the Pyrex rod was set $\frac{3}{8}$ in. back from the cylinder wall and consequently tended to remain clean. Flame color was observed as mixture strength was increased from 75% weak to 100% rich. Compression ratio was always adjusted to the value required for maximum power output.

Mixture 75% to 40% Weak

The color was a brilliant light blue which became tinged with purple as M.S. was increased. The light intensity, as measured by a photomultiplier, was feeble.

Mixture 41% to 39% Weak

In this narrow range the purple tinge of the blue flame was replaced by white with a consequent marked increase in light intensity.

Mixture 39% Weak to 35% Rich

The flame was a brilliant white with an occasional tinge of yellow. Light intensity was so great that visual observations of the flame were necessarily brief.

Mixture 25% to 100% Rich

The brilliant white tended to pink as M.S. was increased to 30% rich. The color then changed to a bright orange as M.S. was further increased to 35% rich. The orange color persisted as M.S. was increased to be 100% rich. Light intensity diminished as color changed from white to pink and then to orange.

Effect of the Combustion of Lubricating Oil

It was shown by the hydrogen engine experiments described in Part XXVII (7) that the decomposition of lubricating oil *vapor* provided carbon nuclei which ignited the mixture with air before completion of the compression stroke. These experiments were carried out at engine speeds rising to 1800 r.p.m. and with normal charge density. Even so, an igniting effect arising from the lubricating oil did not occur until C.R. was raised to 12:1 and the rate of oil passing the piston increased because the top piston ring overlapped the three spark plug holes in the cylinder wall. Enough oil was then vaporized for the production of an igniting concentration of carbon nuclei.

The reactions required for the provision of nuclei of ignition by the vapor of lubricating oil would not be expected in the conditions of low heat load used for the experiments of this Part, and no evidence of such an effect was discerned. Lubricating oil passing the piston was necessarily burnt, at least in part, during combustion of the heptane, especially when air was in excess of that required for a correct mixture. Thus the flame color of heptane–air mixtures leaner than 41% weak was fundamentally a bright blue. The bright flashes of flame ranging in color from orange to white that were then observed appeared to be directly in front of the viewing window, not in the body of the mixture. They were attributed to combustion of the spray of oil thrown up from the periphery of the piston as its direction of motion reversed at t.d.c. It is possible that these bright flashes persisted as mixture strength was increased but were obscured by the intense white light emitted by the burning

carbon nuclei regarded as being responsible for the detonation of heptane–air mixtures richer than approximately 25% weak.

Combustion Knock

The combustion of mixtures leaner than 40% weak that occurred after nuclear ignition was notably silent. As the mixture was enriched, combustion knock increased slowly in intensity until the mixture was 25% weak. Intensity then increased rapidly to become severe at correct mixture. Little change in intensity occurred as M.S. was increased to be 80% rich. Knock intensity diminished slowly as M.S. was further increased.

Cold Starting

A mixture leaner than 40% weak was always used for cold starting. Ignition occurred immediately on raising C.R. to from one to two units higher than the optimum value used for continuous running. The C.R. was then lowered as the engine warmed up and adjusted to the value required for maximum power output for the measured mixture strength.

DISCUSSION

It is of interest to compare the experimental results of this Part with those obtained by others when combustible gaseous mixtures were ignited by rapid compression in a single stroke compression ignition machine and ignition temperature calculated according to the familiar equation,

$$[1] \qquad T_1/T_0 = (P_1/P_0)^{1-1/\gamma} = (V_0/V_1)^{\gamma-1}.$$

Tizard in a paper on the causes of detonation in the end gas in a spark ignition engine (11) described experiments with heptane–air mixtures as carried out with a single stroke compression ignition machine made by Ricardo. The design of the machine is illustrated in the reference quoted. Both the volume and pressure ratios were observed. Thus an apparent value for γ was calculated from the second and third terms of equation [1], which allowed for loss of heat to the cylinder wall during compression and for the concentration of heptane vapor in the mixture with air. The value of γ calculated for a correct mixture was 1.31. It increased to 1.33 for a fuel to air ratio of 0.027 and decreased to 1.22 for a fuel to air ratio of 3.75. These apparent values for γ were obtained when the "delay period" preceding detonation was not maintained at a fixed value. The ignition temperature calculated accordingly varied $\pm 8°$ C. only, from an average value of 291° C. (555° F.). The delay period was taken as the time interval between the completion of compression and the sharp pressure rise caused by detonation. It is probable that if the compression ratios at which ignition occurred had been as required for a constant delay period, the calculated ignition temperature would have had even a more nearly constant value, over the M.S. range of the experiments.

The Effect of Surface Temperature on the Compression Ratio Required for Ignition

It was found by Tizard that the compression ignition temperature of heptane–air mixtures was nearly constant irrespective of the concentration of

heptane but that the C.R. ratio required for the igniting effect varied with the concentration and the delay period. When, however, ignition is by compression in an engine, the temperatures attained by surfaces in the combustion chamber have an important influence on the compression ratio required for the initiation of an igniting effect. The relation between surface temperatures in the combustion chamber of the C.F.R. engine and the occurrence of ignition at optimum values of the compression ratio was obtained by means of the temperature plug used for the experiments of this Part. Noteworthy features of the experimental results as exhibited by the graphs of Fig. 9 are stated below.

When the heptane–air mixture was correct and the plug not cooled, its temperature rose to 1020° F. when the Opt.C.R. was 5.7. The rate of oxidation on the surface of the plug sufficed to start a flame but a transition to nuclear ignition was necessary in order that maximum combustion pressure could occur at the time required for maximum power output as shown by the A indicator diagrams of Fig. 2.

When the plug was cooled to 610° F. to be equal to the temperature of the standard C.F.R. exhaust valve, the Opt.C.R. was 8.0. Then when it was cooled to 325° F. to be equal to the temperature of the sodium cooled exhaust valve, the Opt.C.R. was 9.0. Surface oxidation was not eliminated in either case, but the rate was too low to start ignition; the change in rates was indicated by changes in the length of the fillet which connected compression and combustion pressures.

It is shown by the graphs of Fig. 9 that when M.S. was reduced to be 40% weak, the value of Opt.C.R. remained at 8.0 while the plug temperature was 700° F. or reduced to 400° F. to be equal to that of the standard C.F.R. exhaust valve. At leaner mixtures, Opt.C.R. increased nearly in direct proportion to the decrease in M.S. The temperature attained by the uncooled plug was always higher than that of the exhaust valve as shown by the graphs of Figs. 6 and 7. The difference decreased as M.S. decreased but even with a mixture approximately 75% weak, the plug temperature was 400° F. (Fig. 6) and that of the exhaust valve 200° F. (Fig. 7). When a mixture was 40.5% weak or leaner, Opt.C.R. remained nearly constant as the temperature attained by the plug for a particular mixture was reduced by cooling to a value as low as 200° F., as shown by the graphs of Fig. 5.

Data determined for the relation between plug temperature and Opt.C.R. when the exhaust valve was sodium cooled have been used to obtain the relation between Opt.C.R. and M.S. if the plug temperature were held constant at a temperature of 400° F., which is 40° F. higher than the maximum attained by the valve as shown by the relevant graphs of Fig. 10. The temperature of the valve could not be measured by the T.P. method when the mixture was leaner than approximately 38%, as was the case when the exhaust valve was not cooled.

It will be seen by reference to Fig. 10 that the graphs for the relation between Opt.C.R. and M.S. nearly coincided when mixtures were 39% to 30% weak. A real separation became apparent as M.S. was increased, and with a correct mixture, Opt.C.R. was 8.9 with the sodium cooled valve at a temperature of

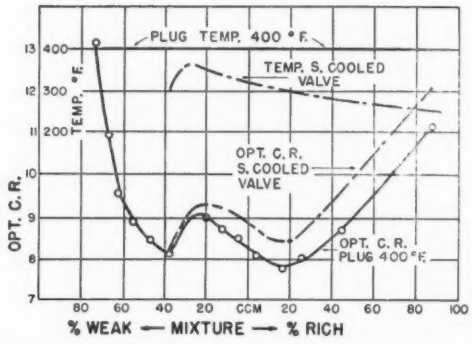

FIG. 10. Solid line graphs—Opt. compression ratios for compression ignition of heptane–air mixtures 72% weak to 90% rich when plug temperature is always 400°F. and the exhaust valve is sodium cooled.

320° F., and 8.3 with the T.P. at a temperature of 400° F. The differences increased as M.S. was increased and with a mixture 80% rich Opt.C.R. was 11.7 for the sodium cooled valve, which then attained a temperature of 260° F., and 10.7 for the temperature plug at a temperature 140° F. higher.

The relatively low heat load in the conditions of the experiments made it possible to show that the *decrease* in Opt.C.R. as M.S. was reduced over the range 25% to 40% weak is a property of a "detonating" fuel. When a nondetonating fuel such as benzene was used in the same conditions and spark timing always adjusted to the optimum value, the corresponding Opt.C.R. *increased* as M.S. was decreased from approximately correct to 40% weak, but ignition by either spark or compression did not occur at leaner mixtures.

The Relation Between the Time of Compression and the Compression Ratio Required for the Explosive Ignition of Correct Heptane–Air Mixtures

The relation is given in Table I as obtained by Tizard when using the Ricardo compression ignition machine, by Taylor *et al.* when using the machine developed in the Massachusetts Institute of Technology (10), and by the C.F.R. engine experiments of this Part when carried out with the standard uncooled exhaust valve, valve timing being taken into account.

Explosive ignition was initiated in Tizard's experiments after a "delay

TABLE I

	Initial pressure	Initial temperature, °F.	Time of compression, sec.	C.R.
Tizard	Atmos.	140°	0.0825	6.3
Taylor *et al.*	Atmos.	150°	0.006	12.3
C.F.R. engine	53% atmos.	100°	0.061	7.9

period" of 0.25 sec. as reckoned from the completion of compression. That is, the time was three times the time of compression. The delay was 0.001 sec. approximately in the Taylor *et al.* experiments, that is, $\frac{1}{6}$ of the time of compression. Explosive ignition was initiated in the engine at approximately 5° of crank revolution after t.d.c., as shown clearly by experiments made when the T.P. was not used, Part XXI (6, Fig. 5) and Part XXV (4, Fig. 7). The delay time if reckoned from the completion of compression at t.d.c. was then 0.002 sec., which is 1/30 of the time of compression although Opt.C.R. was 7.9 only. The delay time must therefore have begun during the compression stroke of the engine.

The true delay time is that required for preflame reactions to produce an igniting concentration of carbon nuclei in the gaseous mixture according to the nuclear theory as stated in Part IV (1). This statement was made in respect of the end gas in a spark ignition engine and applies only to gaseous mixtures that can thus be ignited. It is well known that spark ignition is irregular in the mixture range 20% to 25% weak. It was shown to become completely ineffective as M.S. approached 40% weak, Part XXI (6, p. 235). Further discussion will for the present be restricted accordingly.

Oxidation and decomposition reactions can occur simultaneously during compression in a carburetor engine operated as for the experiments described in this Part. It is shown by the indicator diagrams of Fig. 2 that as the plug temperature was reduced to that of the exhaust valve, the oxidation reaction on the combined surface area of the plug and valve was effective only in providing a fillet connecting compression and explosion pressures. The explosive ignition must therefore have been due to the carbon nuclei produced by a decomposition reaction. The rate of the production of carbon nuclei increases with the increase of temperature and pressure due to an increase of C.R. The concentration of nuclei per unit volume of gases mixture increases directly with increase of pressure. An explanation may thus be provided for the delay time of approximately 0.001 sec. observed by Taylor *et al.* for a correct heptane–air mixture and a C.R. of 12.3. It is possible, however, that the delay time began before compression had been completed, in view of the fact that compression time was six times that of the delay time as it was measured.

Explosive Ignition of the End Gas when Ignition is by Spark

When ignition is started by a spark or by a hot spot provided by a surface in the combustion chamber of an engine, flame is propagated in the compressed fuel–air mixture by the normal thermal process unless explosive ignition occurs in the mixture ahead of the flame front. The phenomenon is commonly described as detonation of the end gas and was observed in the experiments of this Part when a nearly correct heptane–air mixture was ignited by a hot spot provided by the temperature plug, as shown by the A indicator diagrams of Fig. 2. A similar effect was demonstrated by Taylor *et al.* when a heptane–air mixture compressed in the M.I.T. machine was ignited by a spark (10, Fig. 68).

Relevant data for the two experiments are tabulated below.

TABLE II

Method of experiment	F/A ratio	C.R.	Ignition	Approx. time of combustion of end gas
M.I.T. machine	0.066	6.8	Spark	0.3 millisec.
C.F.R. engine	0.064	6.77	Hot spot	0.8 millisec.

The combustion times were taken from pressure time diagrams and although the values are approximate, the longer time required for combustion of the end gas in the engine is consistent with its dilution with residual products to a greater than normal extent because the initial pressure was 53% of atmospheric. It is also to be noted that initial pressure in the M.I.T. machine was 5.5% greater than atmospheric and the mixture 3% richer than that in the engine.

The high speed photographic records taken in the course of experiments with the M.I.T. compression ignition machine show that ignition was initiated by discrete bright spots of flame. Taylor *et al.* comment on the similar bright spots observed by C. D. Miller when high speed photographs were taken of the autoignition of the end gas in an engine (9, pp. 98–143) and further on the theory of King *et al.* that nuclei of free carbon are involved in the autoignition process as shown by experiments with the hydrogen engine described in Part V (8). The theory received further support by the hydrogen engine experiments described later (in Part XXVII (7)).

It should be noted that the bright spots mentioned by Taylor *et al.* appeared prior to autoignition. The phenomenon was therefore not similar to that observed by Miller when autoignition occurred in the end gas of an engine. The bright spots which appeared in the M.I.T. experiments may well have indicated the beginning of ignition on the surface of the glass plate which was necessary for the taking of photographic records of the progress of combustion.

Detonation Pressure Waves

The temperature of a homogenous gaseous fuel – air mixture is not uniform at the end of compression even in a single stroke compression ignition machine, as mentioned by Tizard and later by Taylor *et al.* An even greater lack of uniformity would be expected in an engine because of the local heating effect of the exhaust valve. The decomposition or pyrolysis of the fuel to the extent necessary for the production of an igniting concentration of nuclei would be most advanced in the portion of the mixture in which temperature exceeded the mean value due to compression to the greatest extent. It may safely be assumed that maximum compression temperature was attained by the mixture near the exhaust valve irrespective of turbulence, when ignition was by compression as in the experiments described in this Part. When ignition is by spark the position of maximum temperature in the end gas is difficult to define because it depends on the position of the spark plug relative to that of the exhaust valve, on the characteristics of turbulence, and on the geometry of the combustion space.

Detonation in any event would occur in only that part of the mixture which is sensitive to the effect. That would be the mixture in the end gas in a spark ignition engine and the whole mixture at the end of the compression stroke in a compression ignition engine. The consequent pressure wave as it passed through the remainder of the mixture would raise its somewhat lower temperature to the degree required to start additional pressure waves. There would thus be a complication of pressure waves which would be increased by reflections from the walls of the combustion chamber and by the impact of one wave upon another. It is not surprising therefore that no demarcation of a detonation wave was shown by the flame photographs of Taylor *et al.* although they were taken at the rate of 10 frames per millisecond or by the rate of pressure change diagrams taken in the course of experiments described in this Part. However in all of these diagrams the gas vibrations which followed detonation were shown clearly although their frequency as measured from enlargements was 5.0 per millisecond approximately.

Nuclei of Ignition

Detonation that occurs in the end gas when fuel–air mixtures are ignited by spark is, in accordance with the nuclear theory of ignition as stated in Part IV (1), due to the igniting effect of finely divided carbon derived from decomposition or pyrolysis of the fuel. This carbon accounts for the brilliant white flame of detonating combustion. The flame is blue in operating condition in which detonation does not occur unless the mixture is over rich and vaporization is not complete. Carbon not consumed in the flame appears as a residue on surfaces in the combustion chamber and as black smoke in the exhaust.

When a spark plug was not used, as for the experiments with heptane–air mixtures described in this Part, and C.R. was raised to the value required for ignition with maximum power output, detonation began in part of the whole gaseous mixture, as there was then no end gas. The characteristics of detonating combustion were similar to those described for spark ignition when, as with spark ignition, mixtures were richer than 25% weak.

Mixture strength appears to have a critical value when it is 25% weak. Then as it is increased from that value, residues of finely divided carbon tend to appear on surfaces in the combustion chamber when detonation follows spark or compression ignition. As M.S. decreases from 25% weak, spark ignition tends to become of nil effect. Ignition by compression remains effective but residues of the nuclei of ignition appear to be a mixture of carbon and resin. A corresponding increase in the inflammability of the nuclei of ignition was indicated by a decrease in optimum C.R. as mixture strength was reduced from 25% to 40% weak. Then as mixture strength was further reduced the flame of combustion ceased to be white and became a brilliant blue.

Aldehydes were noticeable in the exhaust as the mixture became leaner than 25% weak. The accompanying increase in the inflammability of carbon nuclei may be due to their absorption and condensation of a particular variety of aldehyde. However, residues of resinous substance increased in quantity when rate of aldehyde formation increased as mixtures leaner than 40% weak were

used, as described in Part XXIV (3, p. 235). Corresponding values of Opt.C.R. increased and flame became a bright blue. This indicated that nuclei of ignition no longer contained carbon. The combustion of these lean mixtures occurred in two stages and was nearly silent.

Experiments carried out especially to determine the role of aldehydes in the compression ignition of mixture leaner than can be ignited by a spark will be described in the second paper on the subject of this Part.

ACKNOWLEDGMENTS

The experiments described in this Part were carried out in the Department of Mechanical Engineering, University of Toronto, with the co-operation of Professor E. A. Allcut, Head of the Department, and with the aid of an Extra-mural Grant from the Defence Research Board, Ottawa, Canada. The authors are indebted to the Chairman of the Board for permission to publish this paper.

REFERENCES

1. KING, R. O. Can. J. Research, F, 26: 228. 1948.
2. KING, R. O. and ALLAN, A. B. Can. J. Technol. 30: 44. 1952.
3. KING, R. O. and ALLAN, A. B. Can. J. Technol. 32: 220. 1954.
4. KING, R. O. and ALLAN, A. B. Can. J. Technol. 33: 335. 1955.
5. KING, R. O., DURAND, E. J., ALLAN, A. B., and HANSEN, E. J. T. Can. J. Technol. 30: 29. 1952.
6. KING, R. O., DURAND, E. J., ALLAN, A. B., HANSEN, E. J. T., and BOWEN, V. E. Can. J. Technol. 30: 222. 1952.
7. KING, R. O. and RAND, M. Can. J. Technol. 33: 445. 1955.
8. KING, R. O., WALLACE, W. A., and MAHAPATRA, B. Can. J. Research, F, 26: 264. 1948.
9. MILLER, C. D. S.A.E. Quart. Trans. Jan. 1947.
10. TAYLOR, C. F., TAYLOR, E. S., LIVENGOOD, J. C., RUSSELL, W. A., and LEARY, W. A. S.A.E. Quart. Trans. April. 1950.
11. TIZARD, H. T. North East Coast Inst. Engrs. & Shipbuilders, May. 1921.

COMPARISON OF THE FATTY ACID COMPOSITION OF RAPESEED AND MUSTARDSEED OILS[1]

By B. M. Craig

ABSTRACT

The fatty acid compositions of solvent extracted oils from Argentine, Polish, and Turkish types of rapeseed, commercial lots of Swedish and Montana rapeseed oil, and a commercial sample of mustardseed oil were determined. The iodine values ranged from 100.8 for Argentine to 123 for Turkish and mustardseed oils. Small variations were found in the total amounts of C_{16} and C_{20} acids and large variations in the C_{18} and C_{22} acids. The variations in the content of palmitic, stearic, hexadecenoic, arachidic, and behenic acids were small. The linolenic acid contents of Turkish rapeseed and mustardseed oils were 6% higher than for the other oils, which differed from one another by less than 2%. Linoleic, oleic, and erucic acids showed maximum variations of 16 to 27, 7 to 27, and 18 to 52%, respectively.

A number of investigations of the fatty acid composition of rapeseed oils have been made in recent years (10) but no comparative work has been done between varieties or types of rapeseed. The increasing production of rapeseed in Western Canada over the past three years and the growing interest in breeding varieties prompted a preliminary survey to determine the extent to which oils from different types and varieties differ in their fatty acid composition. The iodine values of rapeseed oils can vary from 90 to 125. A knowledge of the fatty acid composition of oil from different varieties should be valuable in a breeding program to produce oils with the desired fatty acid composition or with a major amount of a single fatty acid. Reports concerning the nutritional aspects of erucic acid oils make it desirable to know the variation of this particular fatty acid with the variety of rapeseed (1, 2, 3, 6, 7, 8).

MATERIALS AND METHODS

The Argentine and Polish oils were obtained by laboratory extraction of commercial lots of the seed with Skellysolve "F". Samples of these types were provided by Mr. A. D. Miller of the Saskatchewan Co-operative Oil Mill, Saskatoon, Sask., and belong to the species *Brassica napus* and *Brassica campestris* respectively. Turkish oil was solvent extracted from a sample of Turkish rapeseed (*Brassica napus*) obtained from Dr. W. J. White, Forage Crops Division, Department of Agriculture, at the University of Saskatchewan. Samples from commercial lots of rapeseed and mustardseed oils from Montana and rapeseed oil from Sweden were supplied by Geo. Degen and Company, New York. The varieties or types of seed from which these oils were extracted are unknown.

The procedure used for determining fatty acid composition has been described (4, 5, 10). The methyl esters of the fatty acids were prepared from

[1]*Manuscript received May 28, 1956.*
Contribution from the National Research Council of Canada, Prairie Regional Laboratory, Saskatoon, Saskatchewan. Issued as Paper No. 225 on the Uses of Plant Products and as N.R.C. No. 4027.

the glyceride oils by the dimethyl sulphate procedure (9) and were fractionally distilled. The fatty acid composition was determined from the spectrophotometric analyses, iodine values, saponification values, and refractive indices of the individual fractions. The agreement between the properties of the original esters and the summation of the fractions was within the experimental error as in previous work (4, 5, 10) and this coupled with the negligible loss in diene and triene acids indicated an error of less than one per cent for the major constituent acids.

RESULTS

Iodine values, saponification values, refractive indices, and unsaponifiable matter of the oils are given in Table I. The iodine values range from 100.8 for Argentine to 123 for Turkish and mustardseed oils. The percentage by

TABLE I

PROPERTIES OF RAPESEED AND MUSTARDSEED OILS

	Swedish	Argentine	Polish	Turkish	Montana	Montana mustard-seed
Iodine value	104.0	100.8	108.5	123.8	107.8	123.3
Refractive index	1.4693	1.4683	1.4669	1.4699	1.4692	1.4711
Saponification value	171.7	173.7	174.9	177.1	178.9	180.9
Non-saponifiable matter	1.0	1.1	1.2	1.3	1.2	1.4
C_{16}, %	3.0	3.6	2.8	3.3	2.7	3.5
C_{18}, %	34.9	40.0	56.6	56.3	57.5	64.3
C_{20}, %	9.2	13.5	12.4	13.0	12.6	13.0
C_{22}, %	51.9	41.8	27.0	26.1	26.0	17.8

weight of the distilled fractions from each oil is given in Table I. The same reflux ratio and cutoff point between fractions were used for the distillation of the methyl esters from each oil. The fractions were selected by the boiling point range at 10 mm. pressure and were as follows: C_{16}, up to 195°C.; C_{18}, 195° to 215°C.; C_{20}, 215° to 235°C., and C_{22}, 235° to 247°C. The major portion of each fraction distilled at 187°, 205° to 208°, 226°, and 247°C. respectively, and the change-over between fractions would constitute approximately 0.3% of the total. The data shown in Table I indicate that the amount of C_{16} acids is relatively constant for all the oils. The content of C_{20} acids is relatively constant except for Swedish rapeseed oil. The major variation in fatty acid content on the basis of chain length is between the C_{18} and C_{22} fractions. In terms of increasing amounts of C_{18} acids the rapeseed oils fall in the order, Swedish, Argentine, Turkish, Polish, and Montana. The mustardseed oil has the highest percentage of C_{18} acids. The relation in the content of

C_{22} acids follows the same order, with Swedish having the greatest and mustardseed the least. The variations in saponification values as shown in Table I are indicative of the same trend but the limited accuracy of the saponification value determination and the complex mixture of fatty acids do not permit a calculation of the relative amounts of each fraction from the saponification value of the original esters.

The fatty acid compositions of the oils are given in Fig. 1. The dienoic and

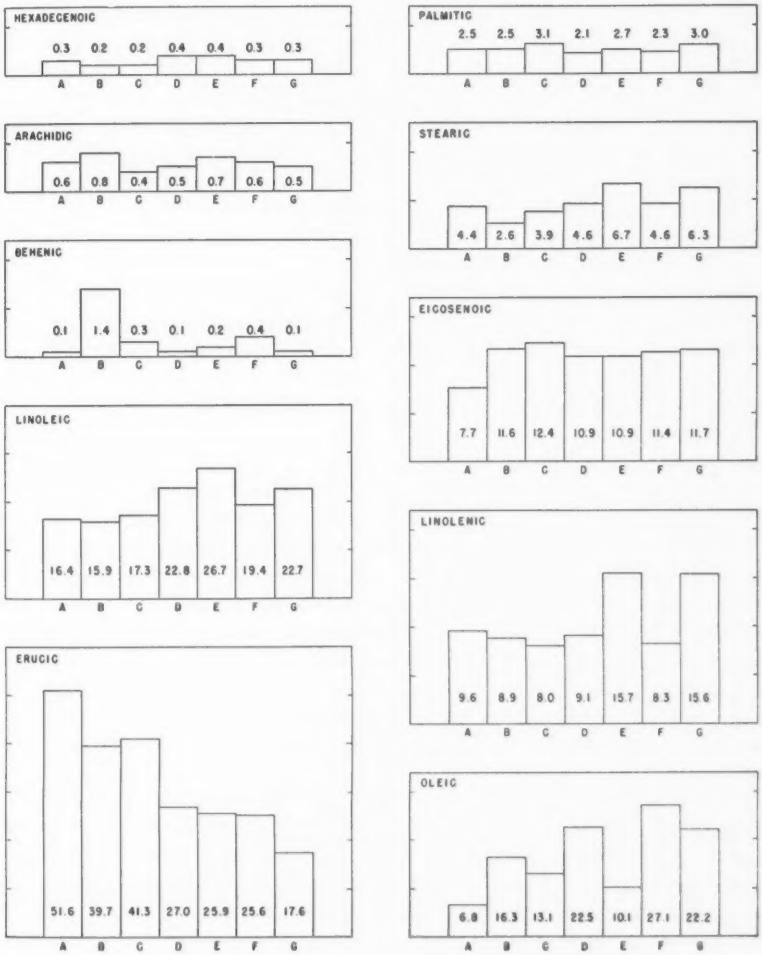

FIG. 1. Fatty acid composition of rapeseed oils and mustardseed oils.

A—Swedish
B—Argentine (8)
C—Argentine
D—Polish
E—Turkish
F—Montana
G—Mustardseed

trienoic acids in the various fractions were totalled and are shown collectively as linoleic and linolenic acids. The total amounts of these acids in the C_{16}, C_{20}, and C_{22} fractions approximate 1.0 and 0.6% respectively for each of the oils. The fatty acid composition of a commercial sample of Argentine rapeseed oil which was previously determined in this laboratory (10) was included for comparison.

DISCUSSION

The data in Fig. 1 show that there are minor variations in the contents of palmitic and hexadecenoic acids as would have been expected from the small variations found for the C_{16} percentages from distillation data in Table I. The palmitic acid had a concentration range of 2.1 to 3.1%. The amounts of C_{20} acids from the distillation data were relatively constant except for the esters from Swedish oil. The same trend is shown in eicosenoic and arachidic acids in Fig. 1. The eicosenoic acid shows a range from 10.9 to 12.4% except for Swedish oil, which has 3 to 5% less than the other oils. The variation is small for arachidic acid as might be expected for a minor acid.

The Turkish rapeseed and mustardseed oils, which have the highest iodine values, have similar and high contents of linolenic acid. The variation in linolenic acid content among the remaining oils is small although the difference in iodine values between Argentine and Polish rapeseed oils is eight units. Differences are found for linoleic acid between Swedish and Argentine rapeseed oils and between Polish and Montana rapeseed oils and mustardseed oil as groups. The Turkish rapeseed oil has the highest content of linoleic acid. The variation in linoleic acid between these groups is from 15.9 to 26.7%.

The major differences are shown in the amounts of oleic and erucic acids. The oleic acids range from a low of 6.8% for Swedish rapeseed oil to a high of 27.1% for Montana rapeseed oil. With the exception of Turkish rapeseed oil the oleic acid content follows the variation in iodine values. The erucic acid shows a trend which follows the variation in saponification values except for mustardseed oil. The oils may be grouped in decreasing order as follows: Swedish, Argentine, Polish, Turkish, Montana, and mustardseed oil. The Polish, Turkish, and Montana rapeseed oils are similar in the amount of erucic acid.

The commercial sample of Montana rapeseed oil seems to be from Polish type rapeseed on the basis of iodine value, distillation data, and fatty acid composition.

This preliminary survey of fatty acid composition of rapeseed and mustardseed oils from several sources indicates that there are major differences which cannot be predicted from iodine values or saponification values of the original oils or methyl esters. These differences are mainly in the content of oleic, linoleic, and erucic acids. Further research would be required to determine the effect of environment on varietal compositions.

ACKNOWLEDGMENTS

The author wishes to acknowledge the analytical work which was done by Mr. T. M. Mallard and Mr. L. L. Hoffman.

REFERENCES

1. CARROLL, K. K. Endocrinology, 48: 101. 1951.
2. CARROLL, K. K. J. Biol. Chem. 200: 287. 1953.
3. CARROLL, K. K. and NOBLE, R. L. Endocrinology, 51: 476. 1952.
4. COLE, L. N. and CRAIG, B. M. Can. J. Technol. 31: 196. 1953.
5. CRAIG, B. M. Can. J. Technol. 31: 202. 1953.
6. THOMASSON, H. J. J. Nutrition, 56: 455. 1955.
7. THOMASSON, H. J. J. Nutrition, 57: 17. 1955.
8. THOMASSON, H. J. and BOLDINGH, J. J. Nutrition, 56: 469. 1955.
9. YOUNGS, C. G. and CRAIG, B. M. J. Am. Oil Chemists' Soc. 28: 521. 1951.
10. YOUNGS, C. G., MALLARD, T. M., CRAIG, B. M., and SALLANS, H. R. Can. J. Chem. 29: 871. 1951.

THE PHENOL EXTRACTION OF LUBRICATING OILS[1]

By R. M. Butler,[2] A. E. Spence,[3] A. R. Barncroft,[4] and A. C. Plewes

ABSTRACT

The properties of the product obtained by the extraction of a particular lubricating oil distillate with a given solvent are not completely determined by the specification of an average physical property such as refractive index, density, or viscosity index. This is shown to be true by the variation in the ultraviolet absorption spectrum and the Sligh oxidation number for oils produced by the phenol extraction of a Leduc intermediate lubricating oil distillate. In each series of oils of a given refractive index those produced under the most selective conditions (i.e. highest yield) have the lowest concentration of aromatics and the lowest Sligh number. It is also shown that the positions of the tie lines in a Hunter–Nash diagram depend upon the conditions within the extractor.

INTRODUCTION

Although solvent extraction has long been used for the treatment of lubricating oils and other complex petroleum mixtures, the theory of such processes is not yet complete. A major advance was made by Hunter and Nash (8, 9, 10, 11), who showed that the triangular diagram which was first proposed by Gibbs (5) for the representation of the composition of three component mixtures could also be used to represent the composition of lubricating oil – solvent mixtures. In order to do this the composition of the oil was represented by an additive property plotted along one side of the triangle. In practice the solvent concentration is shown as a volume fraction, and a property which is additive on a volume basis is used to express the oil composition. Suitable properties are density, refractive index, and viscosity gravity constant (7).

Density may be shown to be additive on a volume basis provided that there is no volume change on mixing; this is essentially true for all hydrocarbon mixtures.

It is found experimentally that a linear relation exists between the refractive index and the density of a series of oils prepared by the extraction of a given feedstock (16). As a result of this linear relation, refractive index is also additive on a volume basis. Use is frequently made of this fact in the preparation of material balances for industrial petroleum plants.

Hunter and Nash showed how the compositions of the raffinate and extract phases at various points in an extractor could be determined by a graphical method from diagrams of this type. In particular they showed how it was possible to determine the number of theoretical stages required for any particular separation. Several variations of the Hunter and Nash method have also been developed (3, 14, 17, 18).

[1]*Manuscript received May 24, 1956.*
Contribution from the Chemical Engineering Department, Queen's University, Kingston, Ontario, Canada.
[2]*Present address: Imperial Oil Research Department, Sarnia, Ontario.*
[3]*Present address: Imperial Oil Limited, Halifax, Nova Scotia.*
[4]*Present address: Atomic Energy of Canada Limited, Chalk River, Ontario.*

In the construction of the triangular equilibrium diagram for an oil–solvent system the solubility curve and tie lines are usually determined from experiments in which the feedstock (e.g. lubricating oil distillate) is mixed with various proportions of the solvent (e.g. phenol). In each case the extract and raffinate layers are separated and analyzed for solvent and oil quality.

If this data is obtained for a sufficient number of mixtures an equilibrium diagram of the type shown in Fig. 1 may be constructed.

When the results of laboratory extractions are compared with those predicted from this type of diagram by means of the Hunter and Nash method, it is found that the number of theoretical stages required in the laboratory for the same yield and quality of the raffinate is greater than that predicted from the equilibrium diagram (4, 10, 13, 15). In the experiments described in the above references the phases were brought into contact by being shaken in

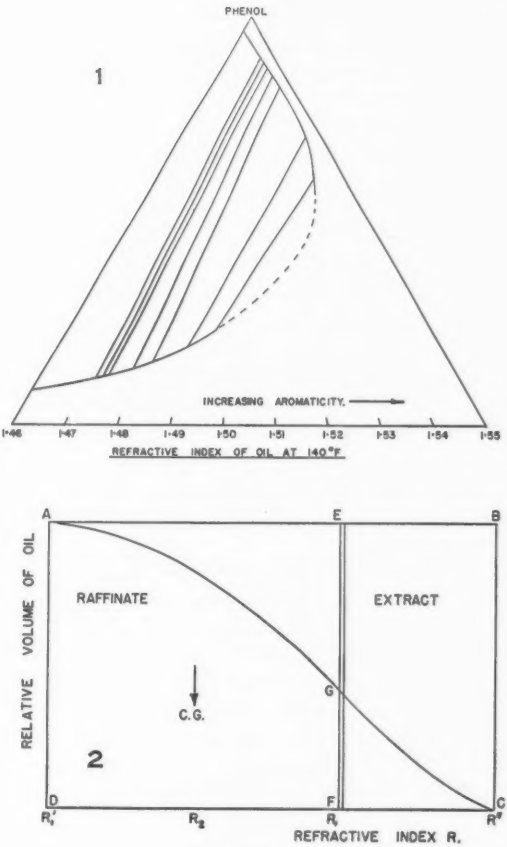

FIGS. 1 and 2.

separatory funnels and decanted from one funnel to the next in such a manner that the cascade could be said to contain a definite number of theoretical stages. There is very little doubt that the laboratory stages were essentially equivalent to theoretical stages.

As will be shown in the experimental work described later in this paper, the main reason for the difference between the number of stages determined from the Hunter and Nash diagram and from the laboratory extractions is that the tie lines determined from single stage extractions of the feed are not the same as those corresponding to the conditions in a countercurrent treater. It is just as unreasonable to expect that the specific gravity of the oil in the extract phase is a definite function of the specific gravity of the oil in the raffinate phase as it would be to expect the specific gravity* of the vapor in a multicomponent fractionator to be a definite function of the liquid phase specific gravity. In the latter case the difference between the liquid and vapor is dependent upon the fractionation conditions. A liquid consisting of a wide range of materials evolves a vapor of lower specific gravity than does a liquid of the same specific gravity consisting of a narrow range of materials. In the analogous case of solvent extraction it would be expected that the extract phase in equilibrium with an oil phase of specified average properties (e.g. gravity, refractive index) would be more aromatic if the oil phase contained materials over a wide range of aromaticity than it would be if the range were narrower.

In the extraction of a specific lubricating oil distillate the relative quantity of materials of various degrees of aromaticity in the raffinate phase at any particular point in the extractor is not only dependent upon the average physical properties of the oil in the raffinate phase (e.g. specific gravity, refractive index, viscosity index, etc.) but it is also dependent upon the extraction conditions (i.e. temperature and temperature gradient, number of stages, solvent to feed ratio, position of feed, etc.). Average physical properties are not in themselves sufficient to describe the properties of treated lubricating oil. Thus, for example, two treated oils prepared by different extraction methods from the same distillate can have quite different compositions and chemical properties even though they may have the same gravity and viscosity index.

The following argument will show that the yield at which the treated oil has been extracted from the feed is a measure of the concentration of highly aromatic materials for oils having the same average physical properties.

In Fig. 2 the area $ABCD$ represents the volume of the feed. The horizontal axis represents refractive index and the vertical axis the relative volumes of oil having each refractive index. Thus the area $(EF)dR$ represents the volume of oil having a refractive index between R_1 and R_1+dR. For simplicity it is assumed that the area $ABCD$ is a rectangle as shown. This assumption is, however, not essential for the argument which follows.

Consider the extraction of the oil represented by the rectangle in Fig. 2.

**Specific gravity of a vapor sample after it has been condensed to a liquid.*

The result of the extraction is that the area is divided into two sections. The refractive index of the treated oil (raffinate) will correspond to the center of gravity of the left hand section and the refractive index of the extract will be at the center of gravity of the right hand section. Consider the production of a raffinate of a given refractive index, say R_2. There is obviously an infinite number of different dividing lines which could be drawn to give this same center of gravity. For a perfect separation the dividing line would be vertical and straight—*EF*. For a practical separation the dividing line will be a curve of the type depicted by *AGC*. If the area *AGCD* is to have the same center of gravity as *AEFD*, then the area *GCF*, which has been added to *AEFD* and has a long moment arm, must be smaller than the area *AEG*, which has been subtracted and has a smaller moment arm. As a result of this argument it may be concluded that in a series of raffinates of the same refractive index produced from the same feedstock, those prepared by the most selective extraction conditions will also be prepared at the highest yield. Furthermore the low yield low selectivity raffinates will contain higher concentrations of highly aromatic high refractive index hydrocarbons. This has been shown to be true in the experimental work described later.

Since the low yield samples in a series of raffinates of equal refractive index (the densities, viscosity gravity constants, and viscosity indices will also be very nearly equal) contain higher concentrations of the highly aromatic materials of the types predominant in the extract, it follows that these low yield oils probably also have chemical stabilities inferior to those obtained at higher yield. Sligh oxidation tests carried out on such series of oils show differences of this type—the low yield oils give high Sligh numbers and the high yield oils give low Sligh numbers. The results of these tests are described later.

It is of practical interest to consider the results of increasing the selectivity of a lubricating oil extraction plant. (The selectivity may be increased by any of the following methods: increasing the number of stages, using more solvent and lower temperatures, using more solvent and more antisolvent, employing a larger reflux section below the feed, using a more selective solvent, etc.). Suppose the new plant is controlled so that it produces raffinate of the same average physical properties as the original plant; two advantages will have been obtained:

1. A larger yield, i.e. more treated oil from the same quantity of feedstock.
2. The concentration of the undesirable highly aromatic components in the treated oil will have been reduced. The new oil, although it is of the same viscosity index as the original oil, will be of superior quality.

Alternatively it would, of course, be possible to obtain an even higher yield of oil of the former quality (from the point of view of the content of highly aromatic materials) if the plant conditions were adjusted so that oil of a somewhat lower viscosity index were produced.

For treated oils produced from a given feedstock, average properties such as refractive index, gravity, viscosity index, and viscosity gravity constant are not by themselves sufficient criteria of quality. A much better description is

given by one of these quantities together with the yield at which the oil has been produced from the feedstock. The results of the experimental work described in the remainder of this paper confirm the ideas which have been introduced here.

EXPERIMENTAL SECTION

Materials Used

1. *Oil samples.*—All of the samples used in this work were prepared by phenol extraction methods from a single 10-gal. sample of waxy Leduc lubricating oil distillate supplied by Imperial Oil Limited which had the following physical properties:

Viscosity at	210° F.	79	S.U.S.
Viscosity at	130° F.	433	S.U.S.
Density at	140° F.	0.8928 gm./ml. (21° API)	
Refractive index at	140° F.	1.4987	

2. *Phenol.*—The phenol used in these experiments was "Analar Grade" as supplied by British Drug Houses (Canada) Limited.

Miscibility Curve

In Fig. 3 the miscibility temperatures of various phenol–oil mixtures are

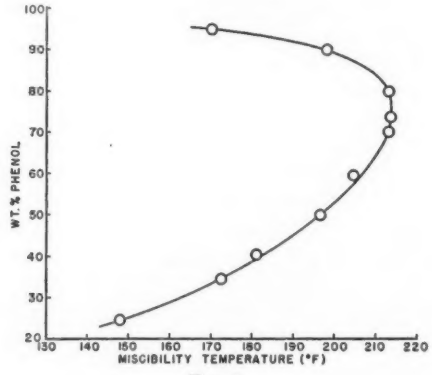

FIG. 3.

shown as a function of composition. It will be noticed that the distillate is completely miscible with phenol at temperatures above 213.5° F.

The Effect of Extraction Conditions Upon Yield

Five sharply extracted oils were prepared by the four stage countercurrent extraction of the distillate sample with phenol. In some cases water was injected into some of the stages near the extract end. The extractions were carried out using the method of batch simulation of continuous countercurrent extraction developed by Watanabe and Morikawa (20) and later employed by Hunter and Nash (10), Rushton (13), and Skogan and Rogers (15). The extraction conditions are shown in Table I.

TABLE I

CONDITIONS FOR THE PREPARATION OF EXTRACTED OIL SAMPLES

Designation of sample	Vol. of phenol per 100 vol. distillate	Temperature of stages, ° F.					Position of feed	Water injection based on 100 vol. feed	R.I. of treated oil at 140° F.	Yield, vol. %
		1	2	3	4	5				
$PD_{77/82}$	0	–	–	–	–	–	–	–	1.4987	100
$R_{IV\ 75}$	75	160	160	160	160	–	1	None	1.4757	65.7
$R_{IV\ 100}$	100	160	160	160	160	–	1	None	1.4730	63.3
$R_{IV\ 100W}$	100	140	140	180	180	–	1	4 vol. to stage 1	1.4798	80.6
$R_{IV\ 200W}$	200	140	140	180	180	–	1	8 vol. to stage 1	1.4693	64.5
$R_{IV\ 200WC}$	200	105	140	140	180	180	2	6 vol. to stage 2		
									1.4708	74.2
								13.3 vol. to stage 1		

In Fig. 4 the yield obtained in these countercurrent extractions has been

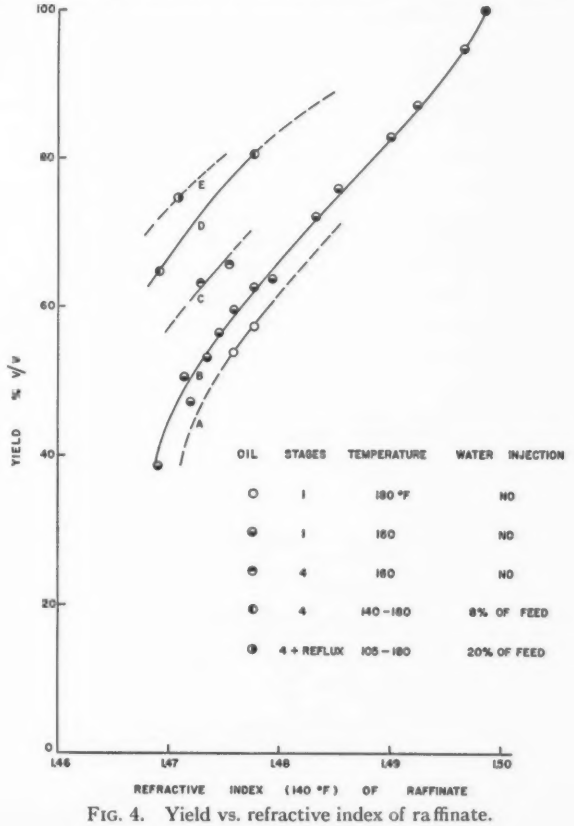

FIG. 4. Yield vs. refractive index of raffinate.

compared with that obtained from single stage extractions with pure phenol at 180° F. and 160° F. It will be noted that the yields obtainable for any particular raffinate refractive index (on a solvent free basis) increase in the following order:

1. Single stage treat at 180° F.
2. Single stage treat at 160° F.
3. Four stage treat at 160° F.
4. Four stage treat with temperature gradient and water injection.
5. Four stage treat with temperature gradient, water injection, and extra cycle oil stage.

On the other hand the solvent requirement is also found to increase in the same order.

Effect of Extraction Conditions Upon Tie Line Position

In the introduction it was suggested that the refractive index of the extract phase should not be solely dependent upon the refractive index of the raffinate phase but should also depend upon the extraction conditions. In particular it was suggested that the difference between the refractive index of the extract and raffinate should be less for sharp extraction conditions, i.e. high yields. This was shown to be true by means of a series of experiments in which the oils described in Table I were treated with various quantities of pure phenol at 160° F. The two layers were separated, analyzed for phenol by the method described in the Appendix, and the refractive index at 140° F. of the phenol free oil in the two phases was determined by means of a Galileo Abbé refractometer. The results are presented in Figs. 5 and 6. In Fig. 5 the difference between the refractive index of the oil in the extract phase and of the oil in the raffinate phase has been plotted against the refractive index of the oil in the raffinate phase. The different types of points indicate the various oils (from Table I) which were shaken with phenol. The small figures written beside the points indicate the volume per cent of the original distillate which is repre-

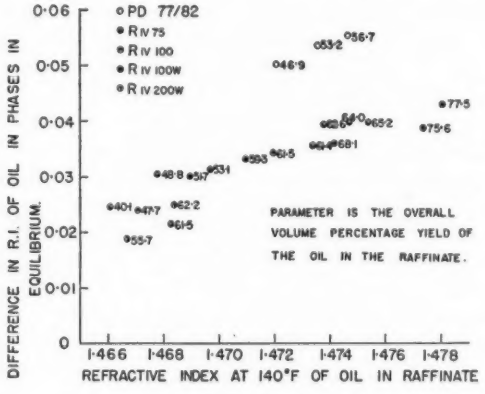

FIG. 5.

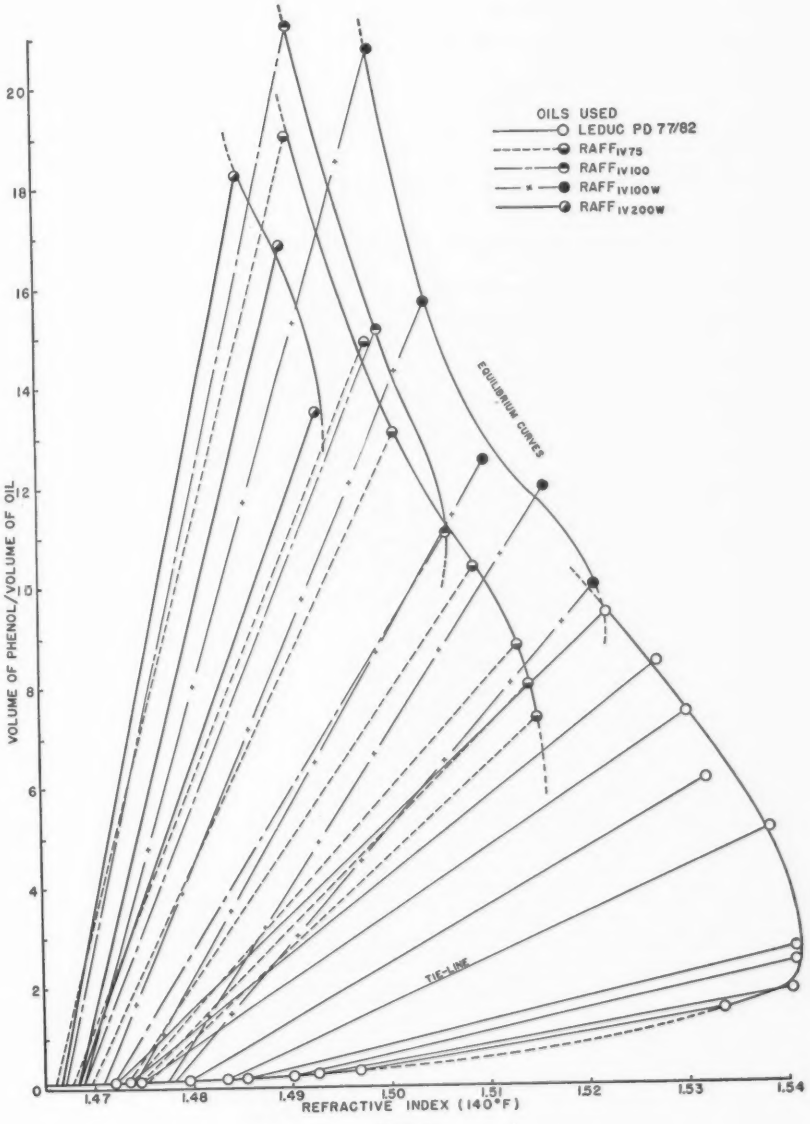
OILS USED
LEDUC PD 77/82
RAFF IV 75
RAFF IV 100
RAFF IV 100W
RAFF IV 200W
EQUILIBRIUM CURVES
TIE-LINE
VOLUME OF PHENOL/VOLUME OF OIL
REFRACTIVE INDEX (140°F)
0
2
4
6
8
10
12
14
16
18
20
1.47
1.48
1.49
1.50
1.51
1.52
1.53
1.54

FIG. 6.

sented by the oil in the raffinate phase (i.e. the yield). It will be noted that the points do not fall along a single curve as they are assumed to in the Hunter and Nash method. For raffinate oil of a given refractive index there is a larger difference between the two phases when the yield is small than when it is larger.

In Fig. 6 the results of the same series of experiments have been plotted on a Janecke type of equilibrium diagram. Again it may be noted that several tie lines may be drawn for a given raffinate refractive index. Fig. 5 also shows that the solubility of the oil in the extract phase depends to some extent on the selectivity of the extraction.

Ultraviolet Absorption Spectra of Treated Oils

The relative aromatic contents of a number of the oils prepared previously were compared by determining ultraviolet absorption spectra by means of a Beckmann D.U. spectrophotometer fitted with a photomultiplier attachment. Other workers have shown that most of the absorption occurring in the wavelength range 240 to 290 millimicrons is caused by aromatic hydrocarbons (2,

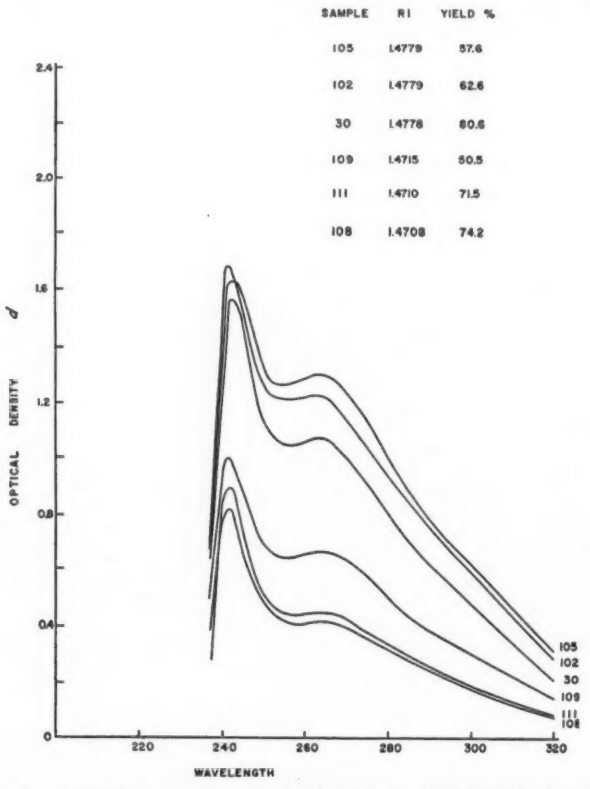

FIG. 7. Absorption spectra of oils in chloroform. (Wavelength in mμ.)

6, 19). Both cyclohexane and chloroform were used as solvents for these determinations and similar results were found with each (1). For the sake of brevity only the results found with chloroform will be reported here.

Analar grade chloroform was employed and it was carefully fractionated by distillation at high reflux in a 5 ft. helix packed column; the middle 80% cut was used. It is doubtful whether this material was completely pure but since the same solvent was used for each determination and the method was one of measuring the difference between the light transmission through the pure solvent and through the solution, it was felt that any impurities which were present would not affect the results.

In each case the solutions which were used had a concentration of 0.0200 gm. of oil in 100 ml. of solution.

Absorption spectra of two different series of three oils of nearly the same refractive index are shown in Fig. 7. It will be noted that in each series different

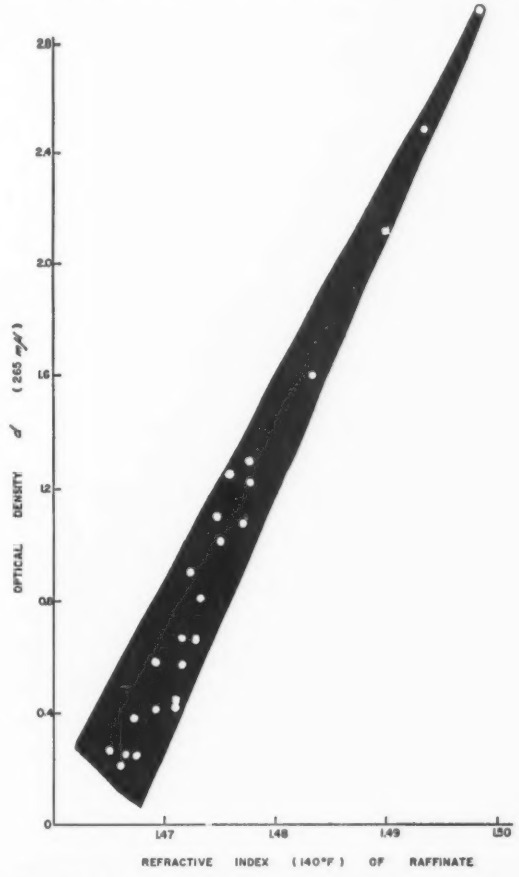

FIG. 8. Optical density vs. refractive index of raffinate.

curves were obtained for oils of the same refractive index. In general it may be seen that the oils produced in the greatest yield (highest selectivity) showed less ultraviolet absorption than oils produced at low yield. This trend was observed in all the spectra which were measured (26 in chloroform and 15 in cyclohexane). It was also found that in each case there was a peak at 265 mμ and the optical density at this wavelength was tabulated as a measure of the entire spectrum. The results are shown in Figs. 8 and 9.

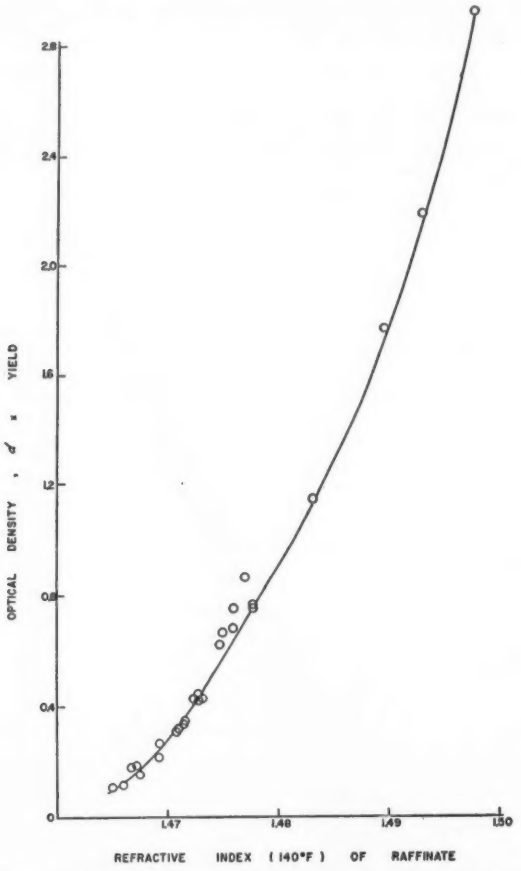

FIG. 9. Optical density × yield vs. refractive index of raffinate.

In Fig. 8 the optical density has been plotted against the refractive index of the oil. As may be expected the heavily extracted low refractive index oils have low optical densities whereas the aromatic high refractive index oils have high optical densities. It is significant that the points do not lie on a smooth curve. For any particular refractive index there is a whole range of optical

densities—the higher ones correspond to low yields and the low ones to high yields.

In Fig. 9, optical density multiplied by yield has been plotted against refractive index. The data fall along a fairly smooth curve when plotted on these coordinates. Again it may be seen that for any particular refractive index the optical density and hence the aromatic content may be high or low depending on the yield.

Sligh Oxidation Tests on Extracted Oils

Sligh oxidation tests (12) were carried out on a number of the samples of extracted oil. The results of these tests are shown in Table II. Each of the Sligh numbers tabulated (mgm. of naphtha insoluble precipitate from a 10 gm. sample of oil oxidized for a period of two and one-half hours at 200°C.) is the mean of four duplicate experiments.

TABLE II

SLIGH OXIDATION TESTS OF TREATED OIL SAMPLES

Sample No.	R.I. at 140° F.	Approximate dewaxed V.I.*	Yield, %	Optical density	Sligh No.
107	1.4667	91.5	71.5	0.257	3.4
31	1.4693	87	64.5	0.418	5.7
103	1.4692	87	38.8	0.579	10.8
108	1.4708	84	74.2	0.429	7.9
111	1.4710	84	71.5	0.453	8.4
109	1.4715	84	50.5	0.669	11.5
28	1.4751	76	65.7	1.010	9.4
101	1.4760	76	59.8	1.260	15.1
106	1.4760	76	54.0	1.250	18.3
30	1.4772	73	80.6	1.190	3.5
102	1.4779	73	62.6	1.225	15.4
105	1.4779	73	57.6	1.303	22.3

**From V.I./R.I. correlation supplied by Imperial Oil Limited for treated oils obtained from this feedstock.*

The figures in Table II have been arranged into four groups. In each group the refractive index of the various samples is nearly constant. It should be noted that in each case the Sligh number varies inversely with the yield. The most selectively extracted high yield oils show the least tendency to oxidize. It appears that the reduction of the "tail" of aromatics which is achieved in the more selective extractions is effective in improving the oxidation stability of the oil.

CONCLUSIONS

The following conclusions may be drawn from the work described here:

1. The position of the tie lines on a Hunter–Nash diagram for the extraction of lubricating oils is dependent upon the conditions within the extractor.

2. A series of oils prepared from a single feedstock by extraction with the same solvent system under various conditions may have different chemical properties although their average physical properties such as refractive index, density, viscosity index, etc., are the same.

3. Increasing the selectivity of an extraction process not only increases the yield for a given product refractive index but also increases the quality of the product.

ACKNOWLEDGMENTS

The authors wish to thank the Queen's University Science Research Committee for their support of this project and Imperial Oil Limited for supplying the sample of lubricating oil distillate.

REFERENCES

1. BANCROFT, A. R. A study of the properties of extracted lubricating oil distillates. Thesis, Queen's University, Kingston, Ontario. 1955.
2. BONDI, A. A. Physical chemistry of lubricating oils. Reinhold Publishing Corporation, New York. 1951.
3. EVANS, T. W. Ind. Eng. Chem. 26: 860. 1934.
4. FERRIS, S. W., BERKHIMER, E. R., and HENDERSON, L. M. Ind. Eng. Chem. 23: 753. 1931.
5. GIBBS, W. Trans. Connecticut Acad. Arts Sci. 3: 176. 1876.
6. GORDON, R. R. and POWELL, H. J. Inst. Petroleum, 31: 428. 1945.
7. HILL, J. B. and COATES, H. B. Ind. Eng. Chem. 20: 641. 1928.
8. HUNTER, T. G. and NASH, A. W. J. Soc. Chem. Ind. 51: 285*T*. 1932.
9. HUNTER, T. G. and NASH, A. W. J. Soc. Chem. Ind. 53: 95*T*. 1934.
10. HUNTER, T. G. and NASH, A. W. Ind. Eng. Chem. 27: 836. 1935.
11. HUNTER, T. G. and NASH, A. W. J. Inst. Petroleum, 22: 49. 1936.
12. PROC. A.S.T.M. I, 35: 335. 1935.
13. RUSHTON, J. H. Ind. Eng. Chem. 29: 309. 1937.
14. SAAL, R. N. J. and VAN DYCK, W. J. D. Proc. World Petroleum Congr. London, 2: 352. 1933.
15. SKOGAN, V. G. and ROGERS, M. C. Oil Gas J. 46(13): 70. 1947.
16. SPENCE, A. E. Solvent extraction of complex mixtures. Thesis, Queen's University, Kingston, Ontario. 1954.
17. THIELE, E. W. Ind. Eng. Chem. 27: 392. 1935.
18. VARTERESSIAN, K. A. and FENSKE, M. R. Ind. Eng. Chem. 28: 1353. 1936.
19. VELLINGER, E. and KLINKENBERG, A. Ann. combustibles liquides, 10: 79. 1935.
20. WATANABE, S. and MORIKAWA, K. J. Soc. Chem. Ind. Japan, 36: 585*B*. 1933.

APPENDIX

Method of Analysis for Phenol in Oil Samples

A small sample (0.05 to 0.25 gm.) of phenol-bearing oil was accurately weighed into a 60 ml. short stemmed separatory funnel. Fifty milliliters of 15% sodium hydroxide solution were added and the funnel was suspended in a steam bath. It was found necessary to place a fine wire under the funnel stopper to prevent the barrel of the stopcock from being pushed out by the expansion of the air in the funnel.

After 15 min., the wire was removed and the funnel agitated. The wire was replaced and the funnel allowed to cool. Two layers were present in the funnel, the phenol free oil layer at the top and the aqueous caustic phenol layer at the bottom. The bottom layer was drained into a 250 ml. conical flask with a

ground glass stopper. The funnel was washed with water and the washings were added to the caustic solution.

The contents* of the flask were acidified with 30 ml. of concentrated hydrochloric acid and brominated with a solution containing 2.784 gm. of potassium bromate and 10 gm. of potassium bromide per liter ($N/10$). The brominating solution was added from a burette until a deep yellow color indicating excess bromine was obtained. The flask was stoppered (glass stoppers must be used) and allowed to stand with occasional agitation for one hour. Two grams of potassium iodide was then added and the liberated iodine, which was equivalent to the excess bromine, was titrated with $N/10$ sodium thiosulphate solution.

$$\% \text{ Phenol} = \frac{1568\{(\text{vol. of Br soln.})(\text{normality of Br soln.}) - (\text{vol. of } Na_2S_2O_3 \text{ soln.})(\text{normality of } Na_2S_2O_3)\}}{\text{Wt. of original sample in gm.}}$$

**From here the method follows that of Scott in Standard methods of chemical analysis. Vol. II. D. Van Nostrand Company, Inc. 1922.*

FUNDAMENTALS OF CHIMNEY PERFORMANCE[1]

By W. G. Brown and W. G. Colborne

ABSTRACT

Tests on geometrically identical, thin-walled, nonradiating chimneys and considerations for other kinds of chimneys showed design data can be obtained from model tests. Methods are outlined for preparing design charts and using models to study wind effects. The performance of the thin-walled nonradiating chimneys (or similar heat exchangers) is shown to depend on the same variables encountered in isothermal flow theory.

INTRODUCTION

The design of chimneys has always been handicapped by a lack of fundamental theory. Performance equations are available for chimneys operating with constant temperature flue gas (never obtained in practice), but apparently no attempts have ever been made to develop theory for more representative operating conditions. With this theory available, limited test data could be used for a wide range of design conditions.

For any chimney, the pressure difference (draft) required to maintain a given rate of gas flow depends on the mean density of the flowing gas and the pressure loss due to fluid friction. These two variables in turn depend on heat lost from the chimney by conduction, convection, and radiation. This heat loss, however, cannot be calculated accurately from existing heat transfer data, hence some experimental performance information is necessary. This paper deals with an investigation of methods for increasing the applicability of existing data and reducing the number of tests necessary to supply further data.

Theory of Chimney Performance

The performance of geometrically identical chimneys of any shape (e.g. Fig. 1), operating with constant temperature flue gas, is given by the following equations:

[1] $D/\Delta\rho gH = 1-K(\rho_1/\Delta\rho)(V_1^2/2gH)$ (for derivation see Appendix I), or

[2] $D = \Delta\rho gH-K\rho_1(V_1^2/2)$

where D = chimney draft (ambient air pressure minus pressure at chimney inlet),

$\Delta\rho$ = difference in density between ambient air and chimney gas,

g = acceleration due to gravity,

H = chimney height,

ρ_1 = flue gas density,

V_1 = flue gas velocity,

K = friction factor, dependent only on Reynold's number $V_1 d/\nu_1$ (d = diameter, ν_1 = kinematic viscosity).

[1]*Manuscript received April 16, 1956.*
Contribution of the Department of Mechanical Engineering, Queen's University, Kingston, Ontario.

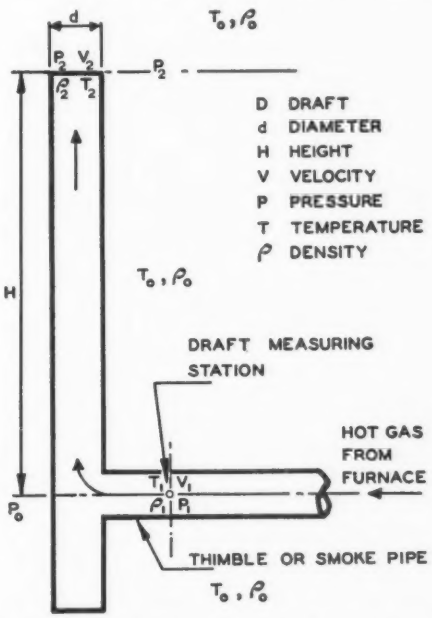

FIG. 1. Conventional chimney layout and nomenclature.

The term $D/\Delta\rho gH$ is usually called chimney efficiency E_a, since it is the ratio of available draft to the draft which would be obtained in the absence of fluid friction and heat loss. Also, $K(\rho_1/\Delta\rho)(V_1^2/2gH) = E_f$ represents the efficiency reduction due to friction, hence equation [1] becomes

$$E_a = 1 - E_f. \tag{3}$$

Equations [1] and [3] may also be written,

$$E_a = \Omega(V_1 d/\nu_1,\ V_1^2/2gH,\ \rho_1/\Delta\rho), \tag{4}$$

where Ω denotes functional dependence.

Although equation [4], relating four dimensionless groups, was derived for constant temperature chimney gas, no new terms would be required for non-isothermal flow of air in thin-walled, nonradiating chimneys, i.e.,

$$E_a = \phi(V_1 d/\nu_1,\ V_1^2/2gH,\ \rho_1/\Delta\rho), \tag{5}$$

(for derivation see Appendix II)

where ϕ denotes functional dependence different from Ω. Hence performance of this kind of chimney could be determined by model tests. To acquire data by this method, however, extensive control over ambient air pressure or temperature would be necessary. Consequently, the experimental part of the present investigation was planned to compare the performance of thin-walled, nonradiating chimneys on the basis of isothermal flow theory.

EQUIPMENT AND PROCEDURE

Equipment

Three model chimneys (nominal heights 4, 6, and 8 ft., complete dimensions given in Table I) were constructed of drawn aluminum tubing to ensure

TABLE I

PHYSICAL DIMENSIONS OF GEOMETRICALLY IDENTICAL THIN-WALLED ALUMINUM CHIMNEYS

Dimension	4 ft. chimney	6 ft. chimney	8 ft. chimney
Height from thimble center line	3.90 ft.	5.85 ft.	7.79 ft.
Inside diameter	3.90 in.	5.86 in.	7.79 in.
Distance from piezometer ring to chimney center line	1.00 ft.	1.51 ft.	2.00 ft.
Distance from piezometer ring to furnace exit	8.0 in.	12.0 in.	16.0 in.
Distance from thimble center line to base of chimney	1.00 ft.	1.51 ft.	2.00 ft.
Chimney wall thickness	0.056 in.	0.068 in.	0.073 in.
Chimney height to diameter ratio	12.00	11.99	12.00

minimum radiation heat loss as well as geometrical identity. The thimble was connected to the chimney at an angle of 90° and all joints were carefully smoothed.

Air was supplied to the model chimneys through a fan, control valve, and electric furnace. The furnace contained three 5000 watt oven heaters in parallel, one controlled with a variable rheostat. The exit section of the furnace consisted of an 18-in.-square plenum chamber to ensure similar entrance conditions for each chimney. Baffles in the plenum chamber caused some mixing of the hot air and protected chimney thermocouples from possible radiation errors.

Measurements

(*a*) *Draft*

Draft was measured with an accuracy better than 0.001 in. water gauge on two calibrated inclined gauges connected to piezometer rings on the chimney thimbles. Gauges and piezometers were connected horizontally to avoid potentially large errors caused by air density differences.

(*b*) *Temperature*

Single 40-gauge copper, 30-gauge constantan thermocouples were installed on center lines at the piezometer ring positions. Temperatures were measured to within an estimated 3°F. on a direct reading potentiometer. Ambient air temperatures were measured with shielded mercury-in-glass thermometers, remote from the chimneys, at three levels corresponding to the equally subdivided heights of the chimneys.

(c) Air Flow

Air flow rates (5 to 100 c.f.m. at 70°F.) were measured by velocity pressure traverses of a 1.50 in. I.D. copper pipe between the fan and furnace. For this purpose a hypodermic needle Pitot tube was connected to a micromanometer accurate to 0.001 in. water gauge.

Scope of Tests

Each chimney was tested to determine:

(1) Variation of friction factor K with Reynold's number. (Measurements at ambient temperature.)

(2) Chimney efficiency at various air flow rates.

(*a*) Effect of $\rho_1/\Delta\rho$ or T_1/T_0 (ratio of chimney inlet to ambient temperature).

(*b*) Variation with chimney size.

All tests were made at night to avoid transient atmospheric effects. In addition K was determined with the chimneys horizontal to avoid errors caused by minor air density differences.

Evaluation of Variables and Properties

Air properties for use in equations [1] to [5] were evaluated at chimney-inlet center-line temperature T_1, and remote ambient air temperature T_0. The air velocity, V_1, was taken as the mass flow per unit area divided by the air density at the chimney-inlet center line.

RESULTS

(1) *Friction Factor K*

Comparison of chimney performance on the basis of isothermal flow theory, equation [1], required knowledge of the friction factor K for evaluation of $E_f = K(\rho_1/\Delta\rho)(V_1^2/2gH)$. Since equation [2] is valid for any constant temperature, K could be determined at ambient temperature. For this condition $\Delta\rho gH = 0$, and D is negative.

Tests were made on all three chimneys since some doubt might arise over the degree of geometrical identity or the validity of equation [2]. Results relating K and Reynold's number (Fig. 2) showed excellent agreement for all chimneys. Below $Re = 3000$, flow appeared to be laminar (slope $= -1$), whereas above $Re = 4000$, turbulent flow was evident (slope $= -0.24$).

(2) *Chimney Efficiency*

Effect of $\rho_1/\Delta\rho$

With nonisothermal flow, chimney efficiency would be expected to vary with $\rho_1/\Delta\rho$ as well as $K(\rho_1/\Delta\rho)(V_1^2/2gH)$. Tests were made at two values of $\rho_1/\Delta\rho$, (1.6 and 3.3), chosen so K would be approximately constant for each chimney when E_f was constant (this was possible since ambient temperature remained approximately constant at 80°F. for all tests). In this way the true effect of $\rho_1/\Delta\rho$ was determined, even though data were compared on the isothermal flow basis. Results (Fig. 3) showed efficiencies of the 6 ft. and 8 ft.

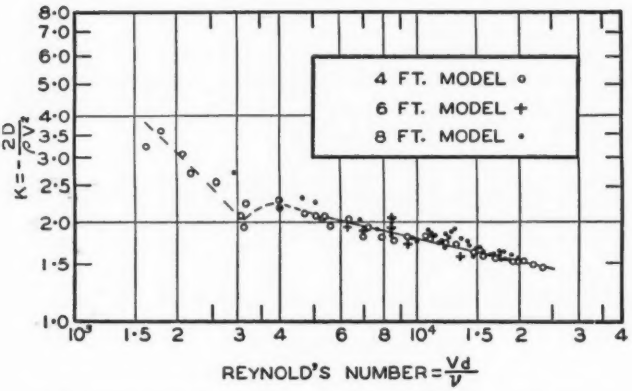

FIG. 2. Isothermal fluid friction in geometrically identical chimneys.

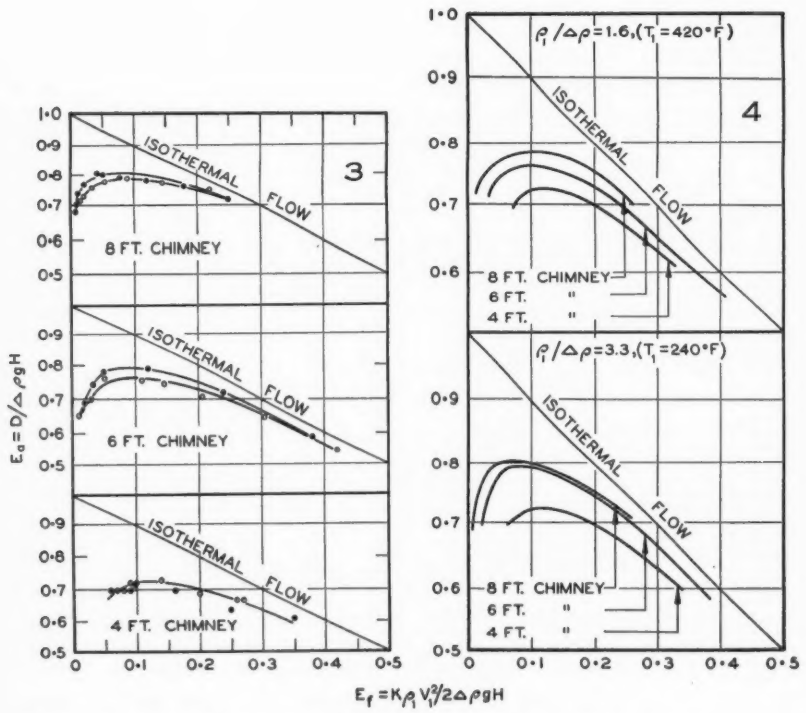

FIG. 3. Chimney efficiency as affected by density – density difference ratio.
○—$\rho_1/\Delta\rho = 1.6(T_1 = 420°\text{F.})$
●—$\rho_1/\Delta\rho = 3.3(T_1 = 240°\text{F.})$

FIG. 4. Chimney efficiency as affected by chimney size.

chimneys increased slightly with increased $\rho_1/\Delta\rho$ (decreased chimney inlet temperature), the effect being most pronounced at low values of E_f where departure from isothermal flow was greatest. For the 4 ft. chimney the effect was masked by experimental error. At high E_f, however, performance of all chimneys approached that of isothermal flow.

Variation with Chimney Size

Composite results for the three chimneys (Fig. 4) showed efficiency increased, yet leveled off, with increased chimney size. Clearly, for the range of maximum efficiency, the performance of large chimneys would not differ greatly from that of the 8 ft. chimney.

DISCUSSION

By comparing test results for thin-walled chimneys on the basis of isothermal theory it has been shown that chimney efficiency increases with chimney size. For this reason performance of large chimneys can be safely predicted from data for smaller chimneys. With this established, consideration can be given to predicting the performance of other kinds of chimneys.

Data by Achenbach and Cole (1) for a brick chimney, 15.5 ft. high above thimble, with 7-in. diameter fire clay liner and 7-in. diameter integral tile thimble (Fig. 5),* are typical of masonry chimneys for which efficiency

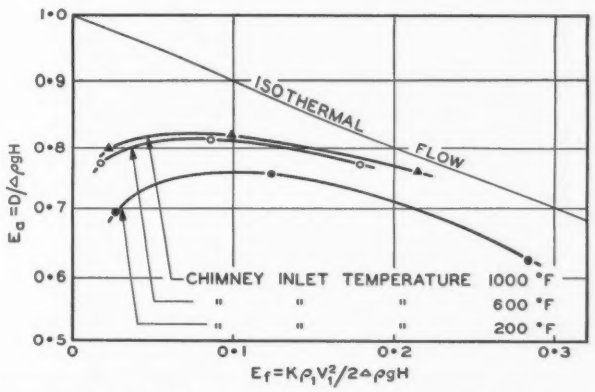

FIG. 5. Performance of a 7 in. I.D. brick chimney, 15.5 ft. high above thimble. (Ambient air temperature 60°F.) Data by Achenbach–Cole.

increases with chimney inlet temperature (decreased $\rho_1/\Delta\rho$). Since this is contrary to results obtained on the thin-walled chimneys further analysis is necessary to explain the effect and to show that efficiency increases with size for any kind of chimney. This can be done by showing how heat loss affects performance.

**Recalculated on the basis of isothermal theory. K determined from Fig. 2 and pipe friction data with assumed relative roughness of 0.01.*

The derivations that follow are not rigid. In particular two assumptions are necessary:

1. Heat loss per unit mass flowing $= C_p(T_1-T_2)$, where T_2 is the chimney exit temperature and C_p is the specific heat of the gas.

2. Temperature corresponding to mean chimney gas density, $T_m = T_1-F(T_1-T_2)$, where F is constant for chimneys of similar internal geometry. Temperature and its inverse are assumed to vary linearly with height. (Data for the 15.5 ft. brick chimney showed $F = 0.6$ to 0.7, no consistent deviations being apparent.)

At constant $K(\rho_1/\Delta\rho)(V_1^2/2gH) = E_f$, the heat loss per unit mass of gas flowing in any chimney is:

$$[6] \qquad \frac{U(T_1-T_0)}{\rho_1\sqrt{\dfrac{2\Delta\rho gHE_f}{K\rho_1}}}\left(\frac{A_s}{A_c}\right) = C_p(T_1-T_2),$$

where A_s, A_c are surface and cross-sectional areas, U is an over-all heat transfer coefficient. Hence

$$[7] \qquad T_m = T_1-F\left[\frac{U(T_1-T_0)}{\rho_1 C_p\sqrt{\dfrac{2\Delta\rho gHE_f}{K\rho_1}}}\left(\frac{A_s}{A_c}\right)\right],$$

$$= T_1-Fx,$$

and

$$[8] \qquad \frac{\Delta\rho_m}{\Delta\rho} = \left(\frac{T_m-T_0}{T_1-T_0}\right)\frac{T_1}{T_m} = 1-\frac{T_1Fx}{(T_1-T_0)(T_1-Fx)} = y,$$

where $\Delta\rho_m$ is the mean density difference.

The magnitude of E_f does not change significantly when recalculated on the basis of T_m; therefore

$$[9] \qquad \frac{D}{\Delta\rho gH} \approx y\left(1-K\frac{\rho_1}{\Delta\rho}\frac{V_1^2}{2gH}\right) = y(1-E_f).$$

Equations [7], [8], and [9] show that chimney efficiency should be less than that for isothermal flow by an amount depending on operating temperatures, chimney size, and over-all heat transfer coefficient. Calculations for $H = 15.5$ ft., $d = 7$ in., $K = 2.6$, $U = 0.5$ B.t.u./hr./sq. ft./°F., $F = 0.65$, and $T_0 = 60$°F. (Fig. 6*a*) gave efficiencies similar to observed results for the 15.5 ft. brick chimney. Additional calculations for a 5.5 ft. and 62 ft. chimney having internal geometry and brick thickness the same as the 15.5 ft. chimney (Fig. 6*b*) showed that efficiency would increase with height. The assumption of constant U and F involved in these latter calculations is valid for constant chimney inlet and ambient air temperature since brick conductance and individual outside natural convection and radiation coefficients remain approximately constant.

The assumption of constant U and F would not be warranted for thin-walled, nonradiating chimneys since convection is the sole heat transfer mechanism. Available heat transfer data (3), however, indicate that U

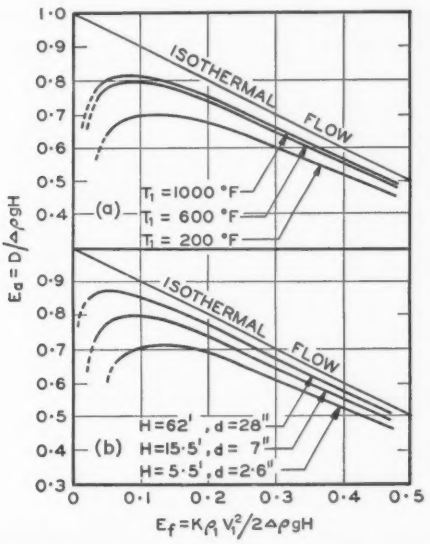

FIG. 6. (*a*) Calculated effect of inlet temperature for a brick chimney 15.5 ft. high, 7 in. internal diameter. (Ambient air temperature 60°F.)
(*b*) Calculated effect of size of brick chimneys. (Chimney inlet temperature 600°F., ambient air temperature 60°F.)

increases with temperature. In turn, this would tend to cause efficiencies that decrease with increased chimney inlet temperature. With radiating walls and flue gas, U values would increase even more with increased temperature, causing decreased efficiencies. Radiation loss, however, should not change the effect of chimney size.

Wind Effects

In practice wind may have considerable influence on chimney performance. Two effects are possible:

1. Reduction of chimney draft by partial conversion of velocity pressure to static pressure at the chimney exit.
2. Increased heat loss through chimney walls.

The first of these effects is likely to be of greatest importance for most chimneys and can probably be studied effectively with models. Considerations similar to those in Appendix II, but assuming negligible gravity influence, indicate that variables may be related as follows:

$$[10] \qquad (P_2 - P_2')/(\rho_0 V_0^2) = \zeta(V_0 d/\nu_0,\ T_2/T_0,\ V_2/V_0,\ \alpha),$$

where ζ denotes functional dependence,

$P_2 - P_2'$ is the difference in static pressure between ambient air and chimney exit at the same level,

V_0, V_2 are wind velocity and chimney exit velocity,

α is the direction angle of the wind.

Equation [10] does not require control of ambient air conditions so design data may be obtained directly from simple model tests.

CONCLUSION

Test results on thin-walled nonradiating chimneys and calculations for other kinds of chimneys have shown that except for wind, existing data can be safely used to estimate performance of larger chimneys of similar geometry and construction. To use this design method, however, data for isothermal fluid friction must be available. When not available, data can be obtained most effectively by model tests since pressure differences can be measured more readily in models than in prototype chimneys.

For masonry chimneys in particular, fairly accurate design charts for different chimney shapes can probably be derived, based on the calculation methods used in this paper. For this purpose the accuracy of equations [7], [8], and [9] could be improved by the use of mean temperatures and mean temperature differences. Some additional test data would be necessary, however, to determine friction losses and semiempirical equation corrections.

APPENDIX I

Chimney Performance with Isothermal Flow

Consider the flow of constant temperature hot gas between chimney inlet (point 1) and chimney exit (point 2), in a chimney of conventional shape (e.g. Fig. 1). Bernoulli's equation yields:

$$P_1 = P_2+\rho_1 gH+K\rho_1 V_1^2/2,$$

where P = pressure,
ρ_1 = gas density,
g = acceleration due to gravity,
H = chimney height,
V_1 = gas velocity,
K = friction factor, which depends only on Reynold's number $V_1 d/\nu_1$
(d = diameter, ν_1 = kinematic viscosity).

Also, $$P_2 = P_0-\rho_0 gH,$$

where ρ_0 = ambient air density. Therefore

[11] $$P_0-P_1 = (\rho_0-\rho_1)gH-K\rho_1 V_1^2/2.$$

On substituting: P_0-P_1 = draft D, $\rho_0-\rho_1 = \Delta\rho$, and dividing by $\Delta\rho gH$, equation [11] becomes

[12] $$D/\Delta\rho gH = 1-K(\rho_1/\Delta\rho)(V_1^2/2gH),$$

[13] $$= \Omega(V_1 d/\nu_1,\ V_1^2/2gH,\ \rho_1/\Delta\rho),$$

where Ω denotes functional dependence.

Equations [12] and [13] are the general equations for isothermal flow in geometrically identical chimneys and are valid for any shape of chimney.

APPENDIX II

Chimney Performance with Nonisothermal Flow

Although equation [13] was derived for constant temperature flue gas, a similar relationship among the same variables is obtained for air in thin-walled nonradiating chimneys even though chimney gas temperature is not constant. In the following derivations the flue gas is assumed to have the same properties as air.

In 1915, Nusselt (4) made use of the fact that the properties of air are proportional to powers of the temperature and derived the following relations for convective heat transfer between geometrically identical bodies and air: for nature convection (i.e. over the outside of a body),

$$h_0 d/k = \psi_1(gd^3/\nu^2,\ T_s/T_0,\ C_p\mu/k); \tag{14}$$

and for forced and natural convection (i.e. inside a pipe or chimney, etc.),

$$h_i d/k = \psi_2(gd^3/\nu^2,\ T_1/T_s,\ C_p\mu/k,\ V_1 d/\nu), \tag{15}$$

where ψ denotes functional dependence,
h_0, h_i = local heat transfer coefficients,
T_s, T_0, T_1 = surface, ambient, and chimney air temperature,
k = thermal conductivity of air,
C_p = specific heat of air,
μ = dynamic viscosity of air,
ν = kinematic viscosity of air.

In these equations the air properties can be evaluated at either temperature in the temperature ratio term.

The heat transfer across the thin walls of chimneys can now be equated, i.e.,

$$h_0(T_s - T_0) = h_i(T_1 - T_s). \tag{16}$$

Equation [16] can be used to eliminate h_0 and h_i from equations [14] and [15] (again, properties of the air can be evaluated at either temperature in any temperature ratio term). Hence,

$$T_s/T_0 = \psi_3(V_1 d/\nu_1,\ gd^3/\nu_1^2,\ T_1/T_0,\ C_p\mu/k). \tag{17}$$

For air $C_p\mu/k$ can be omitted since its value changes only 4.5% between 80° and 450°F. In addition, available heat transfer data (3) indicate that both h_0 and h_i are approximately proportional to $(C_p\mu/k)^{\frac{1}{3}}$. Hence the effect of $C_p\mu/k$ in equations [16] and [17] should be negligible.

Substitutions can be made in equation [17] in accord with the following identities:

$$V_1^2/2gH = (V_1 d/\nu_1)^2\,(\nu_1^2/gd^3)(d/2H);$$

and

$$\rho_1/\Delta\rho = T_0/(T_1 - T_0) = 1/\{(T_1/T_0) - 1\};$$

(absolute pressure variations in the chimney region have negligible effect on density ratios) and,

$$\rho_s/\rho_0 = T_0/T_s.$$

Therefore

[17a] $$\rho_s/\rho_0 = \psi_4(V_1d/\nu_1,\ V_1^2/2gH,\ \rho_1/\Delta\rho).$$

Under the conditions of similarity (2) the value of each of the dimensionless groups Vd/ν, $V^2/2gH$, ρ/ρ_0 at any point in the chimney or its environment must be functionally dependent on all three groups evaluated at the chimney inlet (or any other point not on a surface or in the remote ambient air). Since equation [17a] supports this condition for ρ_s/ρ_0, the complete relations can be written:

[18] $$T_0/T = \rho/\rho_0 = \Theta_1(V_1d/\nu_1,\ V_1^2/2gH,\ \rho_1/\Delta\rho),$$

[19] $$Vd/\nu = \Theta_2(V_1d/\nu_1,\ V_1^2/2gH,\ \rho_1/\Delta\rho),$$

[20] $$V^2/2gH = \Theta_3(V_1d/\nu_1,\ V_1^2/2gH,\ \rho_1/\Delta\rho),$$

where Θ denotes functional dependence.

In developing relations [14] and [15] Nusselt assumed uniform T_s, T_1, T_0. However, the derived equation [17] remains valid when T_s and T_1 are not uniform. If this were not so, the equation could lack only additional temperature ratio terms, but equation [18] shows this is not possible, since all temperature ratio terms depend on the same variables.

Equations [18], [19], and [20] show that with V_1d/ν_1, $V_1^2/2gH$, $\rho_1/\Delta\rho$ constant for geometrically identical chimneys the values ρ/ρ_0, Vd/ν, $V^2/2gH$ are the same at similar points throughout the chimneys. Hence nonisothermal chimney performance is analogous to isothermal performance, equation [13]. Consequently, a similar relation would be expected for chimney efficiency, i.e.,

[21] $$D/\Delta\rho gH = \Theta(V_1d/\nu_1,\ V_1^2/2gH,\ \rho_1/\Delta\rho).$$

This relation can also be obtained directly from Nusselt's differential equations. In deriving equations [14] and [15], however, Nusselt neglected pressure terms. His experimental data and that of later investigators have shown this assumption valid for heat transfer alone.

In practice, the chimney center-line inlet velocity, V_1, will be too low for accurate measurement. The validity of equation [21] does not change, however, if V_1 is defined as follows:

$$V_1 = M/\rho_1 A_c,$$

where M is the total mass flow per unit time; A_c is the chimney cross-sectional area; ρ_1, as before, is the density evaluated at the center-line temperature.

ACKNOWLEDGMENTS

This paper is based on the M.Sc. program of W. G. Brown at Queen's University. Appreciations are due Dean H. G. Conn of The Faculty of Applied Science, Queen's University, for general supervision of the investigation and encouragement during its progress. The project was financed in part by awards of the National Research Council of Canada. The use of facilities of the Division of Building Research, National Research Council, during preparation of the paper is acknowledged.

REFERENCES

1. ACHENBACH, P. R. and COLE, S. D. Trans. Am. Soc. Heating & Ventilating Engrs. 55: 129. 1949.
2. JAKOB, M. Heat transfer. Vol. I. John Wiley & Sons, Inc., New York. 1950. Chaps. 2, 3, and 23.
3. MCADAMS, W. H. Heat transmission. 3rd ed. McGraw-Hill Book Company, Inc., New York. 1954. pp. 172, 219.
4. NUSSELT, W. Gesundh. Ing. 38 (42): 477, 490. 1915.

MOISTURE ABSORPTION BY SOME PACKAGING MATERIALS AT SUBFREEZING TEMPERATURES[1]

By W. G. Brown and C. P. Lentz

ABSTRACT

Moisture absorption by hygroscopic packaging materials can contribute to the surface desiccation of frozen foods, depending on the amount and rate of absorption. Below 32° F. the saturation moisture content of wood and cardboard decreased with temperature, the value at 0° F. being about half that at 40° F. The time for initially dry wood to reach saturation moisture content at 0° F. and 98–100% relative humidity varied by as much as 10 to 15 times depending on species and direction of grain. Absorption times for cardboard depended on kind (corrugated or solid) and strength. The effects of sample thickness, initial moisture content, and air velocity on absorption rate were determined. Methods of preventing surface desiccation of frozen foods by packaging materials are discussed.

INTRODUCTION

Methods for maintaining high relative humidity in cold rooms have been developed to prevent surface desiccation of foods exposed to the atmosphere during cold storage (3, 4). Moisture absorption by packaging materials, however, may still cause serious surface desiccation if their initial moisture content is lower than the equilibrium moisture content corresponding to the temperature and relative humidity in the cold room. This problem is more serious in a jacketed cold room (4), where high relative humidity is maintained by preventing moisture loss from the room, than in a directly humidified room (3).

Most of the information published on the amount and rate of water absorption by wood, cardboard, and related cellulosic materials deals only with above-freezing temperatures (1, 2, 5, 6, 7, 8). The amount of moisture absorbed by these materials increases with decreasing temperature and increases with relative humidity. The characteristic relation between moisture absorption and relative humidity has been discussed in detail (1, 6). The rate of moisture absorption depends on the nature and thickness of the material and on the direction of moisture movement in it (6, 7). Applicable information on drying indicates that the rate of moisture absorption is also a function of the initial and final moisture contents of the material and depends on air velocity (5, 9, 10).

To determine whether significant moisture absorption by packaging materials could occur at cold storage temperatures, and if so, to assess the effectiveness of ways in which the problem could be attacked, information on the amount and rate of moisture absorption at these temperatures was required. Although the work was undertaken mainly to provide information on the cold storage problem, the test program was designed so that the results would also be of more general interest. Equilibrium moisture contents were measured at 98–100% relative humidity at temperatures from −40° F. to

[1]*Manuscript received May 31, 1956.*
Contribution from the Division of Applied Biology, National Research Laboratories, Ottawa, Canada. Issued as N.R.C. No. 4033.

+40° F. for five species of wood and for corrugated cardboard from two sources of manufacture. Moisture absorption rates were determined for six varieties of wood, corrugated cardboard of different types, plain and waxed solid cardboard, and waxed locker paper at 0° F. In addition, the effectiveness of spraying wood with water, as is sometimes done commercially to reduce moisture absorption during storage, was tested.

EQUIPMENT AND PROCEDURE

Samples of wood were $\frac{1}{4}$ in. thick and samples of cardboard were a single layer thick, except where otherwise noted.

In determining equilibrium moisture contents, 5 in. square samples were vacuum dried at 140° F. to constant weight and then placed over ice or water in a sealed glass jar held at the required temperature. The samples were weighed at intervals in the jar until essentially constant weight was reached.

Moisture absorption rates were determined by measuring at suitable intervals the weight increase of 5 in. square samples in a specially constructed cabinet lined with cracked ice and located in a room held at the test temperature (0° F.). The samples were vacuum dried and then cooled to the test temperature over a desiccant before being placed in the cabinet. A small fan driven by a motor outside the cabinet provided air movement at 100–200 f.p.m. for all tests except those in which the effect of reduced air velocity was determined. In these tests the fan was stopped. Moisture movement in the desired direction was obtained by painting the edges of the samples with asphaltic paint. The area of the cracked ice in the cabinet was sufficient to maintain at least 98% relative humidity.

RESULTS AND DISCUSSION

Equilibrium Moisture Content

Moisture content of wood and corrugated cardboard at 98–100% relative humidity decreased with decreasing temperature in the range +40° F. to −40° F. (Fig. 1). The results for wood are the averages from five different

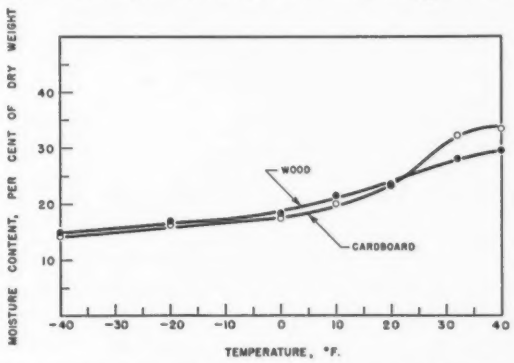

FIG. 1. Saturation moisture contents of wood and corrugated cardboard at subfreezing temperatures.

species (white pine, jack pine, basswood, white birch, white oak). There was no significant difference between species or between sapwood and heartwood of the same species at and below 32° F. Although there was considerable variability at +40° F. (±20%), it was not significant because the same variability was noted in replicates. Similar results were obtained with two samples of corrugated cardboard from different sources of manufacture.

The variation noted above in amount of water absorbed near saturation by different species of wood was discussed by Pidgeon and Maass (6), who suggested that such absorption occurred in the capillary structure of the wood, which could vary between species. They also pointed out that relatively small changes in vapor pressure would cause large changes in the amount of water absorbed because of the relatively large size of the capillary pores.

The variation in moisture content with relative humidity is well known (1, 2, 5, 6) for wood, paper, and other hygroscopic materials. In this study it has been assumed that the relation between relative humidity and moisture content at subfreezing temperatures is similar to that which has been determined at higher temperatures (Fig. 2) and hence only saturation moisture contents have been determined.

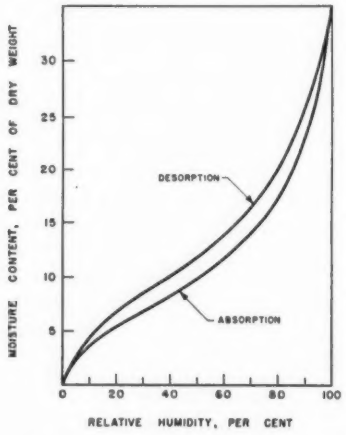

FIG. 2. Variation of moisture content of spruce wood with relative humidity at 68° F. (based on the data of Filby and Maass (2)).

Rate of Moisture Absorption

1. *Wood*

With initially dry samples of $\frac{1}{4}$ in. thick wood exposed to an air velocity of 100–200 f.p.m. at 0° F. and 98–100% relative humidity, average rate of moisture absorption depended on species and, within a species, on whether the sample was sapwood or heartwood (Fig. 3). In addition, the rate of moisture absorption depended on the direction of moisture movement with respect to the grain of the wood. The rate of absorption parallel to or along the grain was

about 15 times as great as in either the radial or the tangential direction in the white pine samples tested. There was no significant difference between absorption rates with radial or tangential flow for any of the samples tested and these are the results in Fig. 3. Although absorption rates for different

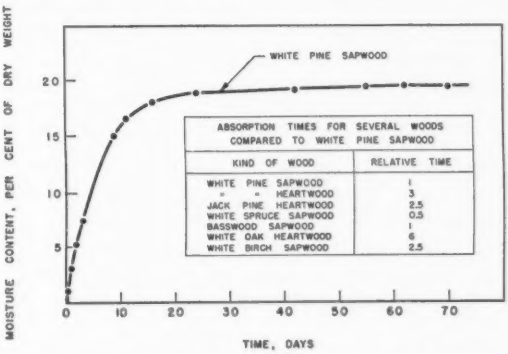

FIG. 3. Moisture absorption times for initially dry woods at 0° F. and 100% relative humidity. (Relative times in the table are based on averages of times at 4, 8, 12, and 16% moisture content.)

samples of the same species of wood from the same stock or lot were in good agreement, the results obtained with samples from different stocks varied by as much as ±50%. The results of Fig. 3 should therefore be used only as a guide.

The difference noted in absorption rates between heartwood and sapwood and the effects of grain have been discussed in terms of microscopic structure by Pidgeon and Maass (6).

2. *Cardboard*

Cardboard absorbed water vapor much more rapidly than wood (Fig. 4). The results obtained with corrugated cardboards of Mullen strengths of 175, 200, and 275 lb. fell between those for the 125 lb. and 350 lb. samples of Fig. 4,

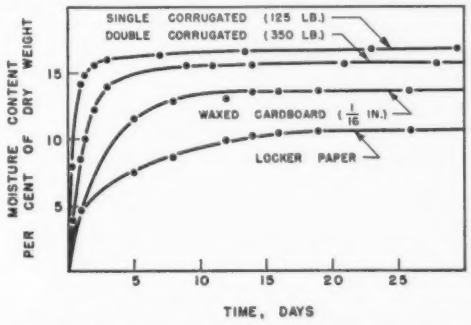

FIG. 4. Moisture absorption times for initially dry cardboard and locker paper at 0° F. and 100% relative humidity. (Mullen strength for corrugated cardboard in parenthesis.)

the rate of absorption decreasing with increasing strength. Solid cardboard 1/16 in. thick absorbed at the same rate as the 350 lb. corrugated cardboard. Maximum variation in absorption rate between comparable samples from four different sources of manufacture was less than $\pm 25\%$ of the mean rate. The lower equilibrium moisture contents of the waxed cardboard and the locker paper might be accounted for by the weight of wax included in the dry weight of the samples.

3. *Effect of Sample Thickness, Initial Moisture Content, and Air Velocity*

Pertinent information on the drying of wood and similar solids (5, 9, 10) at moisture levels below the fiber saturation point indicates that for slab-shaped samples with a large length to thickness ratio, drying time varies as the square of the sample thickness if air film resistance is negligible. Since absorption under these conditions is a similar process in the reverse direction, the same relation between thickness and time should hold; the results of Fig. 5 confirm

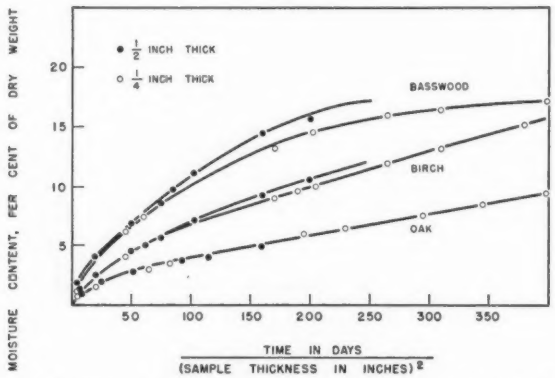

FIG. 5. Relation between absorption time and sample thickness for initially dry wood at 0° F. and 100% relative humidity.

this. In these experiments the samples were thin and the air film resistance (discussed later) was not negligible. This may account for the difference between the results for the $\frac{1}{2}$ in. samples and the $\frac{1}{4}$ in. samples in Fig. 5. It may be noted that the difference decreases as the internal resistance of the wood increases (basswood compared to oak).

The work on drying cited above shows also that the moisture content of a slab of wood at any given time during the drying process depends on its initial moisture content, its final equilibrium moisture content, and the drying time:

$$(W - W_e)/[W_0 - W_e] = f(t)$$

where

W = moisture content at time t,

W_0 = initial moisture content,

W_e = final equilibrium moisture content.

For a given slab $f(t)$ depends only on t, and hence a single value of $f(t)$ is associated with each value of t. Applied to moisture absorption, this relation can be used to calculate the rate of moisture absorption for any initial moisture content if the "initially dry" results are known. Fig. 6 shows the agreement

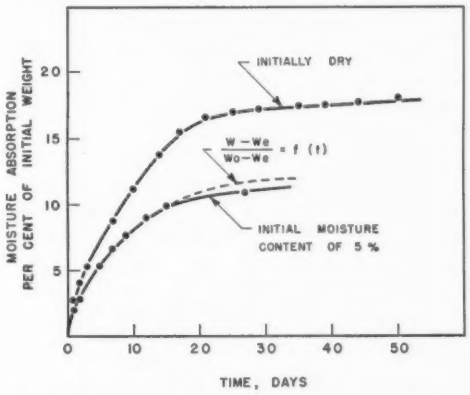

FIG. 6. Effect of initial moisture content on moisture absorption by wood at 0° F. and 100% relative humidity. (Curve $(W-W_e)/(W_0-W_e) = f(t)$ calculated for initial moisture content of 5% from initially dry test results. W, W_0, W_e = moisture contents at time t, initially, and at equilibrium; $f(t)$ = function of time, t.)

between experimental and calculated results for a sample of white pine heartwood $\frac{1}{4}$ in. thick. Similar results were obtained with a sample of cardboard.

Spraying the samples of wood with water for several minutes before they were tested did not change the amount or rate of moisture absorption significantly since less than 2% moisture was gained as a result of spraying.

Reduction in rate of moisture absorption caused by reducing air velocity from 100–200 f.p.m. to a negligible level (natural convection) depended on the resistance of the sample itself to moisture transmission. Absorption times were increased by two-thirds for cardboard, by one-third for white pine $\frac{1}{4}$ in. thick, and by one-fifth for white pine $\frac{1}{2}$ in. thick.

CONCLUSION

The results obtained in these tests indicate that moisture absorption by hygroscopic packaging materials at cold storage temperatures can contribute significantly to surface desiccation of frozen food products, but suggest a simple method of prevention. Since the saturation moisture content of these packaging materials decreases with temperature below the freezing point, their moisture content can be raised before they are used by preconditioning at above-freezing temperatures and relative humidities less than 100%. A moisture content equivalent to saturation at 0° F., for example, is produced by a relative humidity of 80% at 68° F.

Desiccation due to moisture absorption by packaging could also be reduced by adding moisture to the storage room atmosphere to make up for that

absorbed. Since the rate of absorption varies widely with the material, its thickness, and initial moisture content, and the rate of air movement over it, the results of these tests could only be used to estimate the maximum rate of moisture addition required and the approximate time during which moisture should be added. The exact rate of addition can be determined by measuring the relative humidity which should be maintained at or near saturation. This method is not as effective as preconditioning the packaging material. Since packaging materials absorb moisture through both inside and outside surfaces, high humidity at the outside surface will reduce moisture absorption but will not eliminate it. For maximum effectiveness air should circulate on all sides of each container.

ACKNOWLEDGMENT

The authors wish to thank Mr. G. W. Daechsel particularly for technical assistance during the investigation.

REFERENCES

1. BABBITT, J. D. Can. J. Research, A, 20: 143. 1942.
2. FILBY, E. and MAASS, O. Can. J. Research, B, 13: 1. 1935.
3. LENTZ, C. P. Can. J. Technol. 32: 156. 1954.
4. LENTZ, C. P. Can. J. Technol. 33: 265. 1955.
5. PERRY, J. H. Chemical engineers' handbook. 3rd ed. McGraw-Hill Book Company, Inc., New York. 1950.
6. PIDGEON, L. M. and MAASS, O. J. Am. Chem. Soc. 52: 1053. 1930.
7. PIDGEON, L. M. and MAASS, O. Can. J. Research, 2: 318. 1930.
8. PIENIAZEK, S. A. Ice and Refrig. 103: 43. 1942.
9. SHERWOOD, T. K. Ind. Eng. Chem. 21: 12. 1929.
10. SHERWOOD, T. K. Ind. Eng. Chem. 21: 976. 1929.

AN ALL GLASS CIRCULATING PUMP FOR GASES*

By J. S. Watson

The pump described is intended for use in a closed system to maintain continuous gas circulation up to 5 liters per minute at pressures from about 5 mm. Hg to atmospheric pressure.

The design is based on that of Leake (1) but it has been extensively modified. Important differences are that the piston is operated horizontally instead of vertically and that the switching is effected electronically. An interesting feature is that only glass surfaces are exposed to the circulating gas.

Fig. 1 shows the design of the pump, which consists essentially of two

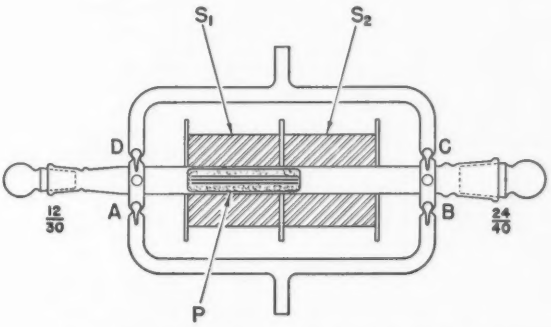

Fig. 1. Diagram of pump (about one-sixth scale).

solenoids S_1 and S_2 energized alternately by d-c. current. A glass piston P (containing an iron core) is thus made to travel backward and forward at a rate which depends on the switching frequency of the current in the solenoids. The result is a double-acting pump, the forward stroke (→) drawing gas through valve A and expelling it through C while on the backward stroke (←) the gas enters via B and is expelled via D. These valves consist of small light pear-shaped glass bulbs seated on constrictions in 15 mm. glass tubing.

The piston consists of a glass tube 18 mm. in diameter, 12 cm. long, ground to fit easily the glass tube in which it slides. A perfect fit is not essential. The piston armature consists of short lengths of iron wire about 20 A.W.G. which partially fill the tube; to prevent any movement of the wire the tube is also packed with glass wool. The total weight of the piston is about 60 gm. The solenoids S_1 and S_2 are wound with 33 A.W.G. cotton covered wire until the resistance is about 5000 ohms. St_1 and St_2 are glass stoppers sizes 12/30 and

Issued as N.R.C. No. 4043.

24/40 respectively. These permit the easy removal of the piston should it require cleaning. In the original model the piston was caused to travel between coils S_1 and S_2 by alternate switching of the current from one coil to the other, and some trouble was experienced as the piston tended to overshoot its position. This trouble has been overcome by allowing some residual current to flow in the coils on the "off" period.

The electronic switch controlling the pump is shown in Fig. 2. It consists

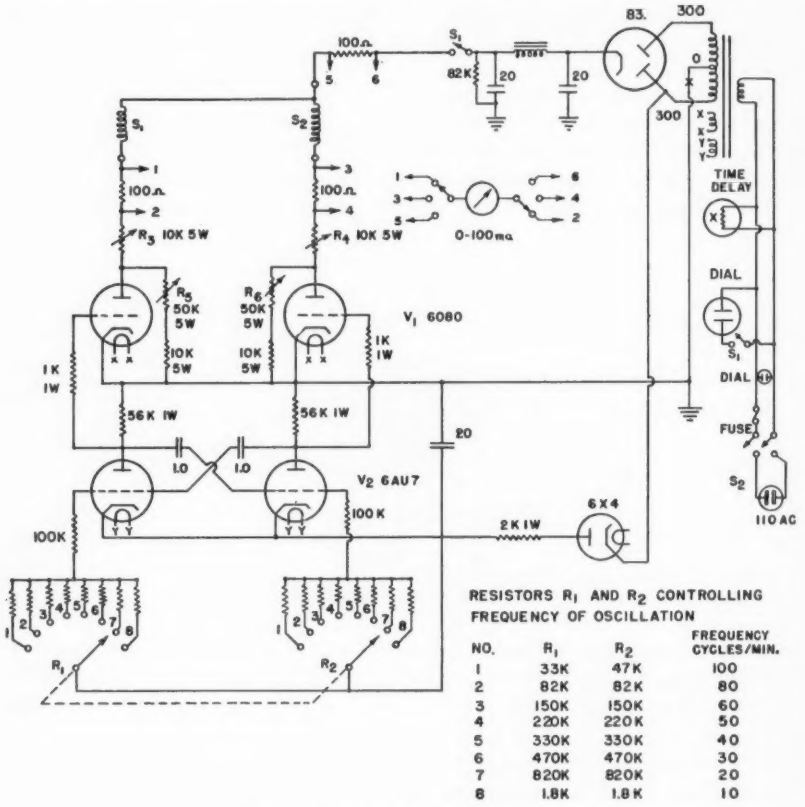

NO.	R_1	R_2	FREQUENCY CYCLES/MIN.
1	33K	47K	100
2	82K	82K	80
3	150K	150K	60
4	220K	220K	50
5	330K	330K	40
6	470K	470K	30
7	820K	820K	20
8	1.8K	1.8K	10

FIG. 2. Electronic switch for pump.

essentially of a symmetrical multivibrator (circuit around V_1) the frequency of which can be altered in steps from 10 to 100 cycles/min. The output voltage is applied to the grids of V_2, one half of which controls the current in S_1 while the other controls the current in S_2. The total current may be adjusted by R_3 and R_4 and the residual current by R_5 and R_6. It has been found that the "on" stroke requires 40–50 ma. while the "off" stroke 10–20 ma. The actual current depends on the pumping speed and pressure of the gas in the system.

The pump has been found to pump gases effectively at rates from 0.5 liter/min. to 5.0 liters/min. at pressures from 5 mm. to 760 mm. It will not, however, operate at a pressure lower than 1 mm. It should also be noted that the pump is intended only to circulate gases and will not pump against a pressure differential greater than a few millimeters of mercury.

ACKNOWLEDGMENTS

Permission to publish the original article was kindly given by Olin Mathieson Chemical Corporation, New Haven, Connecticut, U.S.A. The author is also indebted to Messrs. J. K. Waterman, T. L. Simpson, and G. Ensell, who assisted materially with the design and construction of the pump.

1. LEAKE, L. E. J. Sci. Instr. 434. 1953.

RECEIVED MAY 17, 1956.
OLIN MATHIESON CHEMICAL CORPORATION,
NEW HAVEN, CONN.,
AND
DIVISION OF APPLIED CHEMISTRY,
NATIONAL RESEARCH COUNCIL,
OTTAWA, CANADA.

A NOTE ON THE MEASUREMENT OF VICKERS HARDNESS INDENTATIONS

BY B. S. SATYANARAYANA

INTRODUCTION

The hardness indentations made by the diamond pyramids of Vickers hardness testing machines are found to depart at the top surface of the specimen from the square form expected from geometrical considerations. The indentations in most cases acquire a pincushion type or a barrel shape (1) depending upon the physical nature of the specimen subjected to the hardness test. In the investigations conducted here a fine interference pattern of a pincushion type of indentation is obtained and measurements are conducted on indentations of different sizes. The nature of the fringes enables an accurate measurement of the different positions of the indentations, and the errors involved in the normal measurements of Vickers diamond indentations can be evaluated.

INTERFERENCE PATTERN

The measurement of an interference pattern was made for a macrohardness indentation. The pattern was interesting for the fringes were formed inside the indentation and lent themselves to an accurate measurement of the indentation boundary. The interference pattern outside the indentation merging with the inner interference pattern could also be traced. The inner interference system gives an accurate idea of the rim formation during indentations.

The experimental arrangements for a study of the interference pattern was of the standard type employed in the observation of Newton's rings. The inner pattern was conspicuous only in CR 39, a standard photoelastic material, and is recorded (Fig. 1). The pattern outside the indentation is reduced to the

FIG. 1. Interference pattern of a Vickers indentation.

minimum intensity possible. The measurements of the sides and diagonals of the indentations of different sizes made by the Vickers diamond pyramid for different loads are made by the micrometer eyepiece. The sharp fringes at the boundary of indentation enable an accurate measurement to be made.

DISCUSSION OF RESULTS

The indentations were made by two different diamond pyramids, and the investigations were conducted throughout the normal macroscopic hardness range of indentation. If x is the average length of the sides of an indentation, and d is the measured average length of the two diagonals of an indentation for hardness number calculation, $d/2^{\frac{1}{2}}$ gives the length of the side. But the measured value of x from the fringes is far less than the value $d/2^{\frac{1}{2}}$ (Fig. 2). The difference between the values is expressed as a percentage and it is found that the reduction shows a fairly constant value of 28.5% for different Vickers indentation areas (Table I). The experimental error is not more than 5% in the readings tabulated.

The pincushion appearance of indentation in CR 39 mapped out by the interference fringes suggests that the sinking in occurs mostly at the faces with very little at the ends of the diagonals because the fringes are straight at the centers of all the indentation faces for indentations of different areas.

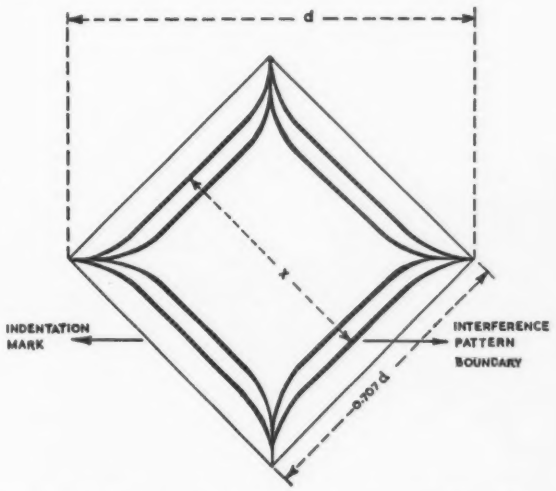

FIG. 2. A sketch of the Vickers indentation fringe pattern with the square mark.

TABLE I

REDUCTION IN SIDES OF VICKERS INDENTATIONS

Average diagonal length, d, mm.	Calculated side length, 0.707 d, mm.	Measured length of side from fringes, x, mm.	Percentage reduction of side length $(0.707d-x)$ $100/0.707d$, %
1.000	0.707	0.504	28.7
0.768	0.544	0.384	29.3
0.664	0.468	0.336	28.4
0.392	0.276	0.200	27.8

The sunk in portion appears as a rectangular strip bordering the faces except for a small portion at the ends of the diagonals (Fig. 2). This was clearly observed during examinations of the indentations under a high power microscope. A regular square mark was present enclosing the pincushion interference pattern though the difference between the diagonal lengths of the interference pattern and the indentation mark was very small. A check to find whether any appreciable difference between the two diagonals exists is still under investigation.

1. TABOR, D. The hardness of metals. Oxford at the Clarendon Press. 1951.

RECEIVED MARCH 13, 1956.
COLLEGE OF MILITARY ENGINEERING,
POONA, INDIA.